THE ANNIHILATION MODEL OF THE TORMAC SHEATH

by

James Henry Hammer

Accelerator and Fusion Division, Plasma
Lawrence Berkeley Laboratory
University of California
Berkeley, California

NOTICE

This report was prepared as an account of work sponsored by the United States Government. Neither the United States nor the United States Department of Energy, nor any of their employees, nor any of their contractors, subcontractors, or their employees, makes any warranty, express or implied, or assumes any legal liability or responsibility for the accuracy, completeness or usefulness of any information, apparatus, product or process disclosed, or represents that its use would not infringe privately owned rights.

DISTRIBUTION OF THIS DOCUMENT IS UNLIMITED

THE ANNIHILATION MODEL OF THE TORMAC SHEATH

James Henry Hammer

Accelerator and Fusion Division, Plasma
Lawrence Berkeley Laboratory
University of California
Berkeley, California

ABSTRACT

A one-dimensional, steady state fluid model is developed to describe the boundary layer between plasma and magnetic field that occurs in the Tormac sheath. Similar systems which may be treatable by the same model are Tokamaks with divertors and reversed field mirrors.

The model includes transport across the magnetic field as well as mirror losses along the field, the latter being represented as "annihilation" terms in the one-dimensional equations. The model equations are derived from the two-dimensional, time dependent hierarchy of equations generated by taking velocity moments of the kinetic equation including collisions. In order to obtain the annihilation equations, several approximations are made: ρ_i/Δ_s is assumed small in order to truncate the infinite hierarchy of fluid equations (ρ_i = the ion gyro radius, Δ_s = the sheath scale length); Δ_s/r_p is assumed small to allow the slab approximation (r_p = the plasma minor radius); r_p/λ_{mfp} is assumed small to allow expansion about the collisionless state (λ_{mfp} = the mean free path) the sheath is assumed to "eat in" steadily, i.e., a balance between particle loss and inward resistive diffusion of open field lines is formed so that there exists a reference frame in which the sheath appears approximately stationary.

With these approximations a set of non-linear ordinary differential equations is generated with independent variable x, the distance across the sheath. Time has been removed from the equations by a change of reference frame. The second spatial dimension y, the poloidal coordinate, is manifested solely in the annihilation terms which arise from the outward flow of loss-cone scattered particles.

The annihilation equations are integrated numerically for a variety of situations: poloidal field reversed and non-reversed sheaths; classical and anomalous collisionality; including or excluding electron-wall interactions. The integration yields profiles for density, pressure, flow velocity, magnetic and electric fields as well as the "eating in" rate of the sheath and the floating electrostatic potential.

Two basic types of solution are found. The first solution has parameters $T_e/T_i|\text{sheath} \sim 1/10$, $e\phi/T_e|\text{sheath} \sim 3$. The sheath width $\Delta_s \gtrsim \rho_i$ and the "eating in" velocity $U_x \sim \rho_i \nu_{ii}$ (ν_{ii} = the ion-ion 90° scattering rate). This type of solution exists for all of the variants of the model mentioned above and confirms the basic Tormac scaling which predicts a confinement time of:

$$\tau_{\text{Tormac}} \cong \frac{r_p}{\rho_i} \tau_{ii}$$

The second solution has parameters $T_e/T_i|\text{sheath} \sim 1$, $e\phi/T_e \sim 1$, $\Delta_s \sim \rho_i$ (anomalously broadened), $U_x \sim 30\rho_i\nu_{ii}$. This solution exists only for the poloidal field reversed sheath. In this case ohmic heating of the electrons overcomes the mirror heat losses resulting in hot electrons, $T_e \sim T_i$. The hot electrons cannot be electrostatically

confined and are lost rapidly. The ions become electrostatically detrapped by the potential until the ions are lost at a rate comparable to the electrons. If this situation were to prevail in Tormac, the confinement time would be degraded until the device lost its confinement advantage over a classical mirror. This solution, however, is sensitive to the detailed structure of the ion-annihilation rate as well as other features of the model and is eliminated for many of the variants described above, e.g. by the addition of a source of cold electrons from the walls.

ACKNOWLEDGEMENTS

I gratefully acknowledge the combined contributions of excellent guidance and valuable ideas from my thesis adviser, Andy Sessler. In the face of many pressing responsibilities, he has always given ample time to the detailed discussion of this work.

Thanks are also due to Wulf Kunkel, Allan Kaufman and Herb Berk for their extensive contributions to this work as well as to my general education in plasma physics. Allen Boozer has also played an important role by originating the annihilation model concept.

Many of my peers have aided in the development of this research, including Mike Mostrom, John Cary, Harry Mynick, Steve McDonald and Robert Littlejohn.

I would especially like to thank Heather Leslie for her unfailing support and the maintenance of my sanity throughout this entire episode.

CONTENTS

Introduction

Chapter I: Review of Tormac theory

Chapter II: Derivation of the model equations

Chapter III: Annihilation fluxes

Chapter IV: Discussion of solutions

Conclusions

Appendix A: Poloidal flow on open field lines

Appendix B: Thermal force terms

Appendix C: Equations modified for an electron source

INTRODUCTION

The Tormac device[1,2] is a high beta toroidal cusp (see Fig. 1) that is "stuffed" with a Tokamak style helical magnetic field. The cusp magnetic field supports most of the plasma pressure, providing an absolute minimum $|B|$ magnetic well that ensures gross plasma stability. The internal rotationally transformed magnetic field constrains particles to move on closed drift surfaces, increasing the confinement time over that of an ordinary, unstuffed cusp where particles stream freely out the open field lines to the walls.

The transition region from the nearly uniform plasma and closed flux surfaces of the interior to the open flux surfaces of the vacuum is called the sheath. An additional advantage of the stuffed cusp over the unstuffed cusp is that particle motion in the sheath may be adiabatic, i.e., particles are better mirror contained on the open flux surfaces (some mirror containment occurs even for an unstuffed toroidally symmetric cusp due to conservation of toroidal canonical momentum).[3]

The confinement time for Tormac is determined by the loss of particles along open field lines. In the absence of instabilities, classical Coulomb collisions cause velocity space scattering of the mirror contained particles into the loss regions, at which point they exit in one transit time $\tau_{tr} \cong r_p/V_{th}$ (r_p = poloidal plasma radius, V_{th} = thermal speed). The sheath is emptied of particles in a time $\tau_{sheath} \cong \tau_{ii}$, the ion-ion collision time.

If the interior plasma and the sheath plasma "decouple" (an

assumption to be examined later), a simple estimate of the overall confinement time for the device may be made:[3]

$$\tau_{Tormac} \cong \frac{r_p}{\Delta_s} \tau_{sheath} \cong \frac{r_p}{\Delta_s} \tau_{ii}$$

Δ_s = sheath thickness = the width of the region where plasma and open field lines coexist.

Assuming no external sources of plasma exist, the nearly uniform interior provides a reservoir of particles to refill the sheath N times where N is the ratio of internal plasma volume to sheath volume ($N \cong r_p/\Delta_s$). To obtain access to the internal plasma particles, the sheath slowly "eats in" due to an inward resistive diffusion of the cusp magnetic field.

The confinement time for an ordinary "unstuffed" cusp is given by the total number of particles in the cusp divided by the flux of particles through the "hole":[4,5]

$$\tau_{cusp} \cong \frac{n r_p^2}{n v_{th} \Delta_{hole}} = \tau_{tr} \frac{r_p}{\Delta_{hole}}$$

Taking the ratio of τ_{cusp} to τ_{Tormac}, assuming $\Delta_s \cong \Delta_{hole}$, yields

$$\frac{\tau_{cusp}}{\tau_{Tormac}} \cong \frac{\tau_{tr}}{\tau_{ii}} \ll 1 \quad \text{for high temperature plasmas}$$

The comparatively long confinement time makes Tormac interesting as a fusion reactor concept. The most crucial parameter constraint on any fusion reactor concept is that the Lawson criterion[6] be satisfied:

$n\tau_E \gtrsim 10^{14}$ for D-T reactions
n = density in cc^{-3}
τ_E = energy confinement time in seconds

For Tormac, assuming $\tau_E \sim \tau_{particle}$, the Lawson criterion becomes

$$n\tau_{ii}\left(\frac{r_p}{\Delta_s}\right) \gtrsim 10^{14}$$

The classical mirror machine for which $\tau_{particle} \sim \tau_E \sim \tau_{ii}$ is known to marginally satisfy the Lawson criterion for some range of parameters ($T_i \sim 100$ KeV, $T_e \sim 10$ KeV, $\beta \sim 1$).[13] Tormac, which operates in a similar regime, constitutes an improvement over a classical mirror machine by the geometrical factor r_p/Δ_s. If Δ_s is on the order of an ion gyro radius as has been predicted,[7,8] then $r_p/\Delta_s \cong r_p/\rho_i \cong 100$ for fusion reactor parameters and the Lawson criterion is easily satisfied.

The above estimate of the Tormac confinement time depends on the crucial assumption that the sheath and the internal plasma must decouple, i.e., particles from the interior must not circulate in and out of the sheath.

If the internal stuffing field is purely toroidal, ∇B and curvature drifts will cause particles to drift across the interior in a direction normal to both $\hat{B}_{tor}$ and $\hat{R}$, the unit vector along the major radius. The characteristic drift time is

$$\tau_{Drift} \cong \frac{r_p}{v_{th}}\frac{R}{\rho_i}$$

The decoupling of the sheath and interior requires $\tau_{Tormac} < \tau_{Drift}$:

$$\tau_{ii}\frac{r_p}{\Delta_s} < \frac{r_p R}{v_t \rho_i}$$

If $\Delta_s \cong \rho_i$, then

$$\tau_{ii} < \frac{R}{r_p}\tau_{tr}$$

For fusion reactor parameters $\tau_{ii}/\tau_{tr} \cong 10^4$ whereas $R/r_p \cong 3$, so that the inequality is violated. The confinement time for a Tormac in the long mean free path regime, stuffed with a purely toroidal field is thus reduced to that of a classical mirror: the interior particles sample the sheath and are lost in a collision time rather than providing a reservoir of isotropic plasma isolated from the mirror-like sheath.

Two possibilities exist for closing particle orbits within the interior. A radial electric field may be produced to cause poloidal $\underline{E}\times\underline{B}$ convection.[9] The combination of $\underline{E}\times\underline{B}$ flow and the ∇B and curvature drifts can result in particle trajectories that are confined within the interior region. Recent calculations have shown, however, that poloidal rotation in a toroidal configuration is heavily damped by parallel viscosity, excluding the possibility of a driven bulk rotation.[10] Flow could be driven in a narrow layer near the sheath, but it is unclear without further study that such a flow would close particle trajectories sufficiently to improve confinement.

In addition, flows in non-circular configurations such as Tormac are subject to a parametric instability that resonantly couples the rotation to Alfvén waves.[11]

To see this examine an infinitesimal tube of toroidal flux following a circulating trajectory. The tube behaves as an Alfvén wave oscillator subjected to a periodic variation in the oscillator frequency due to the non-uniformity of the tube's environment. The equation for the perturbed flow velocity is:[11]

$$\frac{d^2\omega}{d\tau^2} + \left(k^2V_A^2 - \frac{\frac{d^2}{d\tau^2}|\underline{u}|}{|\underline{u}|}\right)\omega = 0$$

$|\underline{u}|$ = magnitude of equilibrium flow

$\frac{d}{d\tau} = \hat{y}\cdot\nabla$

k = toroidal wave vector = $\frac{2\pi n}{R}$

ω = perturbed flow velocity

As an explicit example, take $\frac{1}{|\underline{u}|}\frac{d^2|\underline{u}|}{d\tau^2} = \alpha\Omega_{rot}^2\cos(2\tau\Omega_{rot})$ which yields the Mathieu equation:

$$\frac{d^2\omega}{d\tau^2} + (k^2V_A^2 - \alpha\Omega_{rot}^2\cos(2\Omega_{rot}\tau))\omega = 0$$

α = a constant of order unity for a highly non-circular cross-section. $\Omega_{rot} = 2\pi/(\text{rotation period})$.

This equation is well known to yield bands of instability. For Tormac, $kV_A \sim V_A/R$ (R = major radius), $\Omega_{rot} \sim \frac{|u_o|}{r_p} \sim \frac{V_{thi}}{R}$ typically. Since the plasma β is of order 1 in Tormac, $V_A \sim V_{thi}$ so $k^2V_A^2 \sim \alpha\Omega_{rot}^2$ resulting in an instability with a typical growth time;

$$\tau_{inst} \sim \frac{1}{\Omega_{rot}},$$

The instability transforms rotational energy to wave energy on this time scale.

The large energy drains due to viscous damping and Alfvén wave excitation make rotation an undesirable method for confining particle trajectories.

The second and currently more favored possibility is to induce a toroidal electric field within the interior, driving toroidal currents

that give a helical twist to the stuffing magnetic field. Particles then move on nested toroidal drift surfaces as in the Tokamak device, providing the desired decoupling from the sheath.

The toroidal currents which provide the twist (or rotational transform) are MHD kink unstable if the toroidal current is too large, as is well known from Tokamak theory and experiments.[12] MHD theory places an upper bound on the current given by

$$q \cong \frac{B_T r_p}{B_p R} \gtrsim 1 \qquad \begin{array}{l} q = \text{safety factor} \\ B_p = \text{poloidal field} \\ B_T = \text{toroidal field} \end{array}$$

For Tokamaks, this condition limits the plasma β that is achievable since the poloidal field must support the plasma pressure, i.e., β poloidal = 1.

$$\beta \equiv \frac{8\pi P}{B^2} \cong \frac{8\pi P}{B_T^2} \cong \varepsilon^2 \frac{8\pi P}{B_p^2} \cong \varepsilon^2 \ll 1 \qquad \varepsilon = r_p/R$$

For Tormac most of the pressure gradient is supported on the cusp magnetic field so that β can be of order unity while the internal field satisfies $q > 1$. A high β is desirable in a fusion reactor for economical reasons: high β devices require less investment in magnetic field energy for a given amount of plasma energy.

Thus Tormac is a hybrid of three long-standing fusion reactor concepts: the cusp; the magnetic mirror; and the Tokamak, combining many of the advantages of each. The adiabatic motion of particles allows for mirror confinement of sheath particles and hence a loss rate drastically reduced below that of a pure cusp. The Tokamak type rotational transform decouples the sheath from the interior, providing a reservoir of quiescent isotropic plasma isolated from open field lines.

The essential element of the Tormac scheme is the existence of a relatively narrow sheath. If the sheath width approaches the plasma radius, the confinement time approaches that of an ordinary mirror machine and the concept loses its advantage. If the sheath width is narrow ($\Delta_s \cong 2\rho_i$) and the sheath particles are classically mirror contained (an assumption which will be examined below), then Tormac is superior to any single one of the reactor schemes from which it is hybridized.

The theoretical and experimental understanding of the sheath is somewhat meager (see Chapter I) and many possibilities exist that could degrade the scaling of Tormac. Mirror machines are plagued by instabilities (the DCLC, Lower Hybrid Drift modes, etc.) related to steep density gradients and the inherent loss-cone ion distribution functions. The fluctuating fields of the waves can cause anomalously high scattering of particles into the loss-cone. The sheath possesses both the steep gradients and loss-cone distribution functions that generate these modes, although the instabilities may be limited by finite β and shear effects.

It is found in Tokamaks and magnetic pinches that currents induced at the edge of the plasma drive streaming instabilities that allow anomalously fast current penetration. In Tormac, anomalous resistance could allow the sheath to broaden until the sheath width approaches the plasma radius. As pointed out earlier, Tormac scaling then approaches that of a mirror machine.

It is not clear that a steadily "eating in" sheath is a solution

of the time dependent equations, even in the presence of only classical collisions. For a steadily eating in sheath it is necessary to balance the magnetic diffusion of open field lines into the interior and the particle loss to the walls. If a balance is not achieved, then the sheath varies in time on a time scale shorter than τ_{Tormac}, i.e., the sheath might steepen on a time scale $\cong \tau_{ii}$ until it is so narrow that an instability sets in and generates anomalous transport.

Another complication is the existence of a poloidal field reversed (or neutral) layer near the sheath. From Fig. 1 it is apparent that the internal poloidal field and the cusp poloidal field must oppose at either the inner (small major radius) or outer (large major radius) edge of Tormac. The neutral layer must eat in (i.e., field lines must be reconnected) at the same rate as the sheath eats in.

It is the aim of this thesis to partially resolve some of these problems through a relatively simple and heuristic model of the Tormac sheath called the annihilation model (suggested by A. Boozer).[14] The model treats the sheath as a one-dimensional slab and uses fluid equations with "annihilation" terms. The annihilation terms represent the flow of matter, momentum and energy along the open field lines to the walls due to loss-cone scattering. The effects of classical collisions are included (pitch angle scattering, electron-ion drag, etc.) and anomalous effects can be accounted for in a rough way through multiplying the classical terms by phenomenological coefficients.

The starting point for deriving the model equations is the three-dimensional, infinite hierarchy of moment equations obtained from the

kinetic equation including collisions. The coupled set consisting of the infinite set of moment equations for ions and electrons and Maxwell's equations provides an exact description of the system.

To reduce the infinite set of partial differential equations to the finite set of one-dimensional annihilation equations requires a variety of approximations and assumptions.

The first, and least justifiable approximation is the expansion in gyro-radius/scale length used to truncate the moment equations. The typical Tormac scale lengths in directions other than the direction across the sheath are many gyro radii, validating the expansion for these directions. In the direction across the sheath, structure on the order of the gyro radius (or less) is found.

A rough estimate of the sheath scale length can be obtained from two of the dominant processes in the sheath. Magnetic field diffusion is responsible for the eating in of open field lines:

$$\frac{dB}{dt} \sim \frac{\eta}{4\pi} \frac{\partial^2 B}{\partial X^2} \Rightarrow \frac{dB^2}{dt} \sim \frac{\eta}{4\pi\Delta_s^2} \Delta B^2$$

(ΔB^2 = change in B^2 across the sheath)

$\frac{d}{dt}$ = convective derivative

Mirror losses of particles and energy can be described roughly by:

$$\frac{dnT}{dt} \sim - nT\nu_{Loss} \qquad \nu_{Loss} \cong \nu_{ii} \text{ for classical mirror confinement}$$

If the sheath is to eat in on slow, collisional time scales and the profiles are assumed to change even more slowly on a time scale $\sim \tau_{Tormac}$ (a steadily eating in sheath is established so $\partial/\partial t \cong 0$ in

the reference frame of the sheath), then pressure balance and the quasi-steady condition may be combined to yield:

$$\left(\frac{\partial}{\partial t} + \underline{u}\cdot\nabla\right)(nT + B^2/8\pi) \equiv \frac{d}{dt}(nT + B^2/8\pi) \cong 0 \rightarrow$$

$$nT\nu_{loss} \sim \frac{n}{4\pi\Delta_s^2}\left(\frac{\Delta B^2}{8\pi}\right)$$

Since $\Delta B^2/8\pi \cong nT$, again from pressure balance:

$$\nu_{loss} \sim \frac{n}{4\pi\Delta_s^2} \rightarrow \Delta_s \cong \sqrt{\frac{n}{4\pi\nu_{loss}}}$$

For classical resistivity and ν_{loss} = the ion-ion 90° scattering rate, the sheath scale length becomes

$$\Delta_s \cong \left(\frac{M_e}{M_i}\right)^{1/4}\left(\frac{T_i}{T_e}\right)^{3/4}\frac{\rho_i}{\sqrt{\beta}}$$

$$\cong \rho_i/7 \text{ for } \beta \cong 1,\ \frac{M_e}{M_i} = \frac{1}{3700},\ T_e = T_i$$

For a sheath to be this narrow, the ions must be electrostatically confined across the magnetic field rather than magnetically. The fluid equations obtained from the small gyro radius truncation are invalid in this limit, although it is expected that some of the results remain qualitatively valid. The errors introduced when $\rho_i/\Delta_s > 1$ are in the ion pressure tensor: $\underline{\underline{P}} \neq P_\perp \underline{\underline{I}}_\perp + P_\parallel \underline{\underline{I}}_\parallel$, and in the ion annihilation terms. The annihilation terms, representing mirror losses, are taken to be functions of local parameters only (density, temperature, etc.) which should be replaced by appropriate averages when Δ_s is the

same as the ion orbit size.

The scaling relation $\Delta_s \cong \sqrt{\eta/4\pi\nu_{loss}}$ may predict sheath widths greater than the gyro radius for a variety of circumstances. If the electrons are cool ($T_e/T_i \cong 1/10$) as in a classical mirror, then $\Delta_s \cong \rho_i$ because of the strong temperature dependence in the resistivity and scattering rate. The sheath may also be broadened by anomalous effects, i.e., turbulence due to instabilities.

The narrower the sheath, the larger the current density and the more prone it is to current and gradient driven instabilities (i.e., the Buneman instability or Lower Hybrid Drift). Experimental evidence indicates that sheaths narrower than $\sim\rho_i$ are unstable and therefore anomalously broaden until $\Delta_s \cong \rho_i$. This effect may be modeled in a simple fashion by altering the resistivity by a factor η_{anom}/η_{class}, which yields

$$\Delta_s \gtrsim \rho_i \quad \text{for } \beta \cong 1,\ T_e/T_i \cong 1,\ \frac{\eta_{anom}}{\eta_{class}} \gtrsim \sqrt{\frac{M_i}{M_e}}$$

Further approximations and assumptions are the following:

<u>Toroidal Symmetry</u>. It is assumed that deviations from toroidal symmetry have negligible effect on the system, allowing the reduction to a two-dimensional spatial problem.

<u>A narrow sheath</u>. If the sheath width is small compared to the other poloidal scale lengths ($\cong r_p$), then it is only necessary to consider a small, slab-like region near the sheath (see fig. 3). The slow variation along the sheath can be treated easily, yielding equations with only one significant spatial variable: the distance across

the sheath.

A steadily "eating in" sheath. If the sheath is assumed to eat in at a constant (or slowly varying) rate, then the time variation may be removed by changing to a reference frame where the sheath appears stationary. The existence of a steadily eating in sheath is not obvious; one of the goals of this theory is to discover the regions of parameter space for which solutions do or do not exist.

Krook collisions. The collision terms for the ions are modeled by simple Krook[15] type relaxation terms, except in the annihilation flow where the Fokker-Planck nature of the collisions is taken roughly into account. The sheath ions are far from thermal equilibrium which rules out the usual Chapman-Enskog expansion for the collisional transport. The ion collision terms are chosen so as to conserve matter, momentum and energy and to give results for the transport coefficients which reduce in the appropriate limit to those obtained rigorously in the near thermal equilibrium case. The electrons are assumed close to thermal equilibrium so the usual transport equations are used.[16]

Small Collisionality. Collisions are introduced in a perturbative manner, expanding about collisionless (Vlasov) equilibria. The expansion parameter is $\varepsilon \equiv r_p/\lambda$ where $\lambda = v_{thi}\tau_{loss}$, τ_{loss} = particle loss time. Typically $\tau_{loss} \sim 4\pi\Delta_s^2/\eta$ and $\tau_e < \tau_{loss} < \tau_{ii}$. When collisions are included, constraints on the collisionless quantities are found that remove some of the indeterminacy of the collisionless equations. This is analagous to the MHD theory of Tokamaks where the introduction of a small amount of particle diffusion selects a unique solution from the infinite set of Grad-Shafranov equilibria.[17]

Combining the various assumptions and approximations results in a coupled set of non-linear ordinary differential equations. The equations resemble the usual one-dimensional fluid equations except for the addition of annihilation terms representing mirror losses. Solutions are obtained numerically because of the complexity of the equations, yielding profiles for the density, pressure, magnetic field, flow velocity and electrostatic potential.

The significant results of the model may be summarized as follows:

1. The basic scaling $\Delta_s \sim \sqrt{\eta/4\pi\nu_{loss}}$ is verified in all solutions obtained.

2. The poloidal field reversed and non-poloidal field reversed sheaths yield qualitatively distinct solutions: the density and pressure on the field reversed side fall sharply to zero across the sheath whereas they fall off gradually on the non-reversed side.

The difference stems from the fact that the $\underline{E} \times \underline{B}/B^2$ velocity across the sheath changes sign for the field reversed sheath while remaining of one sign for the non-reversed sheath. In the reference frame where the sheath is stationary, an induced toroidal electric field causes $\underline{E} \times \underline{B}$ convection from the (effectively infinite) reservoir of uniform plasma into the sheath. $\underline{E}_{tor}$ is uniform since $\nabla \times \underline{E} = 0$ but $\underline{B}_{pol}$ changes sign across the field reversed sheath, causing $\underline{E}_{tor} \times \underline{B}_{pol}$ to change sign. On the low density side of the sheath, particles are then convected <u>toward</u> the sheath. In the time independent state the particles on the low density side have been either swept into the sheath or annihilated, so the density drops sharply to zero rather than tailing off.

The $\underline{E}\times\underline{B}$ velocity never changes sign for the non-reversed sheath ($\underline{B}_{pol} > 0$) so that particles are convected from the sheath into the low density region and slowly annihilated as they move. The non-reversed profiles are therefore more gradual.

3. The solution obtained for the non-reversed sheath are similar in some respects to theoretical predictions of mirror parameters:[13]

$$\frac{e\phi}{T_e}\Big|_{sheath} \sim 5 \qquad T_e/T_i\Big|_{sheath} \sim 1/10$$

The electrons rapidly cool once they are convected onto open field lines because of the large heat flow to the walls: electrons that scatter over the confining electrostatic barrier carry energy $e\phi + T_e$ to the walls. The high potential barrier reduces the electron loss rate to the order of the ion loss rate (any solution must have roughly comparable ion and electron loss rates to satisfy quasineutrality)

$$\nu_e e^{-e\phi/T_e} \sim \nu_i$$

Consistent with the relatively cool electrons and low loss rates, the sheath width and eating in velocity are given by:

$$\Delta_s \cong 2\rho_i \qquad u \cong \rho_i\nu_i \qquad (\sim \Delta_s\nu_{loss})$$

4. The solutions for the field reversed case differ from the non-reversed case not only in the way described in (2) but also in that two drastically different types of solution exist.

One of the solutions is similar to the non-reversed solution discussed in (3): $T_e/T_i\big|_{sheath} < 1$, $e\phi/T_e\big|_{sheath} > 1$, $\Delta_{sheath} \sim \rho_i$, $u \sim \rho_i\nu_i$. The important physical processes are the same as described in (3).

The second type of solution has the features: $e\phi/T_e \sim 1$, $T_e/T_i|_{sheath} \gtrsim 1$.

The classical sheath width becomes 0.1 ρ_i. If anomalous resistance is added until $\Delta_s \cong \rho_i$, the resulting eating in rate is

$$u_x \cong 30\rho_i\nu_i$$

An eating in rate of this magnitude demolishes the usual Tormac scaling, reducing the confinement time to on the order of the mirror time, τ_{ii}.

The second solution arises because of an effect not usually important for classical mirror machines: significant ohmic heating of the electrons occurs due to the large current densities associated with the rapid change of the magnetic field across the sheath. The ohmic heating may be greater than the mirror losses of electron energy, resulting in $T_e/T_i \sim 1$.

The electrons may not be electrostatically confined ($e\phi/T_e \gg 1$) in the limit $T_e/T_i \sim 1$ because $e\phi/T_i$ would also be large implying no confinement of ions. For this solution, the electron and ion loss rates are made comparable by adjusting the potential so that:

$$\frac{e\phi}{T_e} \sim \frac{e\phi}{T_i} \sim 1$$

The electron loss rate is not reduced much below ν_e, the electron 90° scattering rate. The ion losses are enhanced by the potential until:

$$\nu_{eff_i}(\phi) \sim \nu_e \qquad \nu_{eff_i}(\phi) = \text{the effective ion collision rate}$$

$$\cong \frac{\nu_i}{\left(1 - \frac{e\phi}{(R-1)T_{\perp i}}\right)^2} \quad \text{(see Chapter III)}$$

The increased ion loss rate when $e\phi/(R - 1)T_{\perp i}$ is significant is related to the small angle nature of Coulomb collisions. It is analagous to the effective collision rate encountered in Tokamak theory[17] where velocity space scattering through a small angle allows detrapping of particles. The velocity space structure of the distribution function becomes narrow, so that scattering through an angle $\ll 90°$ (or an energy $\ll T_{\perp i}$) moves particles into the loss regions.

Because of the large ion loss rates, however, the second type of solution becomes sensitive to the detailed structure of the ion loss term. The solution disappears when the singular behavior is replaced by a more gradual dependence on $e\phi/(R - 1)T_{\perp i}$.

In the ensuing chapters, the derivation and solutions of the annihilation [illegible]l equations are provided in detail. While many elements of the model are heuristic, it is expected that most of the important physical effects are included and that the annihilation model provides at least qualitative insights into the Tormac sheath.

CHAPTER I

In this chapter, the present theoretical understanding of the sheath is reviewed. Theoretical investigations of the sheath have fallen into five categories; the study of particle motion in cusped magnetic fields; self-consistent Vlasov equilibrium theories; high frequency, short wavelength stability theories; magnetohydrodynamic or fluid models that include transport effects; and most recently, time dependent, hybrid fluid-particle simulations. The various approaches are complementary, sacrificing some elements of realism (e.g., self consistency in the particle orbit theory) to give a tractable problem and different insights into the sheath.

1. Particle motion in Tormac was first studied by Levine and co-workers in 1972.[3] The fundamental result they obtained was that conservation of toroidal canonical momentum, P_ϕ, in a toroidally symmetric system causes some particles to be trapped even when their motion is non-adiabatic. Their model assumed a sharp transition of the magnetic field at the vacuum-plasma interface.

When guiding center drifts carry particles across the transition layer of a non-symmetric cusp, adiabatic invariance of the magnetic moment is assumed to be violated. The lack of adiabatic invariance leads to random motion and particle loss in a characteristic time:

$\tau_{transit} \times r_{hole}/r_p$

r_{hole} ($\cong \rho_i$) $\equiv$ the effective "hole" size for the cusp.

For a symmetric cusp, they showed that non-adiabaticity does not imply randomness because of P_ϕ conservation, and some particles remain

trapped in the magnetic well. The trapped particles are lost due to relatively slow effects such as collisions and low level turbulence so that Levine et. al. estimated the confinement time of a symmetric cusp to be:

$$\tau_{cusp} \cong \tau_{ii}$$

If a "stuffing" field in the azimuthal direction is added, isolating the interior from the sheath, they predicted:

$$\tau_{Tormac} \cong \tau_{ii}\ r_p/\Delta_s$$

In 1973 Boozer and Levine[18] extended the previous work by numerically integrating particle orbits for a stuffed line cusp. The transition between the interior and exterior was taken to be of a thickness on the order of an ion orbit size. They arrived at the following conclusions: 1) Particles are indeed trapped. They conjectured that a generalized adiabatic invariant $I = \oint P_\perp dx_\perp$ exists even for a narrow sheath, improving confinement over the non-adiabatic case. 2) The particles move in banana shaped orbits analagous to those found in Tokamaks although much narrower.

$$\Delta_{banana} \cong \rho_{i\ poloidal} = \frac{m_i v_{th}}{eB_{pol}} > \rho_{i\ total} \text{ for Tokamaks}$$
$$\cong \rho_{i\ total} \text{ for Tormac}$$

3) The qualitative nature of the orbits is independent of the sharpness of the $\underline{B}$ profile. 4) The fraction of velocity space in the loss region is a function of the mirror ratio and the stuffing magnetic field. For mirror ratios $R \gtrsim 1.5$, the dependence on the stuffing field was found to be weak.

Additional analytic work on particle orbits in the sheath has been done by H. Mynick.[19] He has established a generalized Hamiltonian guiding center theory, valid even for narrow sheaths $\Delta_s < \rho_i$. This work provides a derivation of the previous conjecture of Boozer and Levine: the generalized adiabatic invariant, I, follows naturally from the theory as a canonical action variable.

2. The Vlasov theory of the sheath is of interest because, for fusion reactor parameters, the sheath is only weakly collisional ($\nu_{ii} \ll \Omega_i$, v_i/r_p). The bulk of the work done to date has been for the slab case, valid when the sheath width is much smaller than the minor cross section and the radius of curvature of the field lines. The slab approximation neglects the finite excursions of drift orbits, away from flux surfaces which is not so serious for Tormac since:

$$\Delta_{drift} = \Delta_{banana} \cong \rho_i$$

The earliest work on the self-consistent Vlasov sheath was done by Grad in 1961[20] for a boundary layer between unmagnetized plasma and a vacuum magnetic field. Grad solved for the "narrowest" sheath assuming $\underline{E} = 0$, $\underline{B}$ unidirectional, and $m_i = m_e$. The numerically calculated sheath profile has a scale length $\sim 5\rho_i$.

In 1976, P. Channell[21] developed an analytic method for finding classes of sheared sheath equilibria, again for the case in which there is no electric field. Channell assumed a distribution function of the form:

$$f(H, P_y, P_z) = e^{-\beta H} g(P_y, P_z)$$

$$H = \frac{P_x^2}{2m} + \frac{(P_y - eAy(x))^2}{2m} + \frac{(P_z - eAz(x))^2}{2m}$$

$\underline{A} = Ay(x)\hat{y} + Az(x)\hat{z}$ = the vector potential
y,z are coordinates lying in the plane of the sheath
x is the coordinate across the sheath

A Hamiltonian framework was developed in which $Ay, Az, P_{Ay} \equiv \partial Ay/\partial x$, $P_{Az} \equiv \partial Az/\partial x$ are treated as canonical variables ($t \rightarrow x$ in Hamilton's equations). The Hamiltonian that determines the variation of $Ay(x)$, $Az(x)$ is given by:

$$H = \frac{P_{Ay}^2}{2} + \frac{P_{Ay}^2}{2} + V(Ay, Az)$$

The potential V is defined as:

$$V(Ay, Az) \equiv \sum_s n_s(Ay, Az) T_s = \sum_s T_s \int d^3\underline{p} e^{-\beta H(\underline{p}, Ay, Az)} g(Py, Pz)$$

This form exploits the fact that the particle Hamiltonian, H, is a function of position through the vector potential only. Hamilton's equations for the fields become:

$$\frac{\partial H}{\partial Ay} = -P_{Ay} = \frac{\partial P_{Ay}}{\partial x} = -\frac{\partial^2 Ay}{\partial x^2}$$

$$\frac{\partial H}{\partial Az} = -P_{Az} = -\frac{\partial P_{Az}}{\partial x} = -\frac{\partial^2 Az}{\partial x^2}$$

These are statements of pressure balance and Ampere's law.

The method of solution is to choose a physically reasonable $V(Ay, Az)$ (typically one for which it's possible to solve Hamilton's equations) then invert the equation relating V and $g_s(Py, Pz)$ to obtain $g_s(Py, Pz)$ explicitly. Channell analytically obtained several sheath-like equilibria for both sheared and unsheared cases. The

characteristic scale was shown to be $\Delta_s \cong \rho_i$, narrower than Grad's "narrowest" sheath since the plasma is magnetized and $M_e \neq M_i$.

Channell's method has recently been generalized by Mynick, Sharp and Kaufman[22] to allow for arbitrary $f(H,P_y,P_z)$ and non-zero electric field. In the generalized version:

$$V_{Channell}(Ay,Az) \rightarrow V(Ay,Az,\phi) \equiv \sum_s P_{xx_s}(Ay,Az,\phi)$$

$$= \sum_s \int d^3\underline{p}\, \frac{p_x^2}{2m} f_s(H(\underline{P},Ay,Az,\phi),Py,Pz)$$

Choosing loss-cone distribution functions to model mirroring effects, Mynick et.al. integrated the field Hamiltonian equations numerically to obtain sheath solutions. The electric field was set equal to zero for the numerical work so that the sheath widths obtained are on the order of ρ_i.

3. The <u>stability</u> of the sheath has been studied by Davidson, Gladd and others.[23,24] The regime studied encompasses high frequency, $\omega \sim \sqrt{\Omega_e \Omega_i}$, short wavelength, $1/\rho_i^2 < k_\perp^2 \lesssim 1/\rho_e^2$, instabilities. In this class are the Lower-Hybrid-Drift, Drift-Cyclotron-Loss-Cone, and Convective-Loss-Cone modes. The goal of the research has been to extend the analysis of these modes to the steep gradients, strong magnetic shear and high β regime of the Tormac sheath.

WKB methods are applied since the mode structure ($k_\perp \lesssim 1/\rho_e$) is much smaller than the sheath width. The dispersion relations obtained show that finite β and magnetic shear effects tend to stabilize these modes.

The Lower-Hybrid-Drift mode, which is thought to cause anomalous resistivity in theta pinch devices, is completely stabilized for

$T_e \cong T_i$, $\rho_i/L_N = 1$, as long as $\beta \gtrsim 3/4$ (this ignores the stabilizing influence of shear). If the effects of shear are considered and finite β effects are ignored, Gladd et.al. find complete stabilization in a sheared field if $L_N/Ls \gtrsim 0.5$ for $0 < \rho_i/L_N < 5$. (L_N,s is the density, shear scale length).

The finite β and magnetic shear stabilization criteria are relatively easy to meet for Tormac since typically $\beta \cong 1$ and $L_N/Ls \cong 1$. In the outer sheath the local β becomes less than 3/4 and perhaps $L_N/Ls < 0.5$, but the density gradient and flow velocity which drive the instability may also be small so that one might expect the instability to be severely curtailed.

The Drift-Cyclotron-Loss-Cone mode (DCLC) is driven by the density gradient and the loss-cone distribution of the ions, and is thought to be a source of anomalously high particle scattering in mirror machines. Gladd, et.al. show that magnetic shear reduces the growth rate but does not completely stabilize the mode. To completely stabilize the DCLC mode, it may be necessary to introduce a stream of low temperature plasma as is done in mirror machines. The effect of finite β is not yet known for the strong gradient case, although it has been shown to be stabilizing in the weak gradient case.

The Convective-Loss-Cone mode is generally found to be less important than the DCLC mode for Tormac parameters.

The lower frequency, $\omega < \Omega_i$, and longer wavelength, $k_\perp \sim \rho_i^{-1}$, regimes have not been studied in depth due to their greater complexity. In these limits, the detailed characteristics of the ion orbits are

needed, as well as the equilibrium profiles since the mode structure is of the same order as the sheath width. A stability formalism has been developed by H. Mynick[19] to treat non-local corrections to the WKB analysis as well as allowing for complex ion orbits, although explicit applications to the Tormac sheath have yet to be made.

4. Another class of sheath theories are the MHD or fluid theories (the model developed in this thesis is included in this class). In these theories, explicit account has been taken of collisional processes such as scattering into the loss cone and electron-ion drag.

In 1976, A. Boozer[25] constructed a flow-out model of the Tokamak divertor, a system similar to the Tormac sheath. Particles in a divertor are lost by streaming to the walls as opposed to the mirroring that occurs in Tormac. A crucial result of his analysis is that the losses are non-ambipolar, i.e., the electron and ion loss rates are not equal on a given field line. The unequal local loss rates can result in strong electric fields across the divertor. The electric fields are not so strong as to violate quasi neutrality so, assuming equal sources of ions and electrons, the integrated (total) losses of each species must be equal. In Boozer's model $T_i \cong 0$ and $T_e \neq 0$ are assumed and the perpindicular scale length is roughly $\rho_i(T_e)$ (the ion gyro-radius calculated at the electron temperature).

Recently M. Mostrom[26] has constructed an annihilation model of the Tormac sheath similar to the one considered in this thesis. The basic approach for both models is to use one-dimensional fluid equations with "annihilation" terms to account for mirror losses (suggested by

A. Boozer). The annihilation terms are necessarily drastic simplifications of the true Fokker-Plank losses. The terms chosen by Mostrom and myself differ in some respects.

In the present model the equations are derived from two-dimensional fluid equations, which yield various relationships between the annihilation fluxes of matter, momentum and energy. These are exploited to remove some of the arbitrariness in Mostrom's model. In addition, the present model allows for the dependence of ion annihilation on the electrostatic potential and includes the effect of cold electrons recycling from the walls.

In both models, the fluid equations are truncated via an expansion in ρ_i/Δ_s. Mostrom assumes a scalar pressure and uses the near thermal equilibrium transport equations derived by Braginskii. In the present version the ion pressure is allowed to be anisotropic to model mirror effects and the transport equations are generalized, although in a somewhat ad hoc fashion.

The model treated in this thesis includes effects of ion poloidal flows which are excluded from Mostrom's model. The ion poloidal flow velocity is found to be a function of the pressure anisotropy, so that it is consistent to set $u_{pol} = 0$ for the scalar pressure case but it is necessary to allow $u_{pol} \neq 0$ in the anisotropic model.

Mostrom treats the case $\underline{B}_{pol} \to 0$ in the interior whereas the present version examines equilibria with arbitrary values of B_{pol} in the interior.

Finally, explicit numerical solutions are obtained in this thesis

as opposed to the asymptotic and order of magnitude results obtained by Mostrom. He found sheath equilibria with two scale lengths: the electron gyro radius and the ion gyro radius. On the first open field lines encountered as plasma moves out from the central region, a substantial fraction of the electrons are lost at a rate ν_{ee}, yielding a scale length $\sqrt{\eta/4\pi\nu_{loss}}$ (see the introduction):

$\sqrt{\eta/4\pi\nu_{ee}} \cong \rho_e$ the electron gryo radius

The electrostatic potential rises rapidly, across the sheath cooling the electrons and reducing the electron loss rate by the factor $e^{-e\phi/T_e}$ until $\nu_{loss_e} \sim \nu_{ii}$. The resistivity at the low electron temperature is large and the scale length $\sqrt{\eta/4\pi\nu_{loss}}$ is of the order of the ion gyro radius.

The model presented in this thesis yields two different types of solution as discussed in the introduction. One of the solutions is similar to Mostrom's except that the plasma floats at a high enough value of the electrostatic potential that the electron loss rate is always considerably less than ν_{ee} and the short scale length is greater than the electron gyro radius. The second solution is quite different because of the possibility of enhancing ion losses at large values of the electrostatic potential. The electrons remain hot for the second solution, $T_e \sim T_i$, and the ion loss rate is increased until:

$\nu_{i_{loss}} \sim \nu_e$

As in Mostrom's model the characteristic scale becomes ρ_e, although the sheath is assumed to anomalously broaden until $\Delta_s \cong \rho_i$.

5. The fifth theoretical approach mentioned at the beginning of the chapter is the construction of a hybrid fluid-particle computer code to model the time dependent state. Investigations into the formation and structure of the sheath with such a code are being carried out currently by M. Vella.[27] The model treats electrons as a resistive fluid and numerically integrates ion orbits to self-consistently determine currents, magnetic and electric fields.

Some results have been obtained concerning the start up of Tormac, showing the initial oscillations and compression as the magnetic field rises. Numerical instabilities have, to date, precluded studies of the approach to dynamic equilibrium and the formation of a narrow sheath.

CHAPTER II

In this chapter, the basic framework of the annihilation model is derived starting from a kinetic description. The model is completed in Chapter III with the choice of explicit annihilation fluxes.

The dynamic Tormac is adequately described by the coupled set of integro-differential equations consisting of the kinetic equation including collisions and Maxwell's equations:

II.1 $$\frac{\partial f_s}{\partial t} + \underline{v}_s \nabla f_s + e_s(\underline{E} + \underline{v}_s x \underline{B})\cdot\nabla_{\underline{v}} f = Cs(f)$$

II.2 $$\nabla x \underline{B} = 4\pi \underline{J} = 4\pi \sum_s e_s \int d^3\underline{v} f_s \underline{v}$$

II.3 $$\nabla\cdot\underline{E} = 4\pi\rho_c = 4\pi\sum_s e_s \int d^3\underline{v} f_s$$

II.4 $$\nabla X \underline{E} = -\,\partial\underline{B}/\partial t$$

II.5 $$\nabla\cdot\underline{B} = 0$$

where $f_s(\underline{x},\underline{v},t)$ is the particle distribution function, normalized such that $n_s(\underline{x},t) = \int d^3\underline{v} f_s$, and $C_s(f)$ is the collision term, i.e., Fokker-Planck or Lenard-Balescu, etc.

Equation II.1 can be replaced by an infinite hierarchy of moment equations dependent only on $\underline{x}$,t rather than $\underline{x}$,$\underline{v}$,t. The moment equations are generated by operating on II.1 with

$\int d^3\underline{v}\ \underline{v}^n\ \{\ \};\ n = 0, 1, 2 \ldots\ldots \infty$

The first four equations generated are

II.6 $$\frac{\partial n}{\partial t} + \nabla\cdot n\underline{u} = 0$$

II.7 $$nm\frac{d\underline{u}}{dt} + \nabla\cdot\underline{\underline{P}} - en(\underline{E} + \underline{u}x\underline{B}) = \underline{C}_1$$

II.8 $$\frac{d\underline{\underline{P}}}{dt} + \underline{\underline{P}}\nabla\cdot\underline{u} + \nabla\cdot\underline{\underline{Q}} + [\underline{\underline{P}}\cdot\nabla\underline{u}]^s = \Omega[\underline{\underline{P}}x\hat{b}]^s + \underline{\underline{C}}_2$$

$$\text{II.9} \quad \frac{d\underline{\underline{Q}}}{dt} + \underline{\underline{Q}}\,\nabla\cdot\underline{u} + \nabla\cdot\underline{\underline{R}} + [\underline{\underline{Q}}\cdot\nabla\underline{u}]^s - \frac{1}{nm}[\underline{\underline{P}}\,\nabla\cdot\underline{\underline{P}}]^s = \Omega[\underline{\underline{Q}}\times\hat{b}] + \underline{\underline{C}}_3$$

Species labels have been supressed. The definitions are the standard ones:

$$n \equiv \int d^3\underline{v}f \qquad \underline{u} \equiv \int d^3\underline{v}f\underline{v}/n \qquad \underline{\underline{P}} \equiv m\int d^3\underline{v}f(\underline{v}-\underline{u})(\underline{v}-\underline{u})$$

$$\underline{\underline{Q}} \equiv m\int d^3\underline{v}\,(\underline{v}-\underline{u})(\underline{v}-\underline{u})(\underline{v}-\underline{u})f$$

$$\underline{\underline{R}} \equiv m\int d^3\underline{v}\,(\underline{v}-\underline{u})(\underline{v}-\underline{u})(\underline{v}-\underline{u})(\underline{v}-\underline{u})f$$

$$\frac{d}{dt} \equiv \frac{\partial}{\partial t} + \underline{u}\cdot\nabla \qquad \Omega \equiv \frac{e|B|}{m}$$

The bracket $[\ ]^s$ means the summation over all cyclic permutations of the tensor indices, i.e.,

$$([\underline{\underline{Q}}\cdot\nabla\underline{u}]^s)_{ijk} = Q_{ijn}\frac{\partial}{\partial x_n}u_k + Q_{kin}\frac{\partial}{\partial x_n}u_j + Q_{jkn}\frac{\partial}{\partial x_n}u_i$$

The collision terms are defined as

$$\underline{\underline{C}}_n = \int d^3\underline{v}\,(\underline{v}-\underline{u})^n C(f)$$

The $\underline{\underline{C}}_n$ obey the well known conservation laws for collisions:[16]

$$\text{II.10} \quad \begin{cases} C_0 = 0 & \text{conservation of particles} \\ \sum_s \underline{C}_{1s} = 0 & \text{conservation of momentum} \\ \sum_s\left(\frac{\mathrm{Tr}\underline{\underline{C}}_{2s}}{2} + \underline{C}_{1s}\cdot\underline{u}_s\right) = 0 & \text{conservation of energy} \end{cases}$$

where the summation is over species (labeled by s).

To obtain a useful set of equations the hierarchy must be truncated, explicit collision terms must be found, and appropriate boundary/initial conditions formulated.

The truncation to a finite set of equations is accomplished via an expansion in ion gyro radius/scale length. As mentioned in the introduction, sheath scale lengths can be $\gtrsim \rho_i$ which would invalidate

the expansion although some results would be expected to remain qualitatively correct. In those cases where the classical scale length is smaller than ρ_i, anomalous resistance will be added until $\Delta_s \gtrsim \rho_i$ on the (experimentally verified) basis that sheaths with $\Delta_s < \rho_i$ are unstable and turbulently broaden until $\Delta_s \cong \rho_i$.[7,8]

The small gyro radius expansion of the moment equations has been carried out by A. McMahon[28] for the case $\underline{\underline{C}}_n = 0$. A simple extension of the lowest order equations with $\underline{\underline{C}}n \neq 0$ results in the following set:

$$\text{II.11} \quad \frac{\partial n}{\partial t} + \nabla\cdot n\underline{u} = 0$$

$$\text{II.12} \quad nm\frac{d\underline{u}}{dt} + \nabla\cdot\underline{\underline{P}} - en(\underline{E} + \underline{u}\times\underline{B}) = \underline{C}_1$$

$$\text{II.13} \quad \begin{cases} \dfrac{dP_\perp}{dt} + P_\perp(\nabla\cdot\underline{u} + \underline{\underline{I}}_\perp : \nabla\underline{u}) = -B\nabla\cdot\dfrac{q_\parallel^\perp b}{B} + \dfrac{\underline{\underline{C}}_2 : \underline{\underline{I}}_\perp}{2} \\ \dfrac{1}{2}\dfrac{dP_\parallel}{dt} + P_\parallel(3/2\nabla\cdot\underline{u} - \underline{\underline{I}}_\perp : \nabla\underline{u}) = -\nabla\cdot(q_\parallel^\parallel b) - q_\parallel^\perp\dfrac{\hat{b}\cdot\nabla B}{B} + \dfrac{\underline{\underline{C}}_\parallel : \hat{b}\hat{b}}{2} \\ \underline{\underline{P}} = P_\perp\underline{\underline{I}}_\perp + P_\parallel\hat{b}\hat{b} \quad , \quad \underline{\underline{I}}_\perp = \underline{\underline{I}} - \hat{b}\hat{b} \end{cases}$$

The only non-zero components of the zeroth order heat flux are $q_\parallel^\perp$, $q_\parallel^\parallel$ representing the flows of perpendicular and parallel energy along the magnetic field. The indeterminacy of $q_\parallel^\perp$, $q_\parallel^\parallel$ is similar to the situation in the collisionless case: there is a large degree of arbitrariness in the lowest order distribution function $f(v_\perp, v_\parallel, x, t)$.

In the usual transport theories,[16,17] the lowest order distribution function is Maxwellian, i.e., the system is close to thermal equilibrium so that $q_\parallel^\parallel$, $q_\parallel^\perp$ are determined:

$$\text{II.14} \quad q_\parallel^\parallel = q_\parallel^\perp = 0$$

In the Tormac sheath ions are mirror contained; the distribution

function possesses a loss-cone and is far from equilibrium so that II.14 is inapplicable. In Chapter III, plausible heat fluxes $q_{\parallel}^{\parallel}$, $q_{\parallel}^{\perp}$ are determined in conjunction with the outgoing flux of particles collisionally scattered into the loss-cone.

The next ingredients needed are explicit collision terms $\underline{\underline{C}}n$. In the theory of collisional transport for plasmas near thermal equilibrium, the collisional fluxes may be derived by Chapman-Enskog methods which utilize an expansion of the distribution function about a Maxwellian.[16] As mentioned, the ions in the sheath are far from thermal equilibrium so that the expansion about a Maxwellian is invalid. On the other hand, the electrons in the sheath are at least partially electrostatically confined and the relaxation time of the distribution function, τ_e, is (usually) less than the sheath time scale so that the distribution function is fairly close to Maxwellian. The Chapman-Enskog transport coefficients are therefore used for the electrons, with the exception of the parallel heat flow which is discussed in Chapter III.

The electron collision terms are

II.15

a) $C_{oe} = 0$

b) $\underline{C}_{1e} = \underbrace{en\,\underline{\underline{\eta}}\cdot\underline{J}}_{\text{resistive drag}} - \underbrace{.71n\nabla_{\parallel}T_e}_{\text{thermal force}}$

c) $\frac{1}{3}\mathrm{Tr}(\underline{\underline{C}}_{2e}) = -2\,\frac{m_e}{m_i}\,\nu_e(P_e - (2/3P_{\perp} + P_{\parallel}/3))$

$+ 2/3\,\underline{\underline{\eta}}:\underline{J}\underline{J} - 2/3\cdot\frac{71}{e}\,\underline{J}\cdot\nabla_{\parallel}T_e$

= electron-ion energy transfer + ohmic heating + work done by thermal force

The conservation laws for collisions determine two of the ion collision terms:

$$\text{II.16} \begin{cases} \text{a)} & C_{oi} = 0 \\ \text{b)} & C_{1i} = -\underline{C}_{1e} \end{cases}$$

To determine the remaining term, $\underline{\underline{C}}_{2i}$, the simple model of collisions developed by Bhatnagar, Gross and Krook[15] is used:

$$\text{II.17} \qquad C(f) = -\sum_s \nu_s(v)(f_s - f_{m_s})$$

s = species label; ν_s = relaxation rate; f_m = local maxwellian

This yields:

$$\text{II.16c} \qquad \underline{\underline{C}}_{2i} = -\nu_{Pi}\left(\underline{\underline{P}}_i - \frac{Tr(\underline{\underline{P}}_i)}{3}\right) - \nu_{Pe}(\underline{\underline{P}}_i - P_e\underline{\underline{I}})$$

ν_{Pi}, ν_{Pe} = appropriate averages of $\nu_s(\underline{v})$

The first term in $\underline{\underline{C}}_{2i}$ can be used in the near thermal equilibrium limit to derive viscous stress terms very similar to the viscous stress found in Chapman-Enskog theory if the identification

$$\text{II.18} \qquad \nu_{Pi} \cong \nu_i, \text{ the } 90° \text{ scattering rate for ion-ion collisions}$$

is made. The second term in $\underline{\underline{C}}_{2i}$ reduces exactly to the electron-ion relaxation rate found in Chapman-Enskog theory if

$$\text{II.19} \qquad \nu_{Pe} = 2\frac{m_e}{M_i}\nu_e \; ; \quad \nu_e = 90° \text{ scattering rate for electrons}$$

With explicit choices for the quantities $q_\parallel^\parallel$, $q_\parallel^\perp$, the set of equations consisting of II.11, 12, 13 for both ions and electrons, the

explicit collision terms II.15, 16 and Maxwell's equations form a complete set, i.e., as many equations as unknowns exist. The relevant Maxwell's equations are II.2, 4, 5. The fourth Maxwell equation, $\nabla\cdot\underline{E} = 4\pi\rho_c = 4\pi\sum_s e_s n_s$, is replaced by the quasi-neutral approximation, $n_e = n_i$.

The equations form a set of partial differential equations for the quantities:

n, $\underline{u}_i$, $\underline{u}_e$, $P_{\perp i}$, $P_{\parallel i}$, P_e ($P_{\perp e} \cong P_{\parallel e}$ is assumed), $\underline{E}$, $\underline{B}$.

To form a mathematically well posed problem, initial values must be chosen for all quantities operated on by $\partial/\partial t$. In addition, appropriate spatial boundary conditions must be chosen, i.e., $\underline{E}\times\hat{n}_{wall} = 0$ near conducting walls, etc.

In general, finding appropriate boundary conditions is a difficult problem. For partial differential equations the choice of boundary conditions is governed by the characteristics of the equations. The characteristic curves, or more generally, characteristic surfaces for a system of partial differential equations:

II.20 $$L_j(\underline{u}) = a^{ij,\nu}(\underline{x},\underline{u})\,\frac{\partial u^i}{\partial x_\nu} + b^j(\underline{x},\underline{u}) = 0$$

u^i = dependent variables $i = 1,k$

x_ν = independent variables $\nu = 1,n$

are determined by the equation

II.21 $$\phi(\underline{x}) = 0$$

where ϕ is a solution to

$$\text{II.22} \qquad \det\left(a^{ij,\nu}\frac{\partial\phi}{\partial x_\nu}\right) = 0$$

The characteristics represent curves along which information propagates in the space $(x_1, \ldots x_n)$. If k real characteristics exist, the equations are called hyperbolic; if no real characteristics exist, the equations are called elliptic. General theory[29] indicates that appropriate boundary conditions may be found for either elliptic or hyperbolic equations, guaranteeing existence and uniqueness of solutions in many cases (as in the Dirichlet and Von Neumann boundary value problems found in electromagnetics).

The equations of interest, II.2, 4, 5, 11, 12, 13, are of mixed type: both real and complex characteristics exist (at least for the case $\partial/\partial t = 0$; which is the situation considered in ensuing sections). There is little general mathematical theory of mixed type equations as far as choosing appropriate boundary conditions and determining the existence and uniqueness of solutions, so each case must be considered separately.

The choice of boundary conditions will be postponed until further reduction of the equations has been performed. In particular, the reduction to a slab model and the elimination of the time dependence will lead to a natural choice of boundary conditions.

In this section additional approximations are employed to simplify the set of equations describing the sheath. The first is the slab

approximation $\Delta s/r_p \ll 1$, which is reasonable since $\Delta s/r_p \cong 1/100$ for fusion reactor parameters. The second is weak collisionality, or $r_p/\lambda \equiv r_p/v_{th_i}\tau_{coll} \ll 1$, ($\tau_{coll} = \min\{\tau_e, \tau_i, 4\pi\Delta_s^2/\eta\}$) which is valid since $r_p/\lambda \gtrsim 10^{-4}$ for fusion reactor parameters. Finally, a steadily "eating-in" sheath will be assumed, which allows a transformation to a reference frame where the sheath is stationary ($\partial/\partial t \to 0$). This assumption will be validated after the fact by explicitly demonstrating that stationary solutions exist.

$\Delta s/r_p \ll 1$ is assumed so that in the neighborhood of the sheath ($|\underline{x}-\underline{x}_0| \sim \Delta s$; $\underline{x}_0$ = a point in the sheath) the field line curvature is negligible and the only gradients of significance are those across the sheath. The system may then be represented by a one dimensional slab (see Fig. 2) to lowest order in $\delta \equiv \Delta s/r_p$.

A locally Euclidian set of coordinates may be introduced:

x = distance across the sheath

y = distance in the poloidal direction

z = distance in the toroidal direction

All quantities are independent of z, the toroidal (symmetry) direction.

Consider first the collisionless case, by which it is meant that the characteristic time scale under consideration satisfies:

II.23 $\quad t \ll \tau_{coll} = \min\{\tau_i, \tau_e, \tau_{res} = 4\pi\Delta_s^2/\eta\}$

If the characteristic time scale also satisfies

II.24 $\quad t \gg t_{tr} \equiv r_p/v_{ti}$,

then a collisionless equilibrium state may be found, i.e.,

$\frac{\partial f}{\partial t} < \underline{v}\cdot\nabla f$ in the Vlasov eqn.

$$\rightarrow \frac{1}{t} < \frac{v_{ti}}{r_p}$$

The collisionless quantities are functions of x only:

$$\text{II.25} \quad \begin{cases} n(x),\ \underline{u}(x) = u_y(x)\hat{y} + u_z(x)\hat{z} \\ P_\perp(x),\ P_\parallel(x),\ P_e(c) \\ \underline{B}(x) = B_y(x)\hat{y} + B_z(x)\hat{z} \\ \underline{E} = -\ \partial\phi_0(x)/\partial x\ \hat{x} \end{cases}$$

The electric field is taken to be in the x direction, $\underline{E} = E_x\hat{x}$, only. From II.4

$$\text{II.26} \qquad \underline{E} = -\nabla\phi = -\ \partial\phi_0/\partial x\ \hat{x}$$

For the collisionless case, the flow velocity in the x direction, u_x, is assumed to vanish.

When collisional effects are included, two changes occur: a slow time variation on the scale τ_{coll} is introduced; and a weak y (poloidal coordinate) dependence appears due to the loss of particles along open field lines. Geometrical effects also introduce a weak y dependence, as discussed below.

When particles on open field lines scatter across the loss boundary in velocity space, they exit moving approximately parallel to a flux surface. The particles scattered at each point along the flux surface accumulate as they stream to the walls, producing a flow pattern as depicted in Fig. 4. The resulting flow velocity has the property

$$\text{II.27} \qquad \frac{\partial u_{pol}}{\partial r_{pol}} \neq 0 \quad \left(\frac{\partial u_y}{\partial y} \neq 0\right)$$

If ε is defined as the collisionality parameter

$$\text{II.28} \qquad \varepsilon \equiv \frac{r_p}{v_{ti}\tau_{coll}}, \quad \tau_{coll} = \min\{\tau_e, \tau_i, 4\pi\Delta_s{}^2/\eta\},$$

then the collisionless equilibrium quantities are altered in the following fashion

$$\text{II.29} \quad \begin{cases} n(x,\varepsilon t,\varepsilon y) \qquad \underline{u} = \varepsilon u_x(x,\varepsilon t,\varepsilon y)\hat{x} \\ \qquad\qquad\qquad\qquad + u_y(x,\varepsilon t,\varepsilon y)\hat{y} \\ \qquad\qquad\qquad\qquad + u_z(x,\varepsilon t,\varepsilon y)\hat{z} \\ P_\perp(x,\varepsilon t,\varepsilon y),\ P_\parallel(x,\varepsilon t,\varepsilon y),\ P_e(x,\varepsilon t,\varepsilon y) \\ \underline{B} = \varepsilon B_x(x,\varepsilon y,\varepsilon t)\hat{x} + B_y(x,\varepsilon t,\varepsilon y)\hat{y} \\ \qquad\qquad\qquad\qquad + B_z(x,\varepsilon t,\varepsilon y)\hat{z} \\ \underline{E} = -\dfrac{\partial\phi_0}{\partial x}(x,\varepsilon y,\varepsilon t)\hat{x} - \varepsilon\dfrac{\partial\phi}{\partial y}(x,\varepsilon y,\varepsilon t)\hat{y} \\ \qquad\qquad\qquad\qquad + \varepsilon E_z\hat{z} \end{cases}$$

The field line curvature effects also produce a y dependence so that $n(x,\varepsilon t,\varepsilon y,\underline{\delta y})$ could be written ($\delta \equiv \Delta s/r_p$). It is assumed that the portion of the sheath studied is near the midplane ($\zeta = 0$ in Fig. 2) so that the curvature effects are quadratic: $n(x,\varepsilon t,\varepsilon y,\delta^2 y)$ and therefore ignorable to lowest order in δ.

If the plasma confined in Tormac is to persist for a long period, $\tau_{tormac} \cong \tau_{ii}\,(r_p/\Delta s)$, ($r_p \rightarrow$ the radius of curvature of the field lines and the plasma minor radius are taken to be of the same order) then

the basic structure of the sheath should not vary on time scales shorter than τ_{tormac}. This requirement motivates the search for a steadily "eating-in" sheath, i.e., a sheath where quantities depend on x,t in the fashion:

$$\text{II.30} \qquad f(x,t) = f(x-u_0(\delta t)t,\ \delta t)$$

where:

$$\text{II.31} \qquad \delta \equiv \frac{\Delta s}{r_p} \sim \frac{\tau_{coll}}{\tau_{tormac}}$$

Combining the prescription defined in II.30 with the expressions II.29 yields:

$$\text{II.32} \quad \begin{cases} n(x-\varepsilon u_0(\delta t)t,\ \varepsilon\delta t, \varepsilon y) \\ \underline{u} = \varepsilon u_x(x-\varepsilon u_0(\delta t)t,\ \varepsilon\delta t, \varepsilon y)\hat{x} \\ \quad + u_y(x-\varepsilon u_0(\delta t)t,\ \varepsilon\delta t, \varepsilon y)\hat{y} \\ \quad + u_z(x-\varepsilon u_0(\delta t)t,\ \varepsilon\delta t, \varepsilon y)\hat{z} \\ \text{- - - - - - - etc. - - - - - -} \end{cases}$$

Keeping only lowest order in ε, δ results in

$$\text{II.33} \quad \begin{cases} x-\varepsilon u_0(\delta t)t \to x-\varepsilon u_0 t \\ \varepsilon\delta t \to 0 \end{cases} \qquad \text{in II.32}$$

If a change of reference frame is made to a frame moving at velocity $\underline{v} = \varepsilon u_0\hat{x}$, then the time dependence completely disappears, yielding

$$
\text{II.34}\quad \begin{cases}
n = n(x) + \varepsilon \dfrac{\partial n}{\partial y}(x)\cdot(y-y_0) \\[2ex]
\underline{u} = \varepsilon u_x(x)\hat{x} + \left(u_y(x) + \varepsilon \dfrac{\partial u_y}{\partial y}(x)(y-y_0)\right)\hat{y} \\[2ex]
\qquad\qquad + \left(u_z(x) + \varepsilon \dfrac{\partial u_z}{\partial y}(x)(y-y_0)\right)\hat{z} \\[2ex]
\underline{\underline{P}}_i = \left[P_\perp(x) + \varepsilon \dfrac{\partial P_\perp}{\partial y}(x)(y-y_0)\right]\underline{\underline{I}}_\perp + \left[P_\parallel(x) + \varepsilon \dfrac{\partial P_\parallel}{\partial y}(x)(y-y_0)\right]\hat{b}\hat{b} \\[2ex]
Pe = Pe(x) + \varepsilon \dfrac{\partial P_e}{\partial y}(x)(y-y_0) \\[2ex]
\underline{B} = \varepsilon B_x(x)\hat{x} + \left(B_y(x) + \varepsilon \dfrac{\partial B_y}{\partial y}(x)(y-y_0)\right)\hat{y} \\[2ex]
\qquad\qquad + \left(B_z(x) + \varepsilon \dfrac{\partial B_z}{\partial y}(x)(y-y_0)\right)\hat{z} \\[2ex]
\underline{E} = \left[-\dfrac{\partial \phi}{\partial x}(x) - \varepsilon \dfrac{\partial^2 \phi}{\partial x \partial y}(x)(y-y_0)\right]\hat{x} \\[2ex]
\qquad\qquad - \varepsilon \dfrac{\partial \phi}{\partial y}(x)\hat{y} + \varepsilon E_z \hat{z}
\end{cases}
$$

In II.34 the y-dependence has been expanded explicitly to first order in ε(y_0 = a point in the slab):

$$f(x,\varepsilon y) = f(x,y_0) + \varepsilon(y-y_0)\frac{\partial f}{\partial y}(x,y_0) + O(E^2)$$

In the reference frame moving at velocity u_0, the sheath appears stationary for times $\tau_{tormac} \gg t \gtrsim \tau_{coll}$.

From the viewpoint of the slab model, the sheath is maintained by a uniform magnetized plasma extending to $x \to -\infty$ that is convecting slowly at velocity $u_0\hat{x}$ toward the sheath. An electric field $\underline{E}$ ε $\underline{E}\cdot\underline{B} = 0$, $\underline{E}\times\underline{B}/B^2 = u_0\hat{x}$ is present in the semi-infinite plasma and is responsible for the convection (In the lab frame $\underline{E} = 0$ in the interior. In the sheath frame $\underline{E}$ arises from the Gallilean transformation

rules for the electric and magnetic field).

Once plasma is convected into the region of open field lines, a flow of matter, momentum and energy develops along the open flux surfaces. The plasma in a moving flux tube is ultimately depleted by the "annihilation" so that $n \to 0$, $\underline{B} \to \underline{B}_{vacuum}$ as $x \to \infty$.

The $\partial/\partial y(\ )$ terms in II.34 represent annihilation effects and may be conveniently related to boundary conditions at the ends of the slab ($y = y_0 \pm L/2$ for a slab length L). By virtue of the weak y-dependence,

$$\text{II.35} \qquad \left.\frac{\partial f}{\partial y}\right|_{y=y_0} \cong \frac{f(y_0+L/2)-f(y_0-L/2)}{L},$$

so that knowing f at the ends of the slab determines $\partial f/\partial y|_{y_0}$. In this manner, certain of the $\partial/\partial y(\ )$ terms will be related to the known mirror loss rates, i.e., the accumulated flux of matter, etc. at the edge of the slab is known from the local mirror losses in the slab, yielding $\partial/\partial y(\text{flux})$ from II.35. In chapter III, explicit expressions will be obtained in this fashion for the fluxes of matter and energy:

$$\frac{\partial}{\partial y}(nu_y)_i,\ \frac{\partial}{\partial y}(nu_y)_e,\ \frac{\partial}{\partial y}q^{\perp}_{\parallel i},\ \frac{\partial}{\partial y}q^{\parallel}_{\parallel i},\ \frac{\partial}{\partial y}q_{\parallel e}\ \left(= \frac{\partial}{\partial y}(q^{\perp}_{\parallel e}+q^{\parallel}_{\parallel e})\right)$$

The expressions II.34 may be inserted into the equations II.2, 4, 5, 11, 12, 13 and expanded to first order in ε, yielding:

II.36

Zeroth order

a) $\frac{\partial P_\perp}{\partial x} - en\left(-\frac{\partial \phi}{\partial x} + u_y B_z - u_z B_y\right) = 0$ for both ions and electrons

b) $\frac{\partial B_y}{\partial x} = 4\pi en\,(u_{iz} - u_{ez})$

c) $\frac{\partial B_z}{\partial x} = -4\pi en\,(u_{iy} - u_{ey})$

d) $\underline{E}_0 = -\frac{\partial \phi}{\partial x}\hat{x}$

First order

for both ions and electrons

e) $u_x \frac{\partial n}{\partial x} + n\frac{\partial u_x}{\partial x} = -\frac{\partial}{\partial y}(nu_y)$

f) $\frac{\partial}{\partial x}\frac{\partial P_{xx}}{\partial y} - \frac{e_s}{n_0}\frac{\partial n_1}{\partial y}\frac{\partial P_\perp}{\partial x} - e_s n\left(-\frac{\partial^2 \phi_1}{\partial x \partial y} + \frac{\partial u_{y1}}{\partial y} B_{z0} + u_{y0}\frac{\partial B_{z1}}{\partial y} - \frac{\partial u_{z1}}{\partial y} By_0 - u_{z0}\frac{\partial B_{y1}}{\partial y}\right) = 0$

g) $nmu_x \frac{\partial}{\partial x} u_y + nmu_y \frac{\partial u_y}{\partial y} + \frac{\partial}{\partial y} P_{yy} - en_0\left(-\frac{\partial \phi_1}{\partial y} - u_x B_z + u_z B_x\right) = C_{1y}$

h) $nmu_x \frac{\partial u_z}{\partial x} + nmu_y \frac{\partial u_z}{\partial y} + \frac{\partial}{\partial y} Pyz - en_0\left(E_z + u_x B_z - u_z B_x\right) = C_{1z}$

II.36

i) $$u_{xi}\frac{\partial P_{\perp i}}{\partial x} + u_{y_i}\frac{\partial P_{\perp i}}{\partial y} + P_{\perp_i}\left(2\left(\frac{\partial u_{xi}}{\partial x} + \frac{\partial u_{yi}}{\partial y}\right) - \frac{B_y}{B^2}\left(B_y\frac{\partial u_{yi}}{\partial y} + B_z\frac{\partial u_{zi}}{\partial y}\right) - \frac{B_x}{B^2}\left(B_y\frac{\partial u_{yi}}{\partial x} + B_z\frac{\partial u_{zi}}{\partial x}\right)\right) = -\frac{B_y}{B}\frac{\partial}{\partial y}q^{\perp}_{\parallel i} + 1/2\,\underline{\underline{C}}_{2i}:\underline{\underline{I}}_{\perp}$$

j) $$u_{xi}\frac{\partial}{\partial x}P_{\parallel i} + u_{yi}\frac{\partial P_{\parallel i}}{\partial y} + P_{\parallel i}\left(\frac{\partial u_{xi}}{\partial x} + \frac{\partial u_{yi}}{\partial y} + \frac{2B_y}{B^2}\left(B_y\frac{\partial u_{yi}}{\partial y} + B_z\frac{\partial u_{zi}}{\partial y}\right) + \frac{2B_x}{B^2}\left(B_y\frac{\partial u_{yi}}{\partial x} + B_z\frac{\partial u_{zi}}{\partial x}\right)\right) = -\frac{2B_y}{B}\frac{\partial q^{\parallel}_{\parallel i}}{\partial y} + \underline{\underline{C}}_{2i}:\delta\delta$$

k) $$u_{xe}\frac{\partial}{\partial x}P_e + u_{y_e}\frac{\partial P_e}{\partial y} + 5/3\left(\frac{\partial u_{xe}}{\partial x} + \frac{\partial u_{ye}}{\partial y}\right) = \frac{\underline{\underline{C}}_e:\underline{\underline{I}}}{3} - 2/3\,\frac{B_y}{B}\frac{\partial}{\partial y}\left(q^{\parallel}_{\parallel e} + q^{\perp}_{\parallel e}\right)$$

l) $$\frac{\partial}{\partial x}\frac{\partial B_y}{\partial y} = 4\pi e\left(n\left(\frac{\partial u_{iz}}{\partial y} - \frac{\partial u_{ez}}{\partial y}\right) + \frac{\partial n_1}{\partial y}\,(u_{iz}-u_{ez})\right)$$

m) $$\frac{\partial}{\partial x}\frac{\partial B_{z1}}{\partial y} = 4\pi e\left(n\left(\frac{\partial u_{iy}}{\partial y} - \frac{\partial u_{ey}}{\partial y}\right) + \frac{\partial n}{\partial y}\,(u_{iy}-u_{ey})\right)$$

n) $$\frac{\partial B_{z1}}{\partial y} = 4\pi e n\,(u_{ix}-u_{ex})$$

one of these is redundant

$$\text{II.36}\begin{cases} \text{o)} \quad \dfrac{\partial B_x}{\partial x} = -\dfrac{\partial B_y}{\partial y} \\ \text{p)} \quad E_z = \text{a constant } (\nabla \times \underline{E} = 0) \\ \text{q)} \quad \underline{\underline{P}}_i = P_\perp \underline{\underline{I}}_\perp + P_\parallel \hat{b}\hat{b} \end{cases}$$

Note that some of the equations (II.36f, l, m) have been operated on with $\partial/\partial y$, which completely eliminates the variable y from the equations. The quantities $\partial U_y/\partial y$, $\partial U_z/\partial y$ . . . are functions of X only to be determined from the various constraints inherent in II.36 as well as from boundary conditions (as in II.35).

Some further manipulations and assumptions are needed before the model reaches its final form. The first of these is to set $B_{1x}(x) = 0$, i.e., assume $\underline{B}$ has no component across the sheath.

If the portion of the sheath studied is at the midplane (as discussed on p. 36), the solutions should have up-down symmetry. $B_{1x} \neq 0$ would slightly cant the field lines, destroying the symmetry so it will be assumed to vanish. Equation II.36o then yields $\partial B_{1y}/\partial y = 0$, as well.

The equations II.36 constitute 17 algebraic and ordinary differential equations for the 21 quantities

$$\text{II.37}\begin{cases} n,\ u_{yi},\ u_{ye},\ u_{zi},\ u_{ze},\ P_{\perp i},\ P_{\parallel i},\ P_e,\ \phi,\ B_y,\ B_z, \\ \dfrac{\partial n}{\partial y},\ u_{xi},\ u_{xe},\ \dfrac{\partial u_{zi}}{\partial y},\ \dfrac{\partial u_{ze}}{\partial y},\ \dfrac{\partial P_{\perp i}}{\partial y},\ \dfrac{\partial P_{\parallel i}}{\partial y},\ \dfrac{\partial P_{ei}}{\partial y},\ \dfrac{\partial \phi_1}{\partial y},\ \dfrac{\partial B_{1z}}{\partial y} \end{cases}$$

with the annihilation fluxes $\dfrac{\partial n u_{yi}}{\partial y}$, $\dfrac{\partial n u_{ye}}{\partial y}$, $\dfrac{\partial q^{\parallel}_{\parallel i}}{\partial y}$, $\dfrac{\partial q^{\perp}_{\parallel i}}{\partial y}$, $\dfrac{\partial q_{\parallel e}}{\partial y}$ specified in terms of the 21 variables in II.37. Four more equations are needed

to close the set, although as further manipulations are performed some decoupling will occur and two variables will drop out.

The two remaining equations are found from global constraints on the collisionless poloidal flow velocities u_{yi}, u_{ye}. In a cusped configuration (Fig. 2) fluid motion in the poloidal direction is inhibited by material boundaries intersecting the open flux surfaces. To have weak interaction with the walls, the plasma density must be small near the boundary and the collisionless flow $\underline{u}_{pol}$ must have no component into the boundary. If any poloidal flow is to exist on the open field lines and satisfy $\nabla\cdot n\underline{u}_p = 0$, then it must circulate away from the walls and hence across flux surfaces (see Fig. 3).

In appendix A the flow across flux surfaces is related to the toroidal stress. The condition $\nabla\cdot n\underline{u}_{pol} = 0$ then gives an approximate formula for the poloidal flow velocity, thus determining a local property, u_y, by applying a boundary condition ($\underline{u}_{pol}\cdot\hat{n}_{wall} = 0$) at the walls. The result is:

$$\text{II.38} \qquad u_{ye} = 0 \qquad\qquad u_{yi} = -\frac{1}{en}\frac{\partial}{\partial x}\left[\frac{(P_{\parallel}-P_{\perp})B_z}{B^2}\right]$$

(approximately isotropic electrons) to lowest order in ρ_i/Δ_s

u_{yi} resembles a diamagnetic flow (instead it is the sum of circulating and "banana" flows) and is first order in ρ_i/Δ_s.*

On the closed field lines, no cusp boundary condition exists (particles can circulate poloidally by simply remaining on a flux

*Note that the fluid equations to lowest order in ρ_i/Δ_s involve many first order as well as zeroth order quantities.

surface) and the poloidal flow velocities are determined by local force balance, the y component of the momentum eqn. II.36g.

With the annihilation fluxes determined in Chapter III, the collision terms II.15, 16 and the poloidal flows II.38, the set II.36 is closed. In order to numerically integrate the equations, they must be cast into the form:

$$\text{II.39} \qquad \frac{d\underline{\xi}}{dx} = \underline{f}(\underline{\xi})$$

where $\underline{\xi}$ = dependent variables = $(n, P_{\perp i}, P_{\parallel i} \ldots)$

$\underline{f}$ = non-linear vector valued function of $\underline{\xi}$

The remainder of this chapter consists of manipulating II.15, 16, 36, 38 into the form II.39 for both the open and closed field line regions.

On closed field lines there are no mirror losses so the collisionally induced y-derivatives vanish, $\partial/\partial y(\ ) = 0$ (except $\partial\phi_1/\partial y = -Ey$ = a constant). The set II.36 becomes:

$$\text{II.40} \quad \begin{cases} \text{a)} & \dfrac{\partial P_\perp}{\partial x} - en\left(-\dfrac{\partial\phi}{\partial x} + u_{yi}B_z - u_{zi}B_y\right) = 0 \\[2ex] \text{b)} & \dfrac{\partial P_e}{\partial x} + en\left(-\dfrac{\partial\phi}{\partial x} + u_{ye}B_z - u_{ze}B_y\right) = 0 \\[2ex] \text{c)} & \dfrac{\partial B_y}{\partial x} = 4\pi J_z = 4\pi en\,(u_{iz}-u_{ez}) \\[2ex] \text{d)} & \dfrac{\partial B_z}{\partial x} = -4\pi J_y = -4\pi en\,(u_{iy}-u_{ey}) \\[2ex] \text{e)} & \dfrac{\partial}{\partial x}\, nu_{xi} = 0 \end{cases}$$

$$
\text{II.40}\quad \begin{cases}
\text{f)} & \dfrac{\partial}{\partial x} n u_{xe} = 0 \\[2ex]
\text{g)} & n m_i u_{xi} \dfrac{\partial}{\partial x} u_y - en\,(E_y - u_{xi} B_z) = -en\eta J_y \\[2ex]
\text{h)} & E_y - u_{xe} B_z = \eta J_y \\[2ex]
\text{i)} & n m_i u_{xi} \dfrac{\partial}{\partial x} u_z - en\,(E_z + u_x\, B_y) = -en\eta J_z \\[2ex]
\text{j)} & E_z + u_{xe} B_y = \eta J_z \\[2ex]
\text{k)} & u_{xi} \dfrac{\partial P_{\perp i}}{\partial x} + 2P_{\perp i} \dfrac{\partial u_{xi}}{\partial x} = -\dfrac{\nu_i}{3}\,(P_\perp - P_\parallel) - \dfrac{2m_e}{m_i}\,\nu_e\,(P_\perp - P_e) \\[2ex]
\text{l)} & u_{xe} \dfrac{\partial P_e}{\partial x} + 5/3\, P_e \dfrac{\partial u_{xe}}{\partial x} = 2/3\, \eta J^2 - \dfrac{2m_e}{m_i}\,\nu_e \left(P_e - \tfrac{2}{3} P_\perp - \dfrac{P_\parallel}{3}\right) \\[2ex]
\text{m)} & u_{xi} \dfrac{\partial P_{\parallel i}}{\partial x} + P_{\parallel i} \dfrac{\partial u_{xi}}{\partial x} = -\dfrac{2}{3}\nu_i\,(P_\parallel - P_\perp) - \dfrac{2m_e}{m_i}\,\nu_e\,(P_\parallel - P_e)
\end{cases}
$$

Eqn.'s a,b combine to yield pressure balance:

$$
\text{II.41}\quad \frac{\partial P_\perp}{\partial x} + \frac{\partial P_e}{\partial x} - J_y B_z + J_z B_y = 0
$$

Eqn.'s e,f yield

$$
\text{II.42}\quad u_{xi} = u_{xe} = \frac{n(-\infty) u_x(-\infty)}{n(x)} \equiv u_x
$$

Combining eqn.'s II.41, II.40e, k, l gives an equation for the density

$$
\text{II.43}\quad \frac{\partial n}{\partial x} = \frac{n}{2P_\perp + \frac{5}{3}P_e} \left(\frac{\left(\nu_i + 2\frac{m_e}{m_i}\nu_e\right)}{3u_x} (P_\perp - P_\parallel) - \frac{2}{3}\, u_x \eta J^2 + J_y B_z - J_z B_y \right)
$$

Combining eqns. II.40g, h and i, k gives

$$\text{II.44} \quad nmu_x \frac{\partial}{\partial x} u_y = 0; \quad nmu_x \frac{\partial}{\partial x} u_z = 0 \Rightarrow$$

$$u_y = 0 + O(\rho_i/\Delta_s)$$

$$u_z = 0 + O(\rho_i/\Delta_s)$$

Flow velocities of first order in finite gyroradius effects can be important since currents of order ρ_i/Δ_s can give lowest order variations in the magnetic field, i.e., diamagnetic flows are $O(\rho_i/\Delta_s)$ but result in lowest order magnetic field variations for $\beta \sim 1$.

To determine the $O(\rho_i/\Delta_s)$ contributions to u_{yi}, u_{zi}, the next order corrections to I..44 must be included. These are gyroviscous terms found from solving II.8 for the off-diagonal pressure components (as done by A. McMahon). The generalization of II.44 is given by:

$$\text{II.45} \quad nmu_x \frac{\partial}{\partial x} u_{yi} + \frac{\partial}{\partial x} Pxy_i = 0$$

$$nmu_x \frac{\partial}{\partial x} u_{zi} + \frac{\partial}{\partial x} Pxz_i = 0$$

$$Pxy_i\, \hat{y} + Pxz_i\, \hat{z} = \left(\frac{P_{\perp i}}{2\Omega_i} \frac{\partial u_{xi}}{\partial x} + \frac{(P_{\parallel i} - P_{\perp i})}{\Omega_i} u_{xi} \frac{B_y^2}{B^2} \frac{\partial}{\partial x}\left(\frac{B_z}{B_y}\right)\right)(\hat{b} \times \hat{x})$$

Since nu_x is a constant from II.42, eqns. II.45 may be integrated:

$$\text{II.46} \quad u_{yi}\, \hat{y} + u_{zi}\, \hat{z} = \frac{P_\perp}{2\Omega mn^2} \frac{\partial n}{\partial x} (\hat{b} \times \hat{x})$$

The second term in P_{xy}, $P_{xz} \propto (P_\parallel - P_\perp)$ is dropped since (as will be verified numerically) the pressure anisotropy on closed field lines is small.

Using II.40h, j to eliminate the currents J_y, J_z results in a set of equations of the form II.39 suitable for numerical integration:

$$
\text{II.47}\quad \left\{
\begin{aligned}
&\text{a)}\quad \frac{\partial n}{\partial x} = \frac{n}{2P_\perp + \frac{5}{3}P_e}\left(\frac{(\nu_i + 2\frac{m_e}{m_i}\nu_e)}{3u_x}(P_\perp - P_\parallel) - \frac{2}{3u_x}\eta J^2 + J_yB_z - J_zB_y\right)\\
&\text{b)}\quad \frac{\partial P_{\perp i}}{\partial x} = \frac{2P_{\perp i}}{n}\frac{\partial n}{\partial x} - \frac{\nu_i}{3u_x}(P_\perp - P_\parallel) - \frac{2\frac{m_e}{m_i}\nu_e}{u_x}(P_\perp - P_e)\\
&\text{c)}\quad \frac{\partial P_\parallel}{\partial x} = \frac{P_\parallel}{n}\frac{\partial n}{\partial x} - \frac{2\nu_i}{3u_x}(P_\parallel - P_\perp) - \frac{2\frac{m_e}{m_i}\nu_e}{u_x}(P_\parallel - P_e)\\
&\text{d)}\quad \frac{\partial P_e}{\partial x} = \frac{5}{3}\frac{P_e}{n}\frac{\partial n}{\partial x} + \frac{2}{3}\frac{\eta J^2}{u_x} - \frac{2\frac{m_e}{m_i}\nu_e}{u_x}\left(P_e - \frac{2}{3}P_{\perp i} - \frac{P_{\parallel i}}{3}\right)\\
&\text{e)}\quad \frac{\partial u_x}{\partial x} = -\frac{u_x}{n}\frac{\partial n}{\partial x} \quad \underline{\text{or}} \quad u_x = \frac{n(-\infty)u_x(-\infty)}{n(x)}\\
&\text{f)}\quad \frac{\partial B_y}{\partial x} = 4\pi J_z\\
&\text{g)}\quad \frac{\partial B_z}{\partial x} = -4\pi J_y\\
&\text{h)}\quad \frac{\partial \phi}{\partial x} = -\frac{1}{en}\frac{\partial P_\perp}{\partial x} + u_yB_z - u_zB_y\\
&\qquad\quad = -\frac{1}{en}\frac{\partial P_\perp}{\partial x} + \frac{P_\perp}{2en^2}\frac{\partial n}{\partial x} \quad \text{using II.46}
\end{aligned}
\right.
$$

$$\text{II.47}\begin{cases} \text{i)} \quad J_z = \dfrac{E_z + u_x B_y}{\eta} \\[2ex] \text{j)} \quad J_y = \dfrac{E_y - u_x B_z}{\eta} \end{cases}$$

The boundary conditions associated with the set II.47 are:

$$\text{II.48} \qquad \begin{array}{lll} \text{as } x \to -\infty & B_y \to B_y(-\infty) & \underline{B}_z \to B_z(-\infty) \\ & n \to n(-\infty) & P_\perp \to P_\parallel \to P_e \to P(-\infty) \\ & u_x \to u(-\infty) & \phi \to \phi(-\infty) \end{array}$$

The constraints $J_z \to 0$, $J_y \to 0$ at $-\infty$ determine the electric fields E_y, E_z

$$\text{II.49} \qquad \begin{aligned} E_y &= u(-\infty)B_z(-\infty) \\ E_z &= -u(-\infty)B_y(-\infty) \end{aligned}$$

Clearly $\underline{E}\cdot\underline{B} \to 0$ as $x \to -\infty$.

The equations II.47 are integrated in from large negative x until the open field lines are encountered. The dividing point between closed and open field lines will be labeled by a particular (although arbitrarily chosen) value of the poloidal magnetic field. If the cusp and interior poloidal fields are antiparallel (the field reversed sheath), then the natural division between open and closed field lines occurs at $B_{pol} = B_y = 0$.

The set of equations for the open field lines analagous to II.47 is more complex. The set II.36 can be simplified by using the result

that u_{yi} is first order is ρ_i/Δ_s and that $u_{ye} = 0$ from II.38. It is also convenient to sum the electron and ion force balance equations to obtain the set:*

$$
\text{II.50}\quad \left\{
\begin{aligned}
&\text{a)}\quad \frac{\partial P_{\perp i}}{\partial x} + \frac{\partial P_e}{\partial x} - enu_{yi}\, B_z + J_z B_y = 0 \\
&\text{b)}\quad u_{xi}\frac{\partial P_{\perp i}}{\partial x} + P_{\perp i}\left(2\left(\frac{\partial u_{xi}}{\partial x} + \frac{\partial u_{yi}}{\partial y}\right) - \frac{B_y}{B^2}\left(B_y\frac{\partial u_{yi}}{\partial y}\right.\right. \\
&\qquad\qquad \left.\left. + B_z\frac{\partial u_{zi}}{\partial y}\right)\right) = -\frac{\partial}{\partial y}q^{\perp}_{yi} - \frac{\nu_i}{3}(P_\perp - P_\parallel) - 2\frac{m_e}{m_i}\nu_e(P_\perp - P_e) \\
&\text{c)}\quad u_{xi}\frac{\partial P_{\parallel i}}{\partial x} + P_{\parallel i}\left(\frac{\partial u_{xi}}{\partial x} + \frac{\partial u_{yi}}{\partial y} + \frac{2B_y}{B^2}\left(B_y\frac{\partial u_{yi}}{\partial y} + B_z\frac{\partial u_{zi}}{\partial y}\right)\right) \\
&\qquad\qquad = -\frac{\partial}{\partial y}q^{\parallel}_{yi} - \frac{2\nu_i}{3}(P_\parallel - P_\perp) - 2\frac{m_e}{m_i}\nu_e(P_{\parallel i} - P_e) \\
&\text{d)}\quad u_{xe}\frac{\partial P_e}{\partial x} + \frac{5}{3}P_e\left(\frac{\partial u_{xe}}{\partial x} + \frac{\partial u_{ye}}{\partial y}\right) = -\frac{2}{3}\frac{\partial}{\partial y}q^e_y + \frac{2}{3}\eta J^2 \\
&\qquad \left\{\text{the annotation } q_y = \frac{B_y}{B}q_\parallel \text{ is used}\right\} \\
&\qquad\qquad - 2\frac{m_e}{m_i}\nu_e\left(P_e - \frac{2}{3}P_{\perp i} - \frac{P_{\parallel i}}{3}\right) \\
&\text{e)}\quad n\frac{\partial u_{xi}}{\partial x} = -u_{xi}\frac{\partial n}{\partial x} - \frac{\partial}{\partial y}(nu_{yi}) \\
&\text{f)}\quad n\frac{\partial u_{xe}}{\partial x} = -u_{xe}\frac{\partial n}{\partial x} - \frac{\partial}{\partial y}(nu_{ye})
\end{aligned}
\right.
$$

*The thermal force terms $\alpha\nabla_\parallel T_e$ are neglected. See Appendix B for an explanation.

II.50

g) $$\frac{\partial P_{\perp i}}{\partial y} + \frac{\partial P_{el}}{\partial y} + en\,(u_{ix}-u_{ex})\,B_z = 0$$

h) $$\frac{\partial u_{zi}}{\partial y} = \frac{\frac{\partial u_{yi}}{\partial y} B_z - \frac{\partial^2 \phi}{\partial x \partial y}}{B_y}$$

i) $$\frac{\partial}{\partial y}\left(P_{\perp i} + \frac{B_y^2}{B^2}(P_{\parallel}-P_{\perp})\right) + \frac{\partial P_e}{\partial y} + en\,(u_{xi}-u_{xe})\,B_z = 0$$

j) $$\frac{\partial \phi_1}{\partial y} = -\,u_{xe}B_z - \eta e n u_{yi}$$

k) $$nmu_{xi}\frac{\partial u_{zi}}{\partial x} = en\,(u_{xi}-u_{xe})\,B_y - \frac{\partial}{\partial y}\left(\frac{B_y B_z}{B^2}(P_{\parallel}-P_{\perp})\right)$$

l) $$J_z = \frac{E_z + u_{xe}B_y}{\eta}$$

m) $$\frac{\partial u_{ez}}{\partial y} = \frac{\partial u_{iz}}{\partial y} - \frac{\partial n/\partial y}{n}(u_{iz}-u_{ez})$$

$$\left\{\begin{array}{l}\text{equivalent to } \dfrac{\partial J_z}{\partial y} = \dfrac{\partial^2 B_y/\partial x \partial y}{4\pi} = 0 \\ \text{see the discussion on p. 42}\end{array}\right\}$$

n) $$\frac{\partial B_{zl}}{\partial y} = 4\pi e n (u_{ix}-u_{ex})$$

o) $$\frac{\partial B_y}{\partial x} = 4\pi J_z$$

p) $$\frac{\partial B_z}{\partial x} = -\,4\pi e n u_{yi}$$

$$\text{II.50}\quad \begin{cases} \text{q)}\ \dfrac{\partial\phi}{\partial x} = -\dfrac{1}{en}\dfrac{\partial P_{\perp i}}{\partial x} + u_{yi}B_z - u_{zi}B_y \\[2ex] \text{r)}\ u_{ye} = 0 \\[2ex] \text{s)}\ u_{yi} = -\dfrac{1}{en}\dfrac{\partial}{\partial x}\left[\dfrac{(P_\parallel - P_\perp)B_z}{B^2}\right] \end{cases}$$

Combining II.50g with II.50i results in

$$\text{II.51}\quad \frac{\partial}{\partial y}\left(\frac{B_y^2}{B^2}(P_\parallel - P_\perp)\right) = B_y^2\frac{\partial}{\partial y}\left(\frac{P_\parallel - P_\perp}{B^2}\right) = 0$$

This can be applied to the term on the right hand side of II.50k:

$$\text{II.52}\quad -\frac{\partial}{\partial y}\frac{B_yB_z}{B^2}(P_\parallel - P_\perp) = -\frac{B_y(P_\parallel - P_\perp)}{B^2}\frac{\partial B_z}{\partial y}$$

Using expression II.50h in II.52 and II.52 in II.50k results in

$$\text{II.53}\quad \begin{aligned} nmu_{xi}\frac{\partial}{\partial x}u_{zi} &= en(u_{xi}-u_{xe})\,B_y - 4\pi en(u_{xi}-u_{xe})\,B_y\frac{(P_\parallel - P_\perp)}{B^2} \\ &= en(u_{xi}-u_{xe})\,B_y\left(1 - \frac{4\pi(P_\parallel - P_\perp)}{B^2}\right) \end{aligned}$$

So:

$$\text{II.54}\quad \frac{\partial u_{zi}}{\partial x} = \frac{eB_y}{m_i}\frac{(u_{xi}-u_{xe})}{u_{xi}}\left(1 - \frac{4\pi(P_\parallel - P_\perp)}{B^2}\right)$$

Equation II.53 shows that the Lorentz force $J_x\hat{x}xB_y\hat{y}$ drives a toroidal ($\hat{z}$) mass flow of ions.

The quantity $\partial u_{zi}/\partial y$, the toroidal annihilation flow, couples to the other variables only through the terms in the ion equations of state

representing exchange of perpendicular and parallel energy, i.e., for a scalar ion pressure, $\partial u_{zi}/\partial y$ decouples from the other variables. $\partial u_{zi}/\partial y$ is given in II.50h.

$$\text{II.50h} \qquad \frac{\partial u_{zi}}{\partial y} = \underbrace{\frac{B_z}{B_y}\frac{\partial u_{yi}}{\partial y}}_{\substack{\text{parallel}\\ \text{streaming}}} - \underbrace{\frac{1}{B_y}\frac{\partial^2 \phi}{\partial x \partial y}}_{\substack{\underline{E}\times\underline{B}\ \text{motion across}\\ \text{field lines}}}$$

To evaluate the $\underline{E}\times\underline{B}$ term, differentiate II.50j

$$\text{II.55} \qquad \frac{\partial^2 \phi_1}{\partial x \partial y} = -\frac{\partial}{\partial x} u_{xe} B_z - \frac{\partial}{\partial x}(\eta e n u_{yi})$$

The second term on the right hand side of II.55 is usually small:

$$\text{II.56} \qquad \frac{e n \eta u_y}{u_{xe} B_z} \sim \frac{e n u_y}{J_z}\frac{B_y}{B_z} \quad \text{from II.50l}$$

The ion poloidal flow is similar to a diamagnetic flow whereas J_z is determined by electron ion drag. Most solutions (as will be seen in Chapter IV) have the property

$$\text{II.57} \qquad \frac{e n u_{yi}}{J_z} \ll 1 \quad \text{on open field lines}$$

The second term in II.55 is therefore neglected:

$$\text{II.58} \qquad \begin{aligned} \frac{\partial^2 \phi_1}{\partial x \partial y} &= -\frac{\partial}{\partial x}(u_{xe} B_z) = -\frac{\partial u_{xe}}{\partial x} B_z - u_{xe}\frac{\partial B_z}{\partial x} \\ &= \left(\frac{u_{xe}}{n}\frac{\partial n}{\partial x} + \frac{1}{n}\frac{\partial (n u_y)_e}{\partial y}\right) B_z + (4\pi e n u_{yi}) u_{xe} \end{aligned}$$

Substituting II.58 into II.50h yields

$$\text{II.59}\quad \frac{\partial u_{zi}}{\partial y} = \frac{B_z}{B_y}\frac{\partial u_{yi}}{\partial y} - \frac{B_z}{B_y}\left(\frac{u_{xe}}{n}\frac{\partial n}{\partial x} + \frac{1}{n}\frac{\partial}{\partial y}(nu_{ye})\right) - \frac{4\pi e n u_{yi}}{B_y}u_{xe}$$

Equations II.59, II.50e, f may be used in II.50b, c, d to obtain the pressure equations:

$$\text{II.60}\quad \left\{\begin{aligned}
&\text{a)}\quad \frac{\partial P_{\perp i}}{\partial x} = \frac{2P_{\perp i}}{n}\left(1 - \frac{u_{xe}}{2u_{xi}}\frac{B_z^2}{B^2}\right)\frac{\partial n}{\partial x} + \frac{P_\perp}{u_{xi}}\left(\Gamma_i - \frac{B_z^2}{B^2}\Gamma_e\right)\\
&\qquad - \frac{4\pi P_\perp}{B^2}\frac{u_{xe}}{u_{xi}}(enu_{yi}B_z) - \frac{\nu_i}{3u_{xi}}(P_{\perp i}-P_{\parallel i}) - \frac{2\frac{m_e}{m_i}\nu_e(P_\perp - P_e)}{u_{xi}}\\
&\qquad - \frac{1}{u_{xi}}\frac{\partial q_{yi}^{\perp}}{\partial y}\\
&\text{b)}\quad \frac{\partial P_{\parallel i}}{\partial x} = \frac{P_\parallel}{n}\left(1 + \frac{2u_{xe}}{u_{xi}}\frac{B_z^2}{B^2}\right)\frac{\partial n}{\partial x} - \frac{2P_\parallel}{u_{xi}}\left(\Gamma_i - \frac{B_z^2}{B^2}\Gamma_e\right)\\
&\qquad + \frac{8\pi P_\parallel}{B^2}\frac{u_{xe}}{u_{xi}}(enu_{yi}B_z) - \frac{2}{3}\frac{\nu_i}{u_{xi}}(P_{\parallel i}-P_{\perp i})\\
&\qquad - \frac{2\frac{m_e}{m_i}\nu_e(P_\parallel - P_e)}{u_{xi}} - \frac{1}{u_{xi}}\frac{\partial q_{yi}^{\parallel}}{\partial y}
\end{aligned}\right.$$

$$\text{II.60} \quad \text{c)} \quad \frac{\partial P_e}{\partial x} = \frac{5}{3}\frac{P_e}{n}\frac{\partial n}{\partial x} - \frac{2\frac{m_e}{m_i}\nu_e}{u_{xe}}\left(P_e - \frac{2}{3}P_\perp - \frac{1}{3}P_\parallel\right) + \frac{\frac{2}{3}\eta J^2}{u_{xe}} - \frac{\frac{2}{3}\frac{\partial}{\partial y}q_y^e}{u_{xe}}$$

where $\Gamma_{\substack{i\\e}} \equiv \frac{1}{n}\frac{\partial}{\partial y}(nu_{y\substack{i\\e}})$ $\left(\text{note that } \frac{1}{n}\frac{\partial}{\partial y}(nu_y) = \frac{\partial u_y}{\partial y} + O\left(\frac{\rho_i}{\Delta_s}\right)\right)$

= the annihilation fluxes

Equations II.60a, b, c and II.50q, s may be combined to yield equations for $\partial n/\partial x$ and u_{yi}:

$$\text{II.61} \quad \begin{cases} \text{a)} \quad \alpha_1 \frac{1}{n}\frac{\partial n}{\partial x} + \beta_1\, enB_z u_{yi} = \gamma_1 - \frac{2}{3}\frac{\eta}{u_{xe}} e^2 n^2 u_{yi}^2 \\ \text{b)} \quad \alpha_2 \frac{1}{n}\frac{\partial n}{\partial x} + \beta_2\, enB_z u_{yi} = \gamma_2 \\ \text{c)} \quad \alpha_1 = 2P_\perp\left(1 - \frac{u_{xe}}{2u_{xi}}\frac{B_z^2}{B^2}\right) + \frac{5}{3}P_e \\ \text{d)} \quad \alpha_2 = 2P_\perp\left(1 - \frac{u_{xe}}{2u_{xi}}\frac{B_z^2}{B^2}\right) - P_\parallel\left(1 + \frac{2u_{xe}}{u_{xi}}\frac{B_z^2}{B^2}\right) \\ \text{e)} \quad \beta_1 = -\left(1 + \frac{4\pi P_\perp}{B^2}\frac{u_{xe}}{u_{xi}}\right) \\ \text{f)} \quad \beta_2 = -\left(\frac{B^2}{B_z^2}\left(1 - \frac{4\pi(P_\parallel - P_\perp)}{B^4}(B_y^2 - B_z^2)\right) + \frac{8\pi\left(P_\parallel + \frac{P_\perp}{2}\right)}{B^2}\frac{u_{xe}}{u_{xi}}\right) \end{cases}$$

$$
\text{II.61}\quad \left\{
\begin{aligned}
&\text{g)}\quad \gamma_1 = -\frac{P_\perp}{u_{xi}}\left(\Gamma_i - \frac{B_z^2}{B^2}\Gamma_e\right) + \frac{\nu_i}{3u_{xi}}(P_\perp - P_\parallel) + \frac{2\frac{m_e}{m_i}\nu_e}{u_{xi}}(P_\perp - P_e) \\
&\qquad + \frac{1}{u_{xi}}\frac{\partial q_{yi}^{\perp}}{\partial y} + \frac{2}{3}u_{xe}\frac{\partial q_y^e}{\partial y} + \frac{2\frac{m_e}{m_i}\nu_e}{u_{xe}}\left(P_e - \frac{2}{3}P_\perp - \frac{1}{3}P_\parallel\right) \\
&\qquad - \frac{\frac{2}{3}\eta J_z^2}{u_{xe}} - J_z B_y \\
&\text{h)}\quad \gamma_2 = -\frac{(2P_\parallel + P_\perp)}{u_{xi}}\left(\Gamma_i - \frac{B_z^2}{B^2}\Gamma_e\right) - \frac{2}{3}\frac{\nu_i}{u_{xi}}(P_\parallel - P_\perp) \\
&\qquad - \frac{2\frac{m_e}{m_i}\nu_e(P_\parallel - P_\perp)}{u_{xi}} + \frac{\nu_i}{3u_{xi}}(P_\perp - P_\parallel) + \frac{1}{u_{xi}}\frac{\partial q_y^{\perp}}{\partial y} \\
&\qquad - \frac{8\pi(P_\parallel - P_\perp)}{B^2}J_z B_y
\end{aligned}
\right.
$$

Equations II.61a, b may easily be solved for $\partial n/\partial x$, u_{yi}. With these results, the open field line equations are in the form II.39 suitable for numerical integration. The closed set is

$$
\text{II.62}\qquad \text{a)}\quad \frac{\partial n}{\partial x} = n\,\frac{(\beta_2\gamma_1 - \beta_1\gamma_2)}{\det} - \frac{2}{3}\frac{\eta n^3\beta_2}{\det\, u_{xe}}u_{yi}^2
$$

II.62

b) $$\frac{\partial P_\perp}{\partial x} = \frac{2P_\perp}{n}\left(1 - \frac{u_{xe}}{2u_{xi}}\frac{B_z^2}{B^2}\right)\frac{\partial n}{\partial x} + \frac{P_\perp}{u_{xe}}\left(\Gamma_i - \frac{B_z^2}{B^2}\Gamma_e\right)$$

$$- \frac{4\pi P_\perp}{B^2}\frac{u_{xe}}{u_{xi}}(enB_z u_{yi}) - \frac{\nu_i}{3u_{xi}}(P_\perp - P_\parallel) - \frac{2\frac{m_e}{m_i}\nu_e(P_\perp - P_e)}{u_{xi}}$$

$$- \frac{1}{u_{xi}}\frac{\partial q_{yi}^\perp}{\partial y}$$

c) $$\frac{\partial P_\parallel}{\partial x} = \frac{P_\parallel}{n}\left(1 + \frac{2u_{xe}}{u_{xi}}\frac{B_z^2}{B^2}\right)\frac{\partial n}{\partial x} - \frac{2P_\parallel}{u_{xi}}\left(\Gamma_i - \frac{B_z^2}{B^2}\Gamma_e\right)$$

$$+ \frac{8\pi P_\parallel}{B^2}\frac{u_{xe}}{u_{xi}}(enB_z u_{yi}) - \frac{2}{3}\frac{\nu_i}{u_{xi}}(P_\perp - P_\parallel) - \frac{2\frac{m_e}{m_i}\nu_e(P_\parallel - P_e)}{u_{xi}}$$

$$- \frac{1}{u_{xi}}\frac{\partial q_{yi}^\parallel}{\partial y}$$

d) $$\frac{\partial P_e}{\partial x} = \frac{5}{3}\frac{P_e}{n}\frac{\partial n}{\partial x} - \frac{2\frac{m_e}{m_i}\nu_e}{u_{xe}}\left(P_e - \frac{2}{3}P_\perp - \frac{1}{3}P_\parallel\right) + \frac{2}{3}\frac{\eta J^2}{u_{xe}}$$

$$- \frac{2}{3u_{xe}}\frac{\partial q_{ye}}{\partial y}$$

e) $$\frac{\partial u_{xi}}{\partial x} = - \frac{u_{xi}}{n}\frac{\partial n}{\partial x} - \Gamma_i$$

f) $$\frac{\partial u_{xe}}{\partial x} = - \frac{u_{xe}}{n}\frac{\partial n}{\partial x} - \Gamma_e$$

$$
\text{II.62}\quad \begin{cases}
\text{g)}\quad \dfrac{\partial B_y}{\partial x} = 4\pi J_z \\[2ex]
\text{h)}\quad \dfrac{\partial B_z}{\partial x} = -\,4\pi e n u_{yi} \\[2ex]
\text{i)}\quad \dfrac{\partial u_{zi}}{\partial x} = \dfrac{eB_y}{m_i}\left(\dfrac{u_{xi}-u_{xe}}{u_{xi}}\right)\left(1 - \dfrac{4\pi(P_{\parallel}-P_{\perp})}{B^2}\right) \\[2ex]
\text{j)}\quad \dfrac{\partial \phi}{\partial x} = -\dfrac{1}{en}\dfrac{\partial P_{\perp}}{\partial x} + u_{yi}B_z - u_{zi}B_y \\[2ex]
\text{k)}\quad u_{yi} = \dfrac{1}{enB_z}\left(\dfrac{\det - \sqrt{\det^2 - \dfrac{8}{3}\dfrac{\eta\alpha^2}{u_{xe}B_z^2}\,(\alpha_1\gamma_2-\alpha_2\gamma_1)}}{\dfrac{2}{3}\dfrac{\eta\alpha_2}{u_{xe}B_z^2}}\right) \\[2ex]
\text{l)}\quad J_z = \dfrac{E_z + u_{xe}B_y}{\eta} \\[2ex]
\text{m)}\quad \det = \alpha_1\beta_2-\alpha_2\beta_1
\end{cases}
$$

The quantities α_1, α_2, β_1, β_2, γ_1, γ_2 are defined in II.61c-h.

$\Gamma_{i,e} \equiv \frac{1}{n}\frac{\partial}{\partial y}(nu_{y:,e})$ = the annihilation flux.

Notice that some decoupling has occurred; the quantities:

II.63 $\partial u_{ez}/\partial y$, $\partial n/\partial y$, $\partial P_{\perp}/\partial y$, $\partial P_{\parallel}/\partial y$, $\partial P_e/\partial y$,

were not needed explicitly. This allows the set II.62 to be closed while some of the quantities II.63 remain indeterminate.

The equations II.62 constitute ten ordinary differential equations for the ten quantities:

II.64 n, $P_{\perp i}$, $P_{\parallel i}$, P_e, u_{xi}, u_{xe}, B_y, B_z, u_{zi}, ϕ

Equations II.62 apply to the region $x > x_0 \equiv$ the dividing point between open and closed field lines. The boundary conditions at x_0 for the ten variables II.64 are provided by matching the closed field line solution continuously to the open field line solution. Several other conditions must be satisfied by the open field line solution:

a) $n,\ P_\perp,\ P_\parallel,\ P_e \to 0$ as $x \to \infty$

b) $nu_{xi} \to 0$ <u>or</u> $\left(n(-\infty)u_x(-\infty) - \int_{x_0}^{\infty} n\Gamma_i dx = 0\right)$

c) $nu_{xe} \to 0$ <u>or</u> $\left(n(-\infty)u_x(-\infty) - \int_{x_0}^{\infty} n\Gamma_e dx = 0\right)$ as $x \to \infty$

d) $\underline{B} \to \underline{B}_{vac}$

e) $\phi \to \phi_0$

The conditions II.65a guarantee that a vacuum region exists at $x \to +\infty$. Conditions II.65b, c guarantee continuity of particles: the equal fluxes of ions and electrons entering the sheath at x_0 must be completely annihilated as $x \to +\infty$.

Conditions II.65b, c imply:

$$\text{II.66} \quad \int_{x_0}^{\infty} n\Gamma_i dx = \int_{x_0}^{\infty} n\Gamma_e dx \quad .$$

The <u>integrated</u> mirror losses of ions and electrons must be equal. This is less restrictive than in an ordinary mirror machine where the <u>local</u> losses must balance:[13]

II.67 $\Gamma_{i_{mirror}} = \Gamma_{e_{mirror}}$,

in order to satisfy quasineutrality. The additional degree of freedom in the sheath of flow across the field lines breaks the constraint II.67.

To explicitly integrate II.62, the annihilation fluxes $\Gamma_{i,e}$, $\frac{\partial}{\partial y} q^{\parallel}_{yi}$, $\frac{\partial}{\partial y} q^{\perp}_{yi}$, $\frac{\partial}{\partial y} q^{e}_{y}$ are needed. These quantities will be derived in chapter III.

CHAPTER III

In this chapter arguments based on mirror losses along the open field lines are used to determine the annihilation fluxes:

$$\text{III.1} \qquad \Gamma_i = \frac{1}{n}\frac{\partial}{\partial y} n u_{yi}\ , \quad \Gamma_e = \frac{1}{n}\frac{\partial}{\partial y} n u_{ye} = \text{particle fluxes}$$

$$\frac{\partial}{\partial y} q^{\perp}_{yi}\ , \quad \frac{\partial}{\partial y} q^{\parallel}_{yi}\ , \quad \frac{\partial}{\partial y} q_{ye} = \text{heat fluxes}$$

The final formulas for these quantities are not exact, but result from physically motivated approximations.

To relate the annihilation fluxes to the mirror loss rates, examine an infinitessimally thin slab of plasma of extent $-L/2 < y < L/2$ that is being convected across the sheath at velocity $u_x(x)$ (see Fig. 5). Plasma is lost from the slab at a rate:

$$\text{III.2} \qquad \frac{\partial N}{\partial t} = -\int_{-L/2}^{L/2} dy \left(\frac{\partial n}{\partial t}\right)_c \ ; \quad \left(\frac{\partial n}{\partial t}\right|_c = \text{local mirror loss rate}$$

N = total number of particles in the slab

And similarly energy is lost at the rate:

$$\text{III.3} \qquad \frac{\partial \varepsilon}{\partial t} = -\int_{-L/2}^{L/2} dy \left(\frac{\partial}{\partial t} n\langle\epsilon\rangle\right|_c dy$$

$$\varepsilon \equiv N\langle\epsilon\rangle\ ; \quad \left(\frac{\partial}{\partial t} n\langle\epsilon\rangle\right|_c = \text{mirror loss rate of energy}$$

ϵ = energy/particle

$= \dfrac{m_i v_\perp^2}{2}$ for ion perp. energy

$$\epsilon = \frac{m_e v^2}{2} \text{ for electron total energy}$$

Implicit in the formulas III.2, 3 is the assumption that the total losses from the slab are the sum of the losses from each point, i.e., particles do not scatter in and out of the loss cone, which is true when $r_p/\lambda_{mfp} \ll 1$.

The particle and energy losses are manifested as fluxes at the ends of the slab:

III.4

$$\text{a)} \quad nu_y\Big|_{L/2} - nu_y\Big|_{-L/2} = \frac{\partial N}{\partial t}$$

$$\text{b)} \quad (q_y + \langle\epsilon\rangle nu_y)\Big|_{L/2} - (q_y + \langle\epsilon\rangle nu_y)\Big|_{-L/2} = \frac{\partial \varepsilon}{\partial t}$$

The combination $q_y + \langle\epsilon\rangle nu_y$ appears because the heat flow q_y does not include <u>convective</u> loss of energy ($\langle\epsilon\rangle = \int d^3\underline{v}\epsilon f/n$, $q \sim \int d^3\underline{v}\ \epsilon f(\underline{v}-\underline{u})$).

In slab geometry the loss rates are independent of y and the fluxes are linear in y to lowest order in r_p/λ_{mfp} (see Chapter II, Sec. 2.2).

III.5

$$nu_y\Big|_{+L/2} - nu_y\Big|_{/L/2} = L\frac{\partial}{\partial y}(nu_y) = -\int \frac{\partial n}{\partial t}\Big|_c dy$$

$$= -L\frac{\partial n}{\partial t}\Big|_c$$

$$\Rightarrow$$

$$\frac{\partial}{\partial y} nu_y = -\frac{\partial n}{\partial t}\Big|_c$$

In a similar fashion the heat flux follows from III.4b:

$$\frac{\partial q_y}{\partial y} = -\left(\frac{\partial n}{\partial t}\langle\epsilon\rangle\right|_c - \frac{\partial}{\partial y}\left(\langle\epsilon\rangle\, n u_y\right)$$

III.6

$$= -\left(\frac{\partial n}{\partial t}\langle\epsilon\rangle\right|_c + \langle\epsilon\rangle\left(\frac{\partial n}{\partial t}\right|_c - \underbrace{n u_y \frac{\partial\langle\epsilon\rangle}{\partial y}}_{\mathcal{O}\left(\frac{\rho_i}{\Delta_s}\right)}$$

The last term on the right hand side of III.6 may be dropped to lowest order in ρ_i/Δ_s since $u_y = \mathcal{O}(\rho_i/\Delta_s)$.

To obtain explicit expressions for the annihilation fluxes, estimates for

$$\left(\frac{\partial n\langle\epsilon\rangle}{\partial t}\right|_c, \left(\frac{\partial n}{\partial t}\right|_c,$$

must be obtained. A complication arises when the sheath is $\sim\rho_i$ in thickness: the ion losses are not dependent on local quantities only since an ion samples a wide range of plasma parameters in the course of an orbit. This effect will be ignored, consistent with the approximation $\rho_i/\Delta_s \ll 1$ used in truncating the hierarchy of fluid equations (see Chapter II, Sec. 2.1), so the mirror losses will be determined by local parameters only.

The mirror loss rates for electrons have been calculated by Pastukhov[30] and R. Cohen, et al[31] in the electrostatically confined limit, $T_e/e\phi \ll 1$:

$$\text{III.7}\quad \begin{cases} \text{a)}\ \left.\frac{\partial n}{\partial t}\right|_c = -3n\nu_{ei}\left(\frac{2R}{2R+1}\right)\frac{e^{-e\phi/T_e}}{\ln(4R+2)}\ T_e/e\phi \qquad (z=1\ \text{assumed}) \\ \text{b)}\ \left.\frac{\partial}{\partial t}\left(\frac{3}{2}nT_e\right)\right|_c = (e\phi+T_e)\left(\left.\frac{\partial n}{\partial t}\right|_c\right. \end{cases}$$

The physical interpretation of the dominant terms in these expressions is simple: only particles near the top of the potential barrier, $mv^2/2 \sim e\phi$, can be scattered out of the electrostatic well (see Fig. 6), hence the classical mirror losses are reduced roughly by the ratio of the velocity space density near the top of the well to the velocity space density at $mv^2/2 \cong T_e$:

$$\text{III.8}\quad \left.\frac{\partial n}{\partial t}\right|_c \sim \nu_e\left(\frac{f\left(\frac{mv^2}{2}=e\phi\right)}{f\left(\frac{mv^2}{2}=T_e\right)}\right)\sim\nu_e\ e^{-e\phi/T_e}$$

When electrons leave the confined region, they take along energy:

$$\text{III.9}\quad \frac{\partial}{\partial t}\left(\frac{3}{2}nT_e\right|_c = \left(\frac{\text{Parallel energy}}{\text{Scattered particle}} + \frac{\text{Perpendicular energy}}{\text{Scattered particle}}\right)\left(\left.\frac{\partial n}{\partial t}\right|_c\right.$$

The parallel energy/scattered particle $\cong e\phi$

The perpendicular energy/scattered particle $\cong T_e/2 + T_e/2 = T_e$ ($1/2\ T_e$ for each degree of freedom)

$$\rightarrow \frac{\partial}{\partial t}\left(\frac{3}{2}nT_e\right|_c = (e\phi + T_e)\left(\left.\frac{\partial n}{\partial t}\right|_c\right.$$

in agreement with III.7b.

When the confining electrostatic well is negligibly shallow, $e\phi/T_e < 1$, the electron loss rate approaches that obtained by Futch,

et al.[13] for magnetically confined particles:

$$\text{III.10}\quad \begin{cases} \left.\dfrac{\partial n}{\partial t}\right|_c = -\dfrac{n\nu_{e_{tot}}}{4\log_{10}R} \cong -\dfrac{2.03n\nu_{ei}}{4\log_{10}R} \\[2ex] \dfrac{\partial}{\partial t}\left(\dfrac{3}{2}\,nT_e\right)_c = (e\phi+T_e)\left.\dfrac{\partial n}{\partial t}\right|_c \end{cases}$$

(add e-e collisions using Spitzer's self-collision rate.[32])

To obtain an approximate expression valid for all $e\phi/T_e$, an interpolation is made between the Pastukhov and Futch formulas:

$$\text{III.11}\quad \begin{cases} \text{a)}\ \left.\dfrac{\partial n}{\partial t}\right|_c = \left.\dfrac{\partial n}{\partial t}\right|_{\text{Pastukhov}} \left(\dfrac{\tanh\left(\lambda\left(\frac{e\phi}{T_e}-1\right)\right)+1}{2}\right) \\[2ex] \qquad + \left.\dfrac{\partial n}{\partial t}\right|_{\text{Futch}} \left(\dfrac{\tan\left(\lambda\left(\frac{T_e}{e\phi}-1\right)\right)+1}{2}\right) \\[2ex] \text{b)}\ \dfrac{\partial}{\partial t}\ \dfrac{3}{2}\,nT_e\ \Big|_c = (\phi+T_e)\left.\dfrac{\partial n}{\partial t}\right|_c \end{cases}$$

The ion temperature is generally assumed to satisfy $e\phi/T_{\perp i} \ll 1$ in mirror machines, yielding a loss rate:

$$\text{III.12}\quad \left.\frac{\partial n}{\partial t}\right|_c = -\frac{n\nu_i}{4\log_{10}R}$$

If $e\phi/T_{\perp i} \sim 1$, the potential has a strong effect on ion losses due to the large hole formed in velocity space (see Fig. 6). In addition to increasing the volume of the loss region in velocity space, the presence of a large potential narrows the structure of the confined region, thereby increasing the effective collision frequency, i.e., small angle Coulomb collisions can deplete a narrow structure at a rate

faster than ν_{ii}, the 90° scattering rate.

To obtain a rough estimate of the effect of a large potential, $e\phi/T_{\perp i} \sim 1$, on the ion loss rate, consider the projected distribution function:

$$\text{III.13} \qquad g(v_\perp) \equiv \int_{-\infty}^{\infty} dv_\parallel f(v_\perp, v_\parallel)$$

The distribution function g is depicted qualitatively in Fig. 7. $g = 0$ for $0 < v_\perp < v_0 \equiv \sqrt{2e\phi/m_i(R-1)}$ and the characteristic velocity scale is $\Delta v_\perp$. The maximum value of g is g_0.

The moments of the distribution function do not depend strongly on the fine scale velocity space structure, so they may be calculated approximately from the distribution $\bar{g}(v_\perp)$ depicted in Fig. 7:

$$\text{III.14} \qquad \bar{g}(v_\perp) = \begin{cases} 0 & 0 < v_\perp < v_0 \\ g_0\, v_0/v_\perp & v_0 < v_\perp < v_0 + \Delta v_\perp \\ 0 & v_\perp > v_0 + \Delta v_\perp \end{cases}$$

$\Delta v_\perp$ is chosen so that

$$\int dv_\perp v_\perp \bar{g} = \int dv_\perp v_\perp g = n \Rightarrow$$

$$\text{III.15} \qquad n = g_0 v_0 \Delta v_\perp$$

The perpendicular pressure is given by:

$$nT_\perp \cong \int dv_\perp v_\perp \frac{mv_\perp^2}{2} g = mg_0 v_0 \int_{v_0}^{v_0+\Delta v_\perp} dv_\perp \; v_\perp^2/2$$

III.16

$$= \frac{mg_0 v_0}{2}\left(v_0^2 \Delta v_\perp + v_0 \Delta v_\perp^2 + \frac{\Delta v_\perp^3}{3}\right)$$

In the regime of interest $e\phi/T_\perp \gtrsim 1$, so $v_0 \gtrsim \Delta v_\perp$. Accordingly, the last term on the right hand side of III.16 is dropped:

III.17 $$nT_\perp \cong \frac{m_i g_0 v_0}{2}\left(v_0^2 \Delta v_\perp + v_0 \Delta v_\perp^2\right) = \frac{nm}{2}\left(v_0^2 + v_0 \Delta v_\perp\right)$$

Coulomb collisions generate a Fokker-Planck collision operator, which is modeled roughly by a diffusion equation:

III.18 $$\frac{\partial g}{\partial t} = \frac{1}{v_\perp}\frac{\partial}{\partial v_\perp} v_\perp D \frac{\partial}{\partial v_\perp} g$$

An estimate of the collisional losses is obtained from III.18:

$$\left.\frac{\partial n}{\partial t}\right|_c \cong \int_0^\infty dv_\perp \frac{\partial}{\partial v_\perp} v_\perp D \frac{\partial g}{\partial v_\perp}$$

III.19

$$= - v_0 D(v_0) \left.\frac{\partial g}{\partial v_\perp}\right|_{v_0} \sim - \frac{v_0 D g_0}{\Delta v_\perp} = - \frac{Dn}{\Delta v_\perp^2} \quad \text{from III.15}$$

All that is needed is an estimate of $\Delta v_\perp$. From III.17:

$$T_\perp - \frac{mv_0^2}{2} = \frac{mv_0 \Delta v_\perp}{2} \Rightarrow$$

III.20 $$\frac{\Delta v_\perp}{v_0} = \frac{T_\perp}{mv_0^2/2} - 1 = \frac{(R-1)T_{\perp i}}{e\phi} - 1$$

Using III.20 in III.19 yields:

$$\text{III.21} \qquad \left.\frac{\partial n}{\partial t}\right|_c \sim -\frac{D}{v_t^2}\,\frac{n\left(\frac{e\phi}{(R-1)T_\perp}\right)}{\left(1-\frac{e\phi}{(R-1)T_{\perp i}}\right)^2}\,,\quad v_t^2 \equiv \frac{2T_\perp}{m}$$

The diffusion coefficient is related to the collision frequency via $D/v_t^2 \sim \nu_i$. The expression III.21 does not include the loss cone scattering contribution, since only the integrated distribution function $g(v_\perp) = \int_{-\infty}^{\infty} dv_\parallel f(v_\parallel, v_\perp)$ was treated. The usual loss term may be incorporated in a simple way so that the loss rate approaches the correct limit as $e\phi/T_{\perp i} \to 0$:

$$\text{III.22} \qquad \left(\frac{\partial n}{\partial t}\right|_c = -\,n\nu_i\,\frac{\left(\frac{1}{4\log_{10}R} + \frac{e\phi}{(R-1)T_{\perp i}}\right)}{(1-e\phi/(R-1)T_{\perp i})^2}$$

As $e\phi/(R-1)T_i \to 1$, III.22 predicts infinite ion annihilation. In reality, ions can leave the device no faster than the transit time so that an upper bound on $|\partial n/\partial t|_c|$ is:

$$\text{II.22a} \qquad \left|\left.\frac{\partial n}{\partial t}\right|_c\right| < \frac{n v_{th\parallel}}{L_{\substack{\text{field}\\ \text{line}}}} = \frac{n v_{th\parallel}}{r_p}\,\frac{B_y}{B} \quad \left(L_{\text{field line}} = \text{length of field line} = r_p B/B_y\right)$$

An estimate of the rate of energy loss for the ions follows from the model equation III.18

$$\text{III.23}\quad \left\{\begin{aligned}
\frac{\partial}{\partial t} n\left\langle\frac{mv_\perp^2}{2}\right\rangle_c &\equiv \left(\frac{\partial}{\partial t} nT_\perp\right)\Bigg|_c = \int_{v_0}^{\infty} \frac{mv_\perp^2}{2}\frac{\partial}{\partial v_\perp} v_\perp D \frac{\partial}{\partial v_\perp} g\, dv_\perp \\
&= \frac{mv_\perp}{2} v_\perp D \frac{\partial g}{\partial v_\perp}\Bigg|_{v_0}^{\infty} - \int_{v_0}^{\infty} m dv_\perp\, v_\perp^2\, D \frac{\partial g}{\partial v_\perp} \\
&= \frac{mv_0^2}{2}\left(\frac{\partial n}{\partial t}\Bigg|_c - \left(\underbrace{\cancel{mgv_\perp^2 D}\Big|_0^\infty}_{0} + \int_{v_0}^{\infty} m dv_\perp g \frac{\partial}{\partial v_\perp} v_\perp^2 D\right)\right) \\
&= \frac{mv_0^2}{2}\left(\frac{\partial n}{\partial t}\Bigg|_c - O\left(mD\int v_\perp dv_\perp g\right)\right) \\
&= \frac{mv_0^2}{2}\left(\frac{\partial n}{\partial t}\Bigg|_c - O\left(\frac{m\Delta v_\perp^2}{2}\left(\frac{\partial n}{\partial t}\Bigg|_c\right)\right)\right. \text{ from III.19}
\end{aligned}\right.$$

As in III.17, the $\Delta v_\perp^2$ term is dropped

$$\text{III.24}\qquad \frac{\partial}{\partial t} n\left\langle\frac{mv_\perp^2}{2}\right\rangle_c \cong \frac{mv_0^2}{2}\left(\frac{\partial n}{\partial t}\Bigg|_c\right.$$

Equation III.24 has a simple interpretation: ions remove energy $mv_0^2/2$ when scattered down into the potential hole.

For parallel ion energy, a simple estimate of the loss is:

$$\text{III.25}\qquad \frac{\partial}{\partial t} n\left\langle\frac{mv_\parallel^2}{2}\right\rangle\Bigg|_c \equiv \frac{\partial}{\partial t}\left(\frac{nT_\parallel}{2}\Bigg|_c\right. \cong \frac{T_\parallel}{2}\left(\frac{\partial n}{\partial t}\Bigg|_c\right.$$

The determination of the annihilation fluxes is now complete; substituting III.11, 22, 24, 25 into III.5,6 yields:

III.26

a) $$\Gamma_e = -\frac{1}{n}\frac{\partial n}{\partial t}\bigg|_c$$

b) $$\frac{\partial q_{ye}}{\partial y} = -\left(\frac{\partial}{\partial t} n\left\langle\frac{m_e v^2}{2}\right\rangle\right)_c + \left\langle\frac{m_e v_e^2}{2}\right\rangle \frac{\partial n}{\partial t}\bigg|_c$$

$$= -(e\phi + T_e - \frac{3}{2}T_e)\left(\frac{\partial n}{\partial t}\bigg|_c\right.$$

$$= -(e\phi - T_e/2)\, n\Gamma_e$$

c) $$\Gamma_i = -\frac{1}{n}\frac{\partial n}{\partial t}\bigg|_c$$

$$= \nu_{ii}\frac{\left(\frac{1}{4\log_{10}R} + \frac{e\phi}{(R-1)T_{\perp i}}\right)}{\left(1 - \frac{e\phi}{(R-1)T_{\perp i}}\right)^2}$$

d) $$\frac{\partial q_{yi}^{\perp}}{\partial y} = -\left(\frac{\partial}{\partial t} nT_\perp\right)_c + T_{\perp i}\left(\frac{\partial n}{\partial t}\bigg|_c\right.$$

$$= T_{\perp i}\left(\frac{-mv_0^2}{2T_{\perp i}} + 1\right)\left(\frac{\partial n}{\partial t}\bigg|_c\right.$$

$$= T_{\perp i}\left(1 - \frac{e\phi}{(R-1)T_{\perp i}}\right)\left(\frac{\partial n}{\partial t}\bigg|_c\right.$$

$$= \frac{-n\nu_{ii}T_{\perp i}\left(\frac{1}{4\log_{10}R} + \frac{e\phi}{(R-1)T_{\perp i}}\right)}{(1 - e\phi/(R-1)T_{\perp i})}$$

e) $$\frac{\partial q_{yi}^{\parallel}}{\partial y} = -\left(\frac{\partial}{\partial t}\frac{nT_\parallel}{2}\bigg|_c\right. + \frac{T_{\parallel i}}{2}\left(\frac{\partial n}{\partial t}\bigg|_c\right. = 0$$

Note that the ion perpendicular heat flow is <u>negative</u>. This results from the fact that ions must scatter downward in perpendicular energy in order to leave the system. The ions that exit the device do so with less than the average perpendicular energy, resulting in perpendicular ion heating.

The electron losses given in III.26a, b must be modified if a significant ammount of electron "recycling" occurs. Hot plasma streaming out along the field lines ultimately impacts on a wall where it cools off and vaporizes some of the wall material. The electrons from the resulting accumulation of cold plasma can fall back down the electrostatic potential well and re-enter the main plasma volume, i.e., they are "recycled." A simple model of this effect consists of multiplying the electron loss rate by a phenomenological term:

$$\text{III.27} \qquad \Gamma_e \rightarrow -\frac{1}{n}\left(\frac{\partial n}{\partial t}\right)_c (1 - \alpha)$$

$\alpha \equiv$ fraction of cold electrons re-entering from the walls (taken to be a constant for simplicity)

To estimate the effect of electron "recycling" on energy balance, note that the hot electrons leave carrying energy:

$$\frac{\partial}{\partial t}\left(\frac{3}{2} nT_e\right)_c = (e\phi + T_e)\left(\frac{\partial n}{\partial t}\right)_c$$

Whereas the cold electrons return energy from the walls:

$$\frac{\partial}{\partial t}\left(\frac{3}{2} n\, T_e\right)_{walls} = -\alpha e\phi \left(\frac{\partial n}{\partial t}\right)_c ,$$

Resulting in:

III.28 $$\frac{\partial}{\partial t}\left(\frac{3}{2}\, n\, T_e\right)\Big|_{Total} = \left(e\phi + \frac{T_e}{1-\alpha}\right)\left(\frac{\partial n}{\partial t}\right)(1-\alpha)$$

The heat flux is given by:

III.29 $$\frac{\partial q_{ye}}{\partial y} = \left(\frac{\partial}{\partial t}\ \frac{3}{2}\, n\, T_e\Big|_c - \frac{3}{2}\, T_e\left(\frac{\partial n}{\partial t}\Big|_c (1-\alpha)\right.$$

$$= \left(e\phi + \frac{T_e}{2}\,\frac{(3\alpha-1)}{(1-\alpha)}\right)\Gamma_e$$

For $1 > \alpha > 1/3$ the second term in the brackets is positive, i.e., it represents extra electron cooling. For $\alpha \to 1$, the ratio

III.30 $$\frac{\frac{\partial}{\partial y}\, q_{ye}}{\frac{3}{2}\, n\, T_e \Gamma_e} \to \infty$$

This indicates that the energy lost/particle greatly exceeds the average energy/particle: the cold electrons from the wall provide an infinite energy sink as the fraction of "recycled" electrons approaches unity.

The development of the annihilation model is now complete. The explicit annihilation terms III.26, 27, 29 may be used in the differential equations II.62.

In Chapter IV, the integration of the equations is performed by starting from the asymptotic solutions, $x \to -\infty$, and numerically integrating the equations across the sheath.

CHAPTER IV

4.1

In this chapter, the annihilation equations are integrated for various values of plasma parameters and the resulting solutions are discussed. The development of analytical solutions is limited by the strongly coupled, highly non-linear nature of the equations II.47, 62. Analytic methods will be used to gain qualitative insights and to determine the asymptotic variation of the dependent variables, but numerical techniques must be resorted to in order to obtain detailed solutions.

The first step is to convert II.47, 62 into dimensionless form, using appropriate normalizations for the variables. A natural set of normalizations is the following:

$$\text{IV.1}\quad \begin{cases} n \to \dfrac{n(x)}{n(-\infty)} \quad T_{\perp,\parallel,e} \to \dfrac{T_{\perp,\parallel,e}(x)}{T_B} \quad u_{xi,e} \to \dfrac{u_{xi,e}(x)}{\rho_i \bar{\nu}_i} \\[2ex] \underline{B} \to \dfrac{\underline{B}(x)}{|\underline{B}(-\infty)|} \quad u_{zi} \to \dfrac{u_{zi}}{\sqrt{T_B/m_i}} \quad \phi \to \dfrac{e\phi}{T_B} \\[2ex] x \to x/\rho_i \quad \underline{J} \to \dfrac{\underline{J}}{en(-\infty)\sqrt{T_B/m_i}} \quad E_{y,z} \to \dfrac{E_{y,z}}{\rho_i \bar{\nu}_i |\underline{B}|(-\infty)} \end{cases}$$

where $\rho_i = \dfrac{\sqrt{m_i T_B}}{e|B(-\infty)|}$ $\quad \bar{\nu}_i = \dfrac{4}{3}\dfrac{\sqrt{\pi}}{\sqrt{m_i}}\dfrac{e^4 n(-\infty)}{T_B^{3/2}}\ln\Lambda$

$$T_B \equiv \frac{|B^2|(-\infty)}{8\pi n(-\infty)}$$

The dimensionless closed field line equations are obtained from II.47:

IV.2

a) $$\frac{\partial n}{\partial x} = \frac{n}{2P_\perp + \frac{5}{3}P_e}\left(\frac{(\nu_i+\nu_{ie})}{3u_x}(P_\perp - P_\parallel) - \frac{2\eta J^2}{3u_x} + J_yB_z - J_zB_y\right)$$

b) $$\frac{\partial P_\perp}{\partial x} = \frac{2P_\perp}{n}\frac{\partial n}{\partial x} - \frac{\nu_i}{3u_x}(P_\perp - P_\parallel) - \frac{\nu_{ie}}{u_x}(P_\perp - P_e)$$

c) $$\frac{\partial P_\parallel}{\partial x} = \frac{P_\parallel}{n}\frac{\partial n}{\partial x} - \frac{2}{3}\frac{\nu_i}{u_x}(P_\parallel - P_\perp) - \frac{\nu_{ie}}{u_x}(P_\parallel - P_e)$$

d) $$\frac{\partial P_e}{\partial x} = \frac{5}{3}\frac{P_e}{n}\frac{\partial n}{\partial x} + \frac{2}{3u_x}\eta J^2 - \frac{\nu_{ie}}{u_x}(P_e - \frac{2}{3}P_\perp - P_\parallel/3)$$

e) $$\frac{\partial u_x}{\partial x} = -\frac{u_x}{n}\frac{\partial n}{\partial x}$$

f) $$\frac{\partial B_y}{\partial x} = \frac{J_z}{2}$$

g) $$\frac{\partial B_z}{\partial x} = -\frac{J_y}{2}$$

h) $$\frac{\partial \phi}{\partial x} = \frac{1}{n}\frac{\partial P_\perp}{\partial x} + \frac{P_\perp}{2n^2}\frac{\partial n}{\partial x}$$

i) $$J_z = \frac{E_z + u_xB_y}{\eta}$$

j) $$J_y = \frac{E_y - u_xB_z}{\eta}$$

Where the parameters η, ν_i, ν_{ie}, ν_e are redefined by:

IV.3 a) $$\eta \rightarrow \frac{n(-\infty)e^2}{m_i\bar{\nu}_i}\eta = \frac{m_e}{m_i}\frac{1}{n}\left(\frac{\nu_e}{\bar{\nu}_i}\right) = \sqrt{2}\sqrt{\frac{m_e}{m_i}}\ \frac{1}{T_e^{3/2}}$$

in normalized variables

$$\text{IV.3}\quad \begin{cases} \text{b)}\quad \nu_i \to \dfrac{\nu_i}{\bar{\nu}_i} = \dfrac{n}{(2T_\perp/3 + T_\parallel/3)^{3/2}} \\[2ex] \text{c)}\quad \nu_{ie} \Rightarrow 2\,\dfrac{m_e}{m_i}\,\dfrac{\nu_e}{\bar{\nu}_i} = 2\sqrt{2}\,\sqrt{\dfrac{m_e}{m_i}}\;\; n/T_e^{\,3/2} \\[2ex] \text{d)}\quad \nu_e \to \dfrac{\nu_e}{\bar{\nu}_i} = \sqrt{2}\,\sqrt{\dfrac{m_i}{m_e}}\;\; n/T_e^{\,3/2} \end{cases}$$

The dimensionless open field line equations are obtained from II.62:

$$\text{IV.4}\quad \begin{cases} \text{a)}\quad \dfrac{\partial n}{\partial x} = \dfrac{n(\beta_2\gamma_1 - \beta_1\gamma_2)}{\det} - \dfrac{\frac{2}{3}\eta\, n^3 \beta_2 u_{yi}^2}{u_{xe}\,\det} \\[2ex] \text{b)}\quad \dfrac{\partial P_\perp}{\partial x} = \dfrac{2P_\perp}{n}\left(1 - \dfrac{u_{xe}}{2u_{xi}}\dfrac{B_z^2}{B^2}\right)\dfrac{\partial n}{\partial x} + \dfrac{P_\perp}{u_{xi}}\left(\Gamma_i - \dfrac{B_z^2}{B^2}\,\Gamma_e\right) \\[2ex] \qquad - \dfrac{P_\perp}{2B^2}\dfrac{u_{xe}}{u_{xi}}\, n B_z u_{yi} - \dfrac{\nu_i}{3u_{xi}}\,(P_\perp - P_\parallel) - \dfrac{\nu_{ie}(P_\perp - P_e)}{u_{xi}} \\[2ex] \qquad - \dfrac{1}{u_{xi}}\dfrac{\partial q_{yi}^{\perp}}{\partial y} \\[2ex] \text{c)}\quad \dfrac{\partial P_\parallel}{\partial x} = \dfrac{P_\parallel}{n}\left(1 + \dfrac{2u_{xe}}{u_{xi}}\dfrac{B_z^2}{B^2}\right)\dfrac{\partial n}{\partial x} - \dfrac{2P_\parallel}{u_{xi}}\left(\Gamma_i - \dfrac{B_z^2}{B^2}\,\Gamma_e\right) \\[2ex] \qquad + \dfrac{P_\parallel}{B^2}\dfrac{u_{xe}}{u_{xi}}\, n\, B_z u_{yi} - \dfrac{2}{3}\dfrac{\nu_i}{u_{xi}}\,(P_\parallel - P_\perp) - \dfrac{\nu_{ie}}{u_{xi}}\,(P_\parallel - P_e) \\[2ex] \text{d)}\quad \dfrac{\partial P_e}{\partial x} = \dfrac{5}{3}\dfrac{P_e}{n}\dfrac{\partial n}{\partial x} - \dfrac{\nu_{ie}}{u_{xe}}\left(P_e - \dfrac{2P_\perp}{3} - \dfrac{P_\parallel}{3}\right) + \dfrac{2}{3}\dfrac{\eta J^2}{u_{xe}} - \dfrac{2}{3u_{xe}}\dfrac{\partial q_{ye}}{\partial y} \end{cases}$$

IV.4

e) $$\frac{\partial u_{xi}}{\partial x} = -\frac{u_{xi}}{n}\frac{\partial n}{\partial x} - \Gamma_i$$

f) $$\frac{\partial u_{xe}}{\partial x} = -\frac{u_{xe}}{n}\frac{\partial n}{\partial x} - \Gamma_e$$

g) $$\frac{\partial B_y}{\partial x} = \frac{J_z}{2}$$

h) $$\frac{\partial B_z}{\partial x} = -\frac{J_y}{2} = -\frac{n u_{yi}}{2}$$

i) $$\frac{\partial u_{zi}}{\partial x} = B_y\left(\frac{u_{xi}-u_{xe}}{u_{xi}}\right)\left(1 - \frac{(P_\parallel - P_\perp)}{2B^2}\right)$$

j) $$\frac{\partial \phi}{\partial x} = -\frac{1}{n}\frac{\partial P_\perp}{\partial x} + u_{yi}B_z - u_{zi}B_y$$

k) $$u_{yi} = \frac{1}{nB_z}\left(\frac{\det - \sqrt{\det^2 - \frac{8}{3}\frac{\eta\alpha_2}{u_{xe}B_z^2}(\alpha_1\gamma_2 - \alpha_2\gamma_1)}}{(2/3\,\eta\,\alpha_2/u_{xe}B_z^2)}\right)$$

l) $$J_z = \frac{E_z + u_{xe}B_y}{\eta}$$

m) $$\alpha_1 = 2P_\perp\left(1 - \frac{u_{xe}}{2u_{xi}}\frac{B_z^2}{B^2}\right) + \frac{5}{3}P_e$$

n) $$\alpha_2 = 2P_\perp\left(1 - \frac{u_{xe}}{2u_{xi}}\frac{B_z^2}{B^2}\right) - P_\parallel\left(1 + \frac{2u_{xe}}{u_{xi}}\frac{B_z^2}{B^2}\right)$$

o) $$\beta_1 = -\left(1 + \frac{P_\perp}{2B^2}\frac{u_{xe}}{u_{xi}}\right)$$

IV.4

p) $$\beta_2 = -\left(\frac{B^2}{B_z^2}\left(1 - \frac{1}{2}\frac{(P_\parallel - P_\perp)}{B^4}(B_y^2 - B_z^2)\right) + \frac{(P_\parallel + P_\perp/2)}{B^2}\frac{u_{xe}}{u_{xi}}\right)$$

r) $$\gamma_1 = -\frac{P_\perp}{u_{xi}}\left(\Gamma_i - \frac{B_z^2}{B^2}\Gamma_e\right) + \frac{\nu_i}{3u_{xi}}(P_\perp - P_\parallel) + \frac{\nu_{ie}}{u_{xi}}(P_\perp - P_e)$$

$$+ \frac{1}{u_{xi}}\frac{\partial q_{yi}^\perp}{\partial y} + \frac{2}{3u_{xe}}\frac{\partial q_{ye}}{\partial y} + \frac{\nu_{ie}}{u_{xe}}\left(P_e - \frac{2}{3}P_\perp - \frac{P_\parallel}{3}\right)$$

$$- \frac{2}{3}\frac{\eta J_z^2}{u_{xe}} - J_z B_y$$

s) $$\gamma_2 = -\frac{(2P_\parallel + P_\perp)}{u_{xi}}\left(\Gamma_i - \frac{B_z^2}{B^2}\Gamma_e\right) - \frac{2}{3}\frac{\nu_i}{u_{xi}}(P_\parallel - P_\perp)$$

$$- \frac{\nu_{ie}}{u_{xi}}(P_\parallel - P_e) + \frac{\nu_i}{3u_{xi}}(P_\perp - P_\parallel) + \frac{\nu_{ie}}{u_{xi}}(P_\perp - P_e)$$

$$+ \frac{1}{u_{xi}}\frac{\partial q_{yi}^\perp}{\partial y} - \frac{(P_\parallel - P_\perp)}{B^2}J_z B_y$$

t) $$\det = \alpha_1\beta_2 - \alpha_2\beta_1$$

Several more normalizations have been introduced:

IV.5 $$\Gamma_{i,e} \to \frac{\Gamma_{i,e}}{\bar{\nu}_i} \qquad \frac{\partial q_y^{\perp,\parallel,e}}{\partial y} \Rightarrow \frac{\frac{\partial q_y^{\perp,\parallel,e}}{\partial y}}{n(-\infty)\Gamma_B\bar{\nu}_i}$$

The quantities $\Gamma_{i,e}$, $\partial q_y^{\perp,\parallel,e}/\partial y$ are given in equations III.26, 27, 29.

The equations IV.2, 4 are <u>almost</u> invariant under the following

scaling transformation:

$$\text{IV.6}\quad \begin{cases} \nu_i,\ \nu_{ie},\ \Gamma_i,\ \Gamma_e,\ \dfrac{\partial q_{yi}}{\partial y},\ \dfrac{\partial q_{ye}}{\partial y} \to s\left(\nu_i,\ \nu_{ie},\ \Gamma_i,\ \Gamma_e,\ \dfrac{\partial q_{yi}}{\partial y},\ \dfrac{\partial q_{ye}}{\partial y}\right) \\ \eta \to t\eta \quad u_{xi},\ u_{xe} \to \sqrt{ts}\,(u_{xi}, u_{xe}) \\ J_y,\ J_z,\ u_{yi},\ u_{zi} \to \sqrt{s/t}\,(J_y,\ J_z,\ u_{yi},\ u_{zi}) \\ E_y,\ E_z, \to \sqrt{st}\,(E_y,\ E_z) \qquad x \to \sqrt{t/s}\,x \end{cases}$$

The equations are not invariant under the scaling, IV.6, because of IV.4i, the equation of evolution for the toroidal ion flow velocity. The transformation IV.6 corresponds physically to the fact that the erosion rate is related to the length scale and loss rate via the continuity equations, IV.4e, f.

$$\text{IV.7}\qquad u_x \sim \nu_{loss}\Delta_s \ . \quad (\nu_{loss} \sim \Gamma_i, \Gamma_e)$$

The erosion rate, length scale and resistivity are related by the magnetic diffusion equation or equivalently IV.4g, 1:

$$\text{IV.8}\qquad \frac{B_y}{\Delta_s} \sim \frac{u_x B_y}{\eta} \Rightarrow u_x\Delta_s \sim \eta$$

Combining the estimates IV.7, 8 gives

$$\text{IV.9}\qquad u_x \sim \sqrt{\eta\nu_{loss}} \qquad \Delta_s \sim \sqrt{\frac{\eta}{\nu_{loss}}}$$

as discussed in the introduction. Letting $\nu_{loss} \to s\nu_{loss}$ and $\eta \to t\eta$ in IV.9 gives the scaling law:

$$u_x \to \sqrt{st}\,u_x\ , \quad \Delta_s \to \sqrt{t/s}\,\Delta_s\ ,$$

which is identical to the transformation IV.6.

The transformation fails for IV.4i because the characteristic scale in IV.4i is ρ_{ipol}, the ion gyroradius in the poloidal field. In dimensional units, IV.4i gives roughly:

$$\text{IV.10} \qquad \frac{\partial u_{zi}}{\partial x} \sim \frac{eB_y}{m_i c} \rightarrow u_{zi} \sim \frac{eB_y}{m_i c} \Delta_s \ .$$

The toroidal flow velocity couples to the other variables through the equation for ϕ_0, IV.4j. The term $\propto u_{zi}$ contributes significantly when:

$$\text{IV.11} \qquad \frac{1}{en} \frac{\partial P_\perp}{\partial x} \sim \frac{P_\perp}{en\Delta_s} \sim \frac{u_{zi}}{c} B_y$$

Combining IV.10, 11 yields an estimate of the minimum scale, Δ_{min}, for which u_{zi} plays an important role:

$$\text{IV.12} \qquad \Delta^2_{min} \cong \frac{P_\perp m_i c^2}{e^2 n B_y{}^2} \equiv \rho^2_{ipol}$$

For sheath widths, $\Delta_s < \rho_{ipol}$, the scaling of IV.4i is of minor importance since u_{zi} couples to the other variables only through a small term in IV.4j. The scaling transformation, IV.6, is then approximately valid, providing a useful tool for comparing classically collisional sheath solutions (some of which have $\Delta_s \ll \rho_i$, invalidating the theory) to anomalously collisional sheath solutions with $\Delta_s \sim \rho_i$ ($\eta \rightarrow t\eta$, $\nu_{loss} \rightarrow s\nu_{loss}$; $s,t \gtrsim 1$).

One consequence of the approximate scaling law IV.6 is that if instabilities driven by strong gradients in the sheath increase <u>both</u>

the resistivity and particle loss rates by comparable amounts ($\eta \to t\eta$, $\nu_{loss} \to t\nu_{loss}$) then the scaled solutions have the properties:

$$\text{IV.13} \quad \begin{cases} \Delta_{sscaled} = \sqrt{t/t}\,\Delta_{unscaled} = \Delta_{unscaled} \\ u_{iscaled} = \sqrt{tt}\,u_{unscaled} = tu_{unscaled}, \end{cases}$$

i.e., the sheath erodes faster but the gradients are <u>not</u> relaxed. For such a case a high level of fluctuations may be continually driven by the sharp gradients and the "eating in" rate may greatly exceed the classical value.

In general, in the presence of instabilities the resistivity and loss rate scale differently (ν_{lossi} and ν_{losse} may scale differently also); $\eta \to t\eta$, $\nu \to s\nu$, $s \neq t$. The most optimistic limit (optimistic in terms of the Tormac confinement time) is to take $\eta \to t\eta$, $\nu \to \nu$ so that the turbulence broadens the sheath enough to quench the instabilities, but does not enhance the particle loss rate.

Anomalous effects will be included in this thesis in a fashion somewhat more sophisticated than the simple scaling IV.6. Turbulence will be assumed to set in for $|\underline{v}_e - \underline{v}_i|$ greater than some critical value, v_{crit}. If the turbulence is assumed to be due to lower hybrid drift waves, then a simple model (suggested by H. Berk) similar to that used by N. Krall[33] is the following:

$$\text{IV.14} \qquad \text{a)} \quad \nu_e \to \nu_{eclass} + \begin{cases} 0 & |\underline{v}_e - \underline{v}_i| < v_{crit} \\ \alpha\omega_{pi}\dfrac{v^\lambda}{1+v^\lambda} & |v_e - v_i| > v_{crit} \end{cases}$$

IV.14 b) $\eta \rightarrow \frac{m_e \nu_e}{e^2 n}$ $\qquad v \equiv |v_e - v_i| - v_{crit}$

where
- λ is an ad hoc parameter = rate of rise of turbulent effects
- α is an ad hoc parameter $\alpha \lesssim 1$
- v_{crit} is an ad hoc parameter $v_{crit} \gtrsim v_{thi}$

The ions are assumed to be unaffected, in the spirit of the "optimistic" approach discussed above.

4.2

In order to perform the numerical integration of equations IV.2, 4 knowledge of the asymptotic state $x \rightarrow +\infty$ or $x \rightarrow -\infty$ is necessary. This is required because the numerical solution must have a finite point $x = \pm L$ $(L < \infty)$ as a starting point, otherwise:

IV.15 $$\left.\frac{d\underline{\xi}}{dx}\right|_{x=\pm\infty} \equiv 0 \qquad \underline{\xi} = (n, P_\perp, P_\parallel, P_e \ldots)$$

and the solution never gets off the ground. If the asymptotic solutions are known analytically they may be matched to the numerical solution at $x = \pm L$, providing the boundary values for the integration scheme:

IV.16 $$\underline{\xi} = \underline{\xi}_0(x = \pm L) \neq \underline{\xi}(x = \pm\infty)$$

$$\left.\frac{d\underline{\xi}}{dx}\right|_{x=L} = f(\underline{\xi}_0) \neq 0$$

Only one of the asympototic states is needed, either the large +x solution or the large -x solution. Large -x is chosen for the following reasons: 1) the closed field line equations are simpler, making the asymptotic analysis easier, 2) fewer quantities must be varied to

obtain solutions.

If the integration were begun at large positive x, the boundary conditions II.65 would be given and some quantities (ϕ_0, the potential at the edge of the sheath, the asymptotic temperatures, etc.) would be varied until the boundary conditions at large negative x, II.48, were met. From II.48, the quantities,

$$\text{IV.17} \qquad \frac{B_y}{B_z}(-\infty),\ n(-\infty),\ P_\perp(-\infty),\ P_\parallel(-\infty),\ P_e(-\infty),\ \frac{u_{xi}}{u_{xe}}(-\infty),$$

must assume prescribed values. Other boundary values appearing in II.48 are not prescribed but determined self consistently, i.e., $\phi(-\infty)$, the floating potential and $u_x(-\infty)$, the "eating in" rate. The magnitude of $\underline{B}(-\infty)$ is determined by pressure balance. Thus, when the integration is begun at large positive x, the six independent constraints IV.17 must be satisfied by varying six quantities (boundary values at large positive x, etc.).

When the integration is begun at large -x, the boundary conditions II.48 are given and some quantities must be varied until II.65 are satisfied. The conditions II.65 constitute 7 independent constraints (again ϕ_0 and $|\underline{B}|$ do not represent additional constraints):

$$\text{IV.18} \quad \begin{cases} n,\ P_\perp,\ P_\parallel,\ P_e \to 0 \text{ as } x \to +\infty \\ \\ \dfrac{B_y}{B_z}(+\infty),\ nu_{xi}\Big|_{+\infty} = 0,\ nu_{xe}\Big|_{+\infty} = 0 \end{cases}$$

however, the first four of them are nearly always satisfied, leaving only three constraints. The magnetic field constraint is usually

relaxed since the goal is to find "typical" solutions (one direction of the magnetic field in the y,z plane is as good as another). The constraint may be reapplied if it is desired to compare the theory directly to an experiment where the direction of the vacuum magnetic field is known. The two remaining constraints are:

$$\text{IV.19} \quad \left\{ \begin{array}{l} \text{a)} \quad nu_{xi} \to 0 \\ \\ \text{b)} \quad nu_{xe} \to 0 \\ \qquad \text{as } x \to \infty \end{array} \right\} \quad \text{or equivalently} \quad \left\{ \begin{array}{l} nu_x(-\infty) = \int_0^\infty n\Gamma_i dx \\ \\ nu_x(-\infty) = \int_0^\infty n\Gamma_e dx \end{array} \right.$$

i.e., the conditions that all of the electrons and ions entering the sheath be annihilated. The quantities $u_x(-\infty)$ (the "eating in" rate) and $\phi(-\infty)$ (the floating potential) are varied until equations IV.19 are satisfied.

The asymptotic equations for large -x may be derived from IV.2. The equations are linearized about the asymptotic values of the dependent variables:

$$\text{IV.20} \quad \left\{ \begin{array}{l} n = n(-\infty)(1-\delta n) \quad P_\perp = P_\perp(-\infty)(1+\delta P_\perp) \quad P_\parallel = P_\parallel(-\infty)(1+\delta P_\parallel) \\ P_e = P_e(-\infty)(1+\delta P_e) \quad u_{xi,e} = u_x(-\infty)(1+\delta u) \\ B_y = B_y(-\infty)(1+\delta B_y) \quad B_z = B_z(-\infty)(1+\delta B_z) \quad \phi = \phi(-\infty)+\delta\phi \end{array} \right.$$

The linearized closed field line equations are:

$$\text{IV.21} \quad \left\{ \begin{array}{l} \text{a)} \quad \frac{\partial}{\partial x}\delta n = -\frac{3}{\pi\Gamma}\left(\frac{\lambda_1}{3}(\delta P_\perp - \delta P_\parallel) - 2B_{y\infty}^2 \frac{\partial}{\partial x}\delta B_y - 2B_{z\infty}^2 \frac{\partial}{\partial x}\delta B_z\right) \\ \text{b)} \quad \frac{\partial}{\partial x}\delta B_y = \lambda_0(\delta u + \delta B_y) \end{array} \right.$$

$$\text{IV.21}\quad \begin{cases} \text{c)}\ \dfrac{\partial}{\partial x}\,\delta B_z = \lambda_0(\delta u + \delta B_z) \\[2ex] \text{d)}\ \dfrac{\partial}{\partial x}\,\delta P_\perp = 2T\,\dfrac{\partial}{\partial x}\,\delta n - \dfrac{\lambda_1}{3}\,(\delta P_\perp - \delta P_\parallel) \\[2ex] \text{e)}\ \dfrac{\partial}{\partial x}\,\delta P_\parallel = T\,\dfrac{\partial}{\partial x}\,\delta n + \dfrac{2}{3}\,\lambda_1\,(\delta P_\perp - \delta P_\parallel) \\[2ex] \text{f)}\ \dfrac{\partial}{\partial x}\,\delta P_e = \dfrac{5}{3}\,T\,\dfrac{\partial}{\partial x}\,\delta n \\[2ex] \text{g)}\ \delta u = \delta n \\[2ex] \text{h)}\ \dfrac{\partial}{\partial x}\,\delta\phi = -\,T\,\dfrac{\partial}{\partial x}\,\delta P_\perp - \dfrac{T}{2}\,\dfrac{\partial \delta n}{\partial x} \end{cases} \qquad \begin{cases} \lambda_0 \equiv \dfrac{u_x(-\infty)}{2n(-\infty)} \\[2ex] \lambda_1 \equiv \dfrac{\nu_i(-\infty)}{u_x(-\infty)} \\[2ex] T \equiv \dfrac{P_\perp(-\infty)}{n(-\infty)} \\[2ex] \text{ion-electron energy exchange is neglected} \\ \nu_{ie} \cong 0\ (T_e = T_i) \end{cases}$$

The set IV.21 may be easily solved to yield

$$\text{IV.22}\quad \begin{cases} \text{a)}\ \delta n = \delta n_0\, e^{\lambda(x-x_0)} \\[2ex] \text{b)}\ \delta P_e = -\,\dfrac{5}{3}\,\delta n \\[2ex] \text{c)}\ \delta P_\perp = \dfrac{5}{3}\,\delta n - \dfrac{2B_{z\infty}^2}{T}\,\delta B_z - \dfrac{2B_{y\infty}^2}{T}\,\delta B_y \\[2ex] \text{d)}\ \delta P = \dfrac{5}{3}\,\delta n - \dfrac{2B_{z\infty}^2\,\delta B_z}{T} - \dfrac{2B_{y\infty}^2\,\delta B_y}{T} \\[2ex] \text{e)}\ \delta P_\parallel = \delta P_\perp - 10\delta n + \dfrac{6}{T}\,(B_{y\infty}^2\,\delta B_y + B_{z\infty}^2\,\delta B_z) \end{cases}$$

$$\text{IV.22}\quad \begin{cases} \text{f)}\quad \delta B_y = \dfrac{\lambda_0}{\lambda-\lambda_0}\,\delta n_0\left(e^{\lambda(x-x_0)} - e^{\lambda_0(x-x_0)}\right) + \delta B_{y0}\, e^{\lambda_0(x-x_0)} \\[2ex] \text{g)}\quad \delta B_z = \dfrac{\lambda_0}{\lambda-\lambda_0}\,\delta n_0\left(e^{\lambda(x-x_0)} - e^{\lambda_0(x-x_0)}\right) + \delta B_{y0}\, e^{\lambda_0(x-x_0)} \\[2ex] \text{h)}\quad \delta\phi = -\,T\delta P_\perp - \dfrac{T}{2}\,\delta n \end{cases}$$

where:

$$\text{IV.23}\quad \lambda \equiv \frac{\lambda_0}{2}\left(\left(1 + \frac{6}{\mathrm{III}} - \frac{10}{\mathrm{II}}\frac{\lambda_1}{\lambda_0}\right) + \sqrt{\left(1 + \frac{6}{\mathrm{III}} - \frac{10}{\mathrm{II}}\frac{\lambda_1}{\lambda_0}\right)^2 + \frac{4\lambda_1}{\lambda_0}\left(\frac{10}{\mathrm{II}} + \frac{6}{\mathrm{III}}\right)}\right)$$

and the relation,

$$\text{IV.24}\quad \frac{\lambda_0}{\lambda-\lambda_0}\,\delta n_0 = \delta B_{yo}B_y^2(-\infty) + \delta B_z B_z^2(+\infty),$$

is satisfied. x_0 is an arbitrary point at large -x.

Letting x_0 be the starting point for the numerical integrator yields the boundary conditions:

$$\text{IV.25}\quad \begin{cases} \text{a)}\quad n(x_0) = n(-\infty)(1-\delta n_0) = 1 - \delta n_0 \text{ by IV.1} \\[1ex] \text{b)}\quad P_\perp = T(1+\delta P_{\perp 0}) \\[1ex] \text{c)}\quad P_\parallel = T(1+\delta P_\parallel) \\[1ex] \text{d)}\quad P_e = T(1+\delta P_{e0}) \\[1ex] \text{e)}\quad u_{xi} = u_{xe} = u_x(-\infty)(1+\delta n_0) \\[1ex] \text{f)}\quad B_y = B_y(-\infty)(1+\delta B_{y0}) \end{cases}$$

g) $B_z = B_z(-\infty)(1+\delta B_{z0})$

h) $\phi = \phi(-\infty) + \delta\phi_0$

δn_0 is an arbitrary, small number. $\delta P_{\perp 0}$, $\delta P_{\parallel 0}$, δP_{e0}, $\delta\phi_0$ are given in terms of δn_0, T, λ_0, λ_1 by equations IV.22. One of the perturbed magnetic field quantities (δB_{y0} or δB_{z0}) is determined by IV.24. $\delta B_{y0}/\delta B_{z0}$, however, remains arbitrary.

The choice of $\delta B_{y0}/\delta B_{z0}$ has significant effect on the solutions because of the exponential dependence. As x increases (as the open field line region is approached), the effects of $\delta B_{y0}/\delta B_{z0}$ become exponentially large, significantly affecting the final value of B_y/B_z at $x \to +\infty$. If it were desired to find solutions with a particular direction of the magnetic field at $x \to +\infty$ (as discussed earlier), the parameter $\delta B_{y0}/\delta B_{z0}$ would be varied along with $\phi(x = -\infty)$, $u_x(-\infty)$.

4.3

The numerical scheme for finding solutions consists of two parts; an integrator and a search routine. The integrator advances the dependent variables from $x = -|x_0|$ (x_0 is set equal to zero since the origin is arbitrary) in the closed field line region to x_1, the division point between closed and open field lines. The boundary conditions are given by IV.25 at $x = x_0$ and the equations IV.2 define the function $f(\underline{\xi})$:

$$\text{IV.26} \qquad \frac{d\underline{\xi}}{dx} = f(\underline{\xi}) \qquad \underline{\xi} = (n, P_\perp, P_\parallel, P_e, u_{xi}, u_{xe}, B_y, B_z, u_{zi}, \phi)$$

At $x = x_1$, the function f is redefined by the open field line equations IV.4. An additional dependent variable is introduced,

$u_{zi}(X)$, changing the dimensionality of $\underline{\xi},\underline{f} \rightarrow \underline{\xi}',f'$ (dim $\underline{\xi}'$ = 10, dim $\underline{\xi}$ = 9)

IV.27 $$\frac{d\underline{\xi}'}{dx} = f(\underline{\xi}') \quad \underline{\xi}' = (n,P_\perp,P_\parallel,P_e,u_{xi},u_{xe},B_y,B_z,u_{zi},\phi)$$

The boundary condition on $\underline{\xi}'$ at x_1 is determined by continuity of $\underline{\xi}$ (but <u>not</u> $d\underline{\xi}/dx$, $d^2\underline{\xi}/dx^2$, etc.). The boundary condition for the additional variable, u_{zi}, is:

IV.28 $$u_{zi}(X_1) = 0$$

which follows from the expansion in ρ_i/Δ_s. The evolution equation IV.4i is only valid if $u_{zi} \approx O(1)$. In chapter II, eqn. II.44 demands that:

IV.28a $$u_{zi} = O(\rho_i/\Delta_s) = 0. + O(\rho_i/\Delta_s)$$

on closed field lines. Continuity of u_{zi} across the dividing point x_1 plus consistency within the ρ_i/Δ_s expansion requires the condition IV.28.

The open field line equations, represented schematically by equation IV.27, are then integrated from x_1 to $x_2 \equiv$ the point where $n = P_\perp = P_\parallel = P_e = 0$. The equations IV.4 have a singularity at $n = 0$ so the integration is terminated slightly before x_2.

The termination is made by placing an upper bound on the number of steps taken by the integrator. As the $n = 0$ point is approached, the step size chosen by the integrator becomes smaller and smaller due to the singularity. An infinite number of steps would be required to reach $n = 0$, so some finite (although large) bound is chosen. The final answers are insensitive to the upper bound as long as it is sufficiently large ($\gtrsim$ 1000).

The equations break down near n = 0 for physical reasons as well, due to the invalidity of the quasi-neutral approximation. A simple model may roughly account for this effect. Examine Poisson's equation in the normalized variables defined in IV.1:

$$\text{IV.29} \qquad \frac{\partial^2\phi}{\partial x^2} = \frac{-\omega_i^2}{\Omega_i^2}(n_i - n_e) \left\{ \frac{\omega_i^2}{\Omega_i^2} \text{ evaluated at } X = -\infty \right\}$$

Quasi-neutrality breaks down near $n_i - n_e \sim n_i$

$$\text{IV.30} \qquad \frac{\partial^2\phi}{\partial x^2} \cong \frac{-\omega_i^2}{\Omega_i^2} n_i$$

When Poisson's equation is accounted for, the boundary condition $\partial\phi/\partial x_{\text{plasma}} = \partial\phi/\partial x_{\text{vacuum}}$ must be included. The vacuum electric field is given by:

$$\text{IV.31} \qquad E_{x_{vac}} = -\left.\frac{\partial\phi}{\partial x}\right|_{vac} = \frac{\phi_P - \phi_W}{X_w - X_2} = \frac{\phi_P}{X_w - X_2} \qquad \text{(the walls are at zero potential)}$$

For infinitely distant walls (consistent with the approximation $\Delta_s/r_p \ll 1$):

$$\text{IV.32} \qquad E_{x_{vac}} = 0.$$

To match the plasma and vacuum electric fields, an electrostatic sheath $\sim \lambda_{Debye}$ in thickness and consisting mostly of ions must exist near n = 0. Consider the average of eqn. IV.30 across the electrostatic sheath:

$$\left\langle \frac{\partial^2\phi}{\partial x^2} \right\rangle = -\frac{\omega_i^2}{\Omega_i^2} \langle n_i \rangle \qquad \langle\rangle \equiv \frac{1}{\phi}\int_{\phi}^{\phi_{vac}} d\phi$$

$$\left\langle \frac{\partial^2\phi}{\partial x^2} \right\rangle = \frac{1}{\phi}\int_{X}^{X_{vac}} \frac{d\phi}{dx}\,\frac{d^2\phi}{dx^2}\,dx = -\frac{1}{\phi}\int_{X_{vac}}^{X} \frac{d}{dx}\left(\frac{1}{2}\frac{d\phi}{dx}\right)^2 dx$$

$$= \frac{-1}{2\phi}\left.\frac{\partial\phi}{\partial x}^2\right|_{X_{vac}}^{X} = \frac{-1}{2\phi}\left(\frac{\partial\phi}{\partial x}\right)^2$$

$$\rightarrow \frac{\partial\phi}{\partial x} = \sqrt{\frac{2\omega_i^2}{\Omega_i^2}\langle n_i\rangle\phi} \sim \sqrt{\frac{2\omega_i^2}{\Omega_i^2}\, n\phi}$$

This rough model has the correct limit $\left.\frac{\partial\phi}{\partial x}\right|_{n=0} = 0$. The breakdown of quasineutrality is then accounted for by replacing IV.4j with

$$\text{IV.34} \qquad \frac{\partial\phi}{\partial x} = \min\left\{\frac{-1}{n}\frac{\partial P_{\perp i}}{\partial x} + u_y B_z - u_z B_y,\ \sqrt{\frac{2\omega_i^2}{\Omega_i^2}\, n\phi}\right\}$$

Typically ω_i^2/Ω_i^2 is a large number $\sim 10^5$, 10^6. The numerical results are insensitive to the value of ω_i^2/Ω_i^2 as long as $\omega_i^2/\Omega_i^2 \gtrsim 10^4$.

The integration of the differential equations on the interval $[x_0, x_2]$ is performed using the GH[34] (Gear) differential equation solver available from the system library of the LBL 7600. The Gear method uses the Adams-Moulton finite difference scheme.

The next step is to vary $u_x(-\infty)$, $\phi(-\infty)$ until the boundary conditions IV.19 are satisfied. This is achieved by first constructing the positive quantity:

$$\text{IV.35} \qquad \chi^2 = \left(n^2 + P_\perp{}^2 + P_\parallel{}^2 + P_e{}^2 + (nu_{xi})^2 + (nu_{xe})^2\right)_{x=x_2}$$

As the quantities $\phi(-\infty)$, $u_x(-\infty)$ are varied, they alter the final values of the dependent variables at $x = x_2$, and hence the value of χ^2. The function $\chi^2(\phi(-\infty), u_x(-\infty))$ may be represented as a two dimensional surface embedded in the three dimensional (χ^2,ϕ,u) pace. Solutions satisfying the boundary conditions IV.19 have $\chi^2 = 0$ so that the correct values of $\phi(-\infty)$, $u_x(-\infty)$ lie at the bottom of a valley on the χ^2 surface.

A search routine[35] is used to find local minima in the χ^2 surface discarding the minima where χ^2 is large. The routine picks a random point on the ϕ,u plane, samples enough values of χ^2 to calculate gradients within the surface, then proceeds down the steepest gradient to find the nearest local minimum.

If the value of χ^2 at minimum is greater than some specified value $\chi_0^2 \ll 1$, the point is discarded and a new random point is chosen for the search. This procedure is repeated until a solution, $\chi^2 < \chi_0^2$, is found.

4.4

The numerical scheme outlined in sec. 4.3 has been carried out for a variety of parameters and boundary conditions. The most striking feature of the results is the existence of continuous bands in the ϕ,u plane for which $\chi^2 \ll 1$. The bands exist in nearly all cases, but are found to shrink in length as the ratio r_p/λ_{mfp} increases (recall $\varepsilon \cong r_p/\lambda_{mfp}$ is the expansion parameter used in Chapter II).

The existence of a continuous band implies the existence of a continuous family of near-solutions that approximately satisfy the boundary conditions IV.19. This phenomenon arises because, in the long mean free path limit and for the model ion-annihilation flux used, the condition IV.19a;

$$nu_{xi} \to 0 \text{ as } x \to +\infty$$

or

$$nu_{xi}(-\infty) = \int_{X_1}^{\infty} n\Gamma_i dx$$

is approximately satisfied for a wide range of parameters.

The ion annihilation flux appearing in IV.19a is given approximately by (see eqn. III.26c)

$$\text{IV.36} \qquad \Gamma_i \sim \min\left\{ \frac{\nu_{ii}}{\left(1 - \frac{e\phi}{(R-1)T_{\perp i}}\right)^2} \;,\; \frac{v_{thi}}{r_p} \right\}$$

when $v_{thi}/r_p\nu_{ii}$ becomes large ($r_p/\lambda_{mfp} \to 0$), the quantity Γ_i/ν_{ii} may become large when $(1 - e\phi/(R-1)T_{\perp i}) \to 1$, i.e., the ions may be lost at a very large rate when $e\phi \sim T_i$.

It is a feature of many solutions found that either ϕ increases or $T_{\perp i}$ decreases across the sheath (with increasing x), so that $e\phi/(R-1)T_{\perp i} \to 1$ at some point in the sheath. The large ion annihilation causes $nu_x(-\infty) - \int_{x_1}^{x} n\Gamma_i = nu_{xi}(x)$ to decrease rapidly, although it can never give "over-annihilation" because of singularities in the equations at n, $u_{xi} = 0$, forcing n, u_{xi} to be positive. The result is that

$nu_x(-\infty) - \int_{x_1}^{\infty} n\Gamma_i = O(\varepsilon)$ for a wide range of parameters.

The expression for χ^2 becomes (neglect the pressure, density terms for simplicity)

IV.37 $$\chi^2 = \left(nu_{xe}\Big|_{x_2}\right)^2 + O(\varepsilon^2)$$

$$\cong \left(nu_{xe}\Big|_{x_2}\right)^2 \text{ for } \varepsilon \ll 1$$

The quantity $nu_{xe}\Big|_{x_2} = nu_x(-\infty) - \int_{x_1}^{x_2} n\Gamma_e$ may be estimated from III.7a:

IV.38 $$nu_{xe}\Big|_{x_2} \sim nu_x(-\infty) - \int_{x_1}^{x_2} n\nu_e\, e^{-e\phi/T_e}\, dx$$

$$= u_x(-\infty) - \bar{\nu}_e\, e^{-e\phi(-\infty)/\bar{T}_e}\, \Delta_s$$

$\bar{n}, \bar{T}_e, \bar{\nu}_e$ = appropriate averages over the sheath.

From IV.8 the sheath width is estimated:

IV.39 $$nu_{xe}\Big|_{x_2} \sim u_x(-\infty) - \frac{\bar{\nu}_e \bar{n}}{u_x(-\infty)}\, e^{-e\phi(-\infty)/\bar{T}_e}$$

Thus $\chi^2 \cong 0$ determines a curve in the u,ϕ plane:

IV.40 $$\frac{u_x^2}{\bar{\nu}_e \bar{n}} = e^{-e\phi/\bar{T}_e} \rightarrow \phi(-\infty) = -\bar{T}_e \ln\left(\frac{u_x^2(-\infty)}{\bar{\nu}_e \bar{n}}\right)$$

For the classical case, $\bar{\nu}_{e_{class}}$ and $\bar{\eta}_{class}$ are functions of $\bar{T}_e$. If the dependence of $\bar{T}_e$ on $\phi(-\infty)$ is neglected, IV.40 gives ($\nu_c \equiv \bar{\nu}_{e_{class}}$, $\eta_c \equiv \bar{\eta}_{class}$)

IV.41a $\quad \phi(-\infty) = \bar{T}_e \, (\ln \nu_c \eta_c - 2 \ln u_x(-\infty))$

For the anomalously collisional case (see equation IV.14)

$$\nu_{e_{anom}} \alpha \, \nu_{anom} \tilde{\alpha} \, |\underline{u}_e - \underline{u}_i|^{\lambda}$$

λ is usually chosen to be 2.0. From IV.4ℓ,

$$\nu_{e_{anom}} \alpha \, \eta_{anom} \tilde{\alpha} \, \frac{u_x^{\,2}}{\eta_{anom}^2} ,$$

which yields:

$$\nu_{e_{anom}} \alpha \, \eta_{anom} \tilde{\alpha} \, u_x^{\,2/3}$$

Plugging into IV.40 gives $\phi(u)$ for the anomalous case:

IV.41b $\quad \phi(-\infty) = \bar{T}_e (\ln \nu^* \eta^* - 2/3 \ln u_x(-\infty))$

The quantities ν^*, η^* represent the proportionality factors in the above rough analysis. Inserting reasonable values for $\bar{T}_e$, $\ln \eta_c \nu_c$, $\ln \eta^* \nu^*$ into IV.41a,b yields continua very similar to those actually obtained numerically. Figures (9,10) show the results of fitting the functional forms IV.41a,b to the numerical results (two points on the classical continuum are chosen to determine $\bar{T}_e$, $\ln \eta_c \nu_c$. One point on the anomalous curve is chosen to determine $\ln \eta^* \nu^*$ and the same value of $\bar{T}_e$ is used).

Since the existence of the continuous bands stems from the singular nature of the ion annihilation flux, changes in that singularity alter the length and the structure along the bands. Numerical investigation of cases with different values of the parameter r_p/λ_{mfp} (recall $(r_p/\lambda_{mfp})^{-1}$ is the upper bound of Γ_i/ν_i) shows that the length of the continuous bands decreases and a well defined minimum exists as $r_p/\lambda_{mfp} \to 1$, in agreement with the above arguments. For $r_p/\lambda_{mfp} \ll 1$, the regime of interest for fusion plasmas, investigation of the structure along the bands reveals that (perhaps several) broad minima still exist. Figure (8) shows the shift of the position of one of the minima along the band as a function of r_p/λ_{mfp}, indicating the sensitivity of the solution to variations in the ion annihilation. The curve in Fig. (8) corresponds to the minimum at the smallest erosion rate for the classical, field reversed case (for sufficiently large $r_p/\lambda_{mfp} \gtrsim .02$, the minima at larger erosion rates cease to exist). In the nearly collisionless limit ($r_p/\lambda_{mfp} \ll 1$) the minimum varies on the order of 20% as r_p/λ_{mfp} is varied over several decades. When r_p/λ_{mfp} is significant ($\sim .2$), the upper bound on the ion annihilation flux becomes comparable to typical values of the flux and the erosion rate is substantially decreased. This curve indicates that the most slowly eroding sheath solution is not too sensitive to the detailed structure of the ion annihilation flux, whereas the more rapidly eroding solutions are.

As a further test of the effects of modifying the ion annihilation flux, a different model Γ_i is substituted into the equations. The singularity is removed by the substitution:

$$\text{IV.42} \qquad \frac{1}{\left(1-\frac{e\phi}{(R-1)T_{\perp i}}\right)^2} \rightarrow \exp\left(\frac{2e\phi}{(R-1)T_{\perp i}}\right)$$

Note that these expressions are nearly equal at small values of $e\phi/(R-1)T_{\perp i}$.

The result of the substitution IV.42 is to drastically shrink the length of the band and provide a single well defined minimum near the slowly eroding solution obtained for the singular case (the dashed line in Fig. (8) shows the minimum $u_x(-\infty)$ for the modified, non-singular case). In the non-singular case the rapidly eroding solutions disappear, again indicating that they are sensitive to the details of the ion annihilation flux.

Since the positions and existence of some minima along a band are sensitive to the model ion annihilation flux chosen, and the model ion annihilation flux was crudely determined (see Chapter III), the entire continua will be presented and compared for the different variations of the basic model.

The continua for various cases are shown in figures 9,10 (a continuum is defined by $\chi^2 < .1$). The results are subdivided according to whether they apply t poloidal field reversed or non-reversed sheaths, since these two cases differ markedly. The non-reversed (Fig. 9) solutions will be discussed first.

The curve labeled "A" represents the case of classical resistivity and collisions and no electron wall effects. Points on the large u, small ϕ end of the curve correspond to solutions where the electrons

are more rapidly lost due to lack of electrostatic confinement. The ion losses match the electron losses by electrostatic "detrapping," i.e., $e\phi/(R-1)T_{\perp i} \to 1$. The rapid losses result in a narrow sheath as predicted by the scaling law $\Delta_s \sim \sqrt{\eta/\nu_{loss}}$. Points near the small u, large ϕ part of the curve correspond to solutions where the electrons are well confined electrostatically, their loss rate approaching ν_{ii}. The potential causes a minimum of electrostatic detrapping of the ions and the sheath is correspondingly broader. The continuum follows the theoretical curve IV.41a reasonably closely except near the small ϕ portion of the curve. In this region, the assumption $\overline{T}_e \neq \overline{T}_e(\phi)$ in equation IV.41a breaks down as will be discussed below.

Two local minima exist along the curve, the corresponding density profiles being shown in Figs. 11, 12. In these examples, only a minute fraction of the pressure gradient is supported on closed field lines so that the phenomena of interest occur primarily on the open field lines.

The solutions exhibit some short scale structure near the open-closed dividing point on the scale

$$\text{IV.43} \qquad \Delta_1 = \frac{\eta(T_e)}{u_x} \text{ ; with } T_e \cong T_i \to$$

$$\cong \rho_i/7$$

Within a distance $O(\Delta_1)$ from the open-closed dividing point, the electron temperature decreases until $T_e/T_i \cong 1/10$ and the scale becomes

$$\text{IV.44} \qquad \Delta_2 = \frac{\eta(T_e \cong T_i/10)}{u_x} \cong \rho_i$$

so that the total sheath width is $\Delta_s \gtrsim \rho_i$.

The rapid decrease in the electron temperature is due to the rapid transport of energy along the field lines. From the Pastukhov formula for energy loss (III.7b), the energy lost per particle is

$$\text{IV.45} \qquad \frac{\frac{\partial}{\partial t}\left(\frac{3}{2}nT_e\right)\Big|_c}{\frac{\partial n}{\partial t}\Big|_c} \sim \phi \gtrsim 2T_e \text{ on the first open field line}$$

$$\rightarrow 6T_e \text{ at large X.}$$

The electron temperature levels off once a balance between the parallel heat flow, the ohmic heating and the electron-ion energy transfer is achieved. The result is similar to the theoretical predictions for ordinary mirror machines where $T_e/T_i \sim 1/10$ is found.[13]

The positive curvature of the density profiles in Figs. 11,12 may be explained roughly by a simple model. Ignoring temperature variations, the ion collision rate may be written: $\nu_i = \nu_{io}n(x)$, $\nu_{io} = \nu_i(x = -\infty)$. The ion and electron flow velocities across the sheath rapidly approach the asymptotic rate $\sim \underline{E}\times\underline{B}/B^2$, so $u_{xi} \sim u_{xe}$ may be taken constant. The continuity equation then assumes the form:

$$\text{IV.46} \qquad u_x \frac{\partial n}{\partial x} \cong -n\Gamma_i \cong -n\nu_i \cong -n^2\nu_{10}$$

This may be solved to yield:

$$\text{IV.46a} \qquad n \cong \frac{u_x}{\nu_{io}} \frac{1}{(x+x_1)} = \frac{n_0 x_1}{x+x_1} \quad (x_1 = \text{open closed dividing point})$$

which is qualitatively similar to the positive curvature portions of Fig. 11,12. The functional form IV.46a is less similar to Fig. 12 because

of the effects of electrostatic detrapping of ions in the large x portions of the solution.

The continuum labeled "B" in Fig. 9 represents the set of solutions obtained when the anomalous resistivity given in IV.14 is included ($v_{crit} = 3v_{ith}$, $\lambda = 2$, $\alpha\omega_{pi} = 10^4\ \nu_i(-\infty)$). The same comments made concerning curve "A" apply to curve "B," the only difference being that for a given ϕ, the erosion rate, u_x, is faster due to anomalous resistance. The theoretical curve IV.41b is a good match to the numerical results (note that only one parameter is adjusted to fit the curve).

Only one minimum exists along the curve, the resulting density profile being shown in Fig. 13. The characteristics of the solution are similar to those of the classical solution shown in Fig. 12, except that structure on the short scale, Δ_1, is obliterated by anomalous broadening. The resulting sheath is somewhat broader and "eats in" faster than the classical sheath, although not dramatically so (about twice as fast). The continuum and minimum are sensitive, however, to the details of the anomalous processes, i.e., different values of v_{crit}, λ, $\alpha\omega_{pi}$.

The continuum labeled "C" in Fig. 9 represents the set of solutions obtained when strong electron recycling effects occur. A source of cold electrons is assumed to exist such that the electric field across the sheath is completely nullified (for the modified equations, see Appendix C). This effect tends to shrink the band where $\chi^2 < 1$ and displace it slightly. Because of the shortness of the band, no attempt is made to fit it to the theoretical model IV.41a.

The density profile at the minimum is shown in Fig. 14 and is similar to the solution in Fig. 11 discussed above. When the electric field vanishes, the density tends to drop off asymptotically like a Gaussian (as discussed by A. Boozer). This can be seen from a simple model neglecting temperature variations. Toroidal force balance gives:

$$\text{IV.47} \qquad m_i n\, u_{xi} \frac{\partial u_{zi}}{\partial x} = J_x B_y$$

i.e., the Lorentz force $(\underline{J}x\underline{B})_z$ drives a toroidal mass flow (pressure anisotropy terms are neglected). The electrons tend to be annihilated first due to their greater loss rate, so $J_x = en(u_{xi} - u_{xe}) \sim enu_{xi}$ which yields:

$$\text{IV.48} \qquad \frac{\partial u_{zi}}{\partial x} = \frac{eB_y}{m_i} \rightarrow u_{zi} \cong \frac{eB_{y_{vacuum}}}{m_i}\, x \text{ asymptotically}$$

Ion force balance in the absence of electric fields across the sheath gives

$$\text{IV.49} \qquad \frac{\partial P_\perp}{\partial x} = -\, enu_{zi}B_y \cong \frac{-e^2B_{y_{vac}}^2\, nx}{m_i} \text{ asymptotically}$$

$$\cong T_\perp \frac{\partial n}{\partial x}$$

Equation IV.49 may be solved to yield

$$\text{IV.50} \qquad n \,\tilde{\alpha}\, e^{-x^2/\rho_{iy}^2} \;;\quad \rho_{iy}^2 = \frac{m_i T_{\perp i}}{e^2 B_y^{\,2}}$$

The field reversed sheath is more complex as seen in Fig. 10, the

continua consisting of several disjoint curves for each case (note that gaps between continua may be artifacts of the search routine since the routine can show where solutions exist but cannot prove non-existence for any region. The solutions may simply be hard to find.). The discussion of the non-reversed sheath applies here as well--solutions at large u_x and small ϕ are narrower and lossier while solutions at small u_x and large ϕ tend to be broader and lose particles at the rate $\Gamma_i \sim \Gamma_e \sim \nu_i$.

The "A" curves shown in Fig. 10 represent the case of classical collisions and resistivity. A minimum exists on each distinct band, the density profiles being shown in Fig. 15, 16, 17 (15 is the minimum at the largest value of ϕ, 16 the intermediate value and 17 the lowest).

The solution in Fig. 15 is similar to the classical non-reversed solutions in that structure exists on both the scales $\Delta_1 \cong \rho_i/7$ and $\Delta_2 \cong \rho_i$. The electron temperature drops rapidly on the scale Δ_1 so that:

IV.51 $\quad T_e/T_i \cong 1/10$.

It is a general feature of the field reversed sheaths that they vary more abruptly than the non-reversed solutions, i.e., the curvature of the density profiles in Figs. 15-17 is negative. The steeper profiles are related to the fact that the $\underline{E}\times\underline{B}/B^2$ convection velocity changes sign across the sheath.

To illuminate this phenomenon it is helpful to imagine the time-dependent state before a steadily "eating-in" sheath is established. If the density profile for the initial state is gradual, the diamagnetic

and frictional drifts become small at the outer edge (large +x limit) of the sheath. The fluid flow becomes:

$$\text{IV.52} \qquad u_x = \frac{\underline{E}\times\underline{B}}{B^2} \cdot \hat{x} = \frac{-E_z B_y + E_y B_z}{B^2}$$

The plasma tends to polarize to force $\underline{E}\cdot\underline{B}$ to zero, i.e., if plasma is bounded on open field lines, an electric field $E_{\parallel}$ produces a charge separation at the edges until $E_{\parallel} \rightarrow \lambda_D^2/r_P^2\, E_{\parallel} \ll E_{\perp}$. The condition $\underline{E}\cdot\underline{B} = 0$ requires

$$\text{IV.53} \qquad E_y B_y = -E_z B_z \rightarrow E_y = -E_z\, B_z/B_y$$

Using IV.53 in IV.52 yields

$$\text{IV.54} \qquad u_x \cong -E_z/B_y$$

E_z is a constant across the sheath by the condition $\nabla\times\underline{E} = 0$ (assume the time variation of $\underline{B}$ is negligible), so the fluid flow at large +x and large -x ($u_x(\pm\infty) = -E_z/B_y(\pm\infty)$) are of opposite sign for the field reversed sheath. Matter at the low density edge is swept into the sheath until the profile is steep enough to balance $\underline{E}\times\underline{B}/B^2$ with frictional drifts.

A simple analytical argument reproduces the negative curvature of the density profile found numerically. Since u_{xe} tends to change sign, it is small over a large fraction of the sheath. Neglecting u_{xe}, the equation for the poloidal field becomes (IV.4g):

$$\text{IV.55} \qquad \frac{\partial B_y}{\partial x} \cong \frac{E_z}{2\eta} = \frac{u_x(-\infty)B_y(-\infty)}{2\eta}$$

Ignoring temperature variations, this yields

$$\text{IV.56} \qquad B_y \cong \frac{u_x(-\infty)B_y(-\infty)}{2\eta}(x-x_1)$$

Neglecting the ion poloidal current nu_{yi} (usually a good approximation), the pressure balance equation IV.4a gives:

$$\text{IV.57} \qquad n(T_{\perp i} + T_e) + B_y^2 = B_y^2(+\infty)$$

$$\rightarrow n \cong \frac{2T(-\infty)}{T_{\perp i}+T_e} - \frac{B_y^2(-\infty)}{(T_{\perp i}+T_e)}\left(\left(\frac{u_x}{2\eta}(x-x_1)\right)^2 - 1\right)$$

which closely resembles the profiles in 15, 16, 17.

The solutions in Figs. 16, 17 differ from the solution in Fig. 15 in that the electrons do not cool off, resulting in sheath widths $\Delta_s \sim \eta/u_x$ $(T_e \sim T_i) \sim 0.1\rho_i$. The basic assumption of the theory, $\Delta_s/\rho_i \ll 1$, is strongly violated although the approximate scaling law IV.6 allows scaling to a regime where $\Delta_s/\rho_i < 1$ by letting $\eta \rightarrow \alpha\eta$ ($\alpha \gtrsim 100$). This represents a different method of including anomalous effects than by the expression IV.14. Numerical investigation of such scalings shows that IV.6 is valid as long as the resulting sheath width, Δ_s, is not too many ion gyroradii.

In these solutions the ohmic heating term $\sim \eta J^2$ overcomes the large parallel heat flow so that $T_e/T_i \sim 1$. This may be seen by comparing the two terms in the electron heat balance equation IV.4d.

$$\text{IV.58} \qquad \frac{\text{Ohmic heating}}{\text{Parallal heat flow}} \cong \frac{\eta J^2}{\phi\nu_{loss}} \sim \frac{u_x^2 B_y^2}{\phi\eta\nu_{loss}} \sim \frac{T_i}{\phi}$$

At small values of $\phi(-\infty)$ (where these solutions occur), the ohmic heating overcomes the parallel heat flow. The hot electrons are lost at a rate $\Gamma_e \sim \nu_e$ and the ions are electrostatically detrapped until $\Gamma_i \sim \nu_e$ also. The strong dependence of the sheath electron temperature on ϕ at small values of ϕ explains the deviation of the theoretical curve IV.41a from the numerical results for both the field reversed and non-reversed sheaths. ($\overline{T}_e = \overline{T}_e(\phi)$ in IV.41a at small values of ϕ.)

The hot electron solutions are sensitive to the detailed structure of the ion annihilation flux since a significant ammount of electrostatic detrapping of the ions is required. Unless $\Gamma_i \sim \nu_e$ is possible, these solutions disappear as was illustrated earlier by varying the ion annihilation flux.

The results of including anomalous effects via IV.14 are shown in curve "B" of Fig. 10. The curve is similar in shape to the main branch of curve "A" although shifted to larger values of u_x as predicted by eqn. IV.8.

$$\text{IV.59} \qquad u_{xanom} \rightarrow \sqrt{\frac{\eta_{anom}}{\eta_{class}}}\, u_{xclass}$$

The curve is similar to the theoretical curve IV.41b. Note that only one minimum exists in the anomalous case as opposed to three in the classical case. The surviving minimum corresponds to the slowest eroding solution of the three classical solutions, again illustrating the relative insensitivity of the slow solution to perturbations of the model and the relative sensitivity of the rapid solutions to such perturbations.

The density profile corresponding to the minimum on curve "B" is shown in Fig. 18. The profile is similar to that in Fig. 15 except for the broadening of the structure on the scale length $\Delta_1 \sim \rho_i/7$ and the relaxation of the abrupt decrease to zero density.

Curve "C" shows the results of adding a large electron source to the classical equations for the field reversed case. The continua are similar to curve "A," the classical case without electron recycling and fit the theoretical curve IV.41a reasonably well. Again the most-slowly eroding solution survives this perturbation, as well as a solution at faster erosion rate.

The two minima are shown in Figs. 19, 20 (19 is the minimum at large ϕ, 20 is the minimum at small ϕ). The positive curvature in Fig. 19 is due to strong effects of the electron source. The solution in Fig. 20 differs from the large-erosion-rate solutions in the other cases in that the electrons remain cool due to the electron source and the sheath is correspondingly broader. As for the non-reversed case, the asymptotic density variation is approximately Gaussian in Figs. 19, 20.

The preceeding results do not represent an exhaustive study of all interesting parameter regimes, but rather a study of some typical parameters relevant to a Tormac fusion reactor ($\beta_{\perp i}(-\infty) = 1.$, $R(+\infty)$ = vacuum mirror ratio = 3., $|B_y/B_z|\ (-\infty) \cong .2$, etc.). The annihilation model could be a useful tool for investigating a wide range of plasma parameters.

CONCLUSIONS

The purpose of this thesis has been to develop a simple, heuristic model of the Tormac sheath that includes the effects of cross-field transport as well as mirror losses along magnetic field lines. The different variants of the model studied include the purely classical case, the anomalous case with a simple model of enhanced collisions and resistivity, and the case of a large electron source on open field lines that shorts out strong electric fields across the sheath.

The model applies to the long mean-free-path limit and the results may be compared to an experiment in this regime. Explicit predictions of the confinement time as well as density, temperature, magnetic and electric field profiles have been made.

The model is sufficiently general to treat any system possessing a boundary layer between plasma on closed magnetic field lines and a region of open field lines where mirroring effects are important. Examples other than the Tormac sheath are reversed field mirrors and Tokamaks with divertors. It is hoped that the author, or others, may see fit to apply the methods of this thesis to these other systems.

The annihilation model equations are derived from "first principles": the time dependent, two-dimensional fluid equations including collisional effects (one dimension is assumed ignorable due to axial symmetry). The infinite hierarchy of fluid equations is truncated by an expansion in gyroradius/scale length.

Further analytical progress is made by expansions in the parameters

Δ_s/r_p, r_p/λ_{mfp} along with the assumption of a steadily "eating in" sheath. The final result is a set of ten strongly coupled, non-linear, ordinary differential equations describing the dynamic of plasma across a one dimensional slab. The two dimensional effects (fluxes of matter, momentum and energy along magnetic field lines) are reduced to sink terms in the one dimensional fluid equations. The sink terms (annihilation terms) are determined by simple models of mirror losses.

The annihilation model equations are solved numerically by integrating the set of ordinary differential equations from the asymptotic values of the dependent variables at large -x (the independent variable) across the sheath to the point where the density vanishes. Two parameters ($u_x(-\infty)$, the eating in rate of the sheath and $\phi(-\infty)$, the plasma floating potential) are varied until the total number of electrons and ions annihilated on open field lines equals the flux of electrons and ions convected into the sheath.

The numerical results may be summarized as follows:

1) the scale length and erosion rate of the solutions are consistent with the estimates described in the introduction:

$$u_x \sim \sqrt{\eta \nu_{loss}} \qquad \Delta_s \sim \sqrt{\frac{\eta}{\nu_{loss}}} \qquad \begin{array}{l} \eta = \text{resistivity} \\ \nu_{loss} = \text{particle loss rate} \end{array}$$

The resistivity and loss rate in these formulas are strong functions of the solution parameters, i.e., T_e/T_i, $e\phi/T_e$, v_{crit} = critical velocity for the onset of anomalous effects, etc.

2) Continuous bands of near-solutions are found in the parameter

plane $u_x(-\infty)$, $\phi(-\infty)$ rather than well defined, discrete points as would seem to follow from the imposed boundary conditions. The continua exist due to the singular nature of the ion mirror loss rate which becomes large as $e\phi/(R-1)T_{\perp i} \to 1$ (R = the mirror ratio). Various points along the continuous curves where the boundary conditions are locally the best satisfied are identified as solutions, although some of these solutions are sensitive to details of the ion loss rate. The solutions at small erosion rate, $u_x(-\infty)$, and large floating potential, $\phi(-\infty)$, seem to be relatively stable to alterations of the model whereas the solutions at large erosion rate and small floating potential are quite model dependent, i.e., variations in the type of singularity in the ion loss rate may cause these solutions to disappear.

3) The solutions at small erosion rate, $u_x(-\infty)$, have some similar characteristics for a wide range of different conditions: poloidal field reversed or non-reversed sheaths, sheaths where anomalous effects are included, and sheaths where significant amounts of cold electrons from the walls are present. Typical parameters for these solutions are:

$$\left.\frac{T_e}{T_i}\right|_{\substack{\text{open field}\\ \text{lines}}} \sim 1/10 \,, \qquad \left.\frac{e\phi}{T_e}\right|_{\substack{\text{open field}\\ \text{lines}}} \sim 3$$

The scale length, Δ_s, and erosion rate, u_x, consistent with these parameters and the expressions in 1) above are:

$$u_x(-\infty) \sim \rho_i \nu_{ii} \qquad \Delta_s \gtrsim \rho_i$$

Thus the annihilation model provides a confirmation of the usual confinement time predicted for Tormac:

$$\tau_{Tormac} \cong \frac{r_p}{\rho_i} \tau_{ii}$$

4) The solutions at larger erosion rate occur only for the field-reversed case and disappear when the ion loss rate is non-singular. Typical parameters are

$$\left.\frac{T_e}{T_i}\right|_{\substack{\text{open field}\\ \text{lines}}} \cong 1 \qquad \frac{e\phi}{T_e} \lesssim 1$$

To obtain sheath solutions within the range of validity of the theory ($\Delta_s/\rho_i < 1$) the approximate scaling law IV.6 must be invoked, letting $\eta \to 100\eta$. The resulting erosion rate and sheath width are:

$$\Delta_s \sim \rho_i \quad , \quad u_x(-\infty) \sim 30\rho_i\nu_i$$

If this state prevailed, the advantage of Tormac as a fusion reactor concept would be demolished, the confinement time approaching that of a classical mirror machine.

5) The existence and characteristic behavior of the two solutions is closely tied to electron heat balance.

Electron heat balance for the first type of solution ($T_e/T_i \ll 1$) is dominated by the mirror losses of energy parallel to field lines. The cool electrons are confined by a high electrostatic barrier which reduces the electron loss rate until

$$\nu_{e_{loss}} \sim \nu_e \, e^{-e\phi/T_e} \sim \nu_{ii}$$

For the second type of solution ($T_e/T_i \sim 1$) the electron heat balance is dominated by ohmic heating. The resulting warm electrons are not electrostatically confined; rather the ions are electrostatically removed until the integrated losses of both species are equal:

$$\frac{\nu_i}{\left(1 - \frac{e\phi}{(R-1)T_{\perp i}}\right)^2} \sim \nu_e$$

Thus, the warm electron, rapidly eroding solution depends strongly on the singularity in the ion loss rate.

6) For both the field-reversed and non-reversed sheaths, simple analytic models reproduce many of the qualitative features of the solutions (see sec. IV.4).

The annihilation model represents a first attempt at describing the transport of matter, momentum and energy across the sheath; it contains many heuristic elements which must be improved upon if a more thorough understanding is to be gained. Several improvements, in order of increasing difficulty, might be the following:

a) Particles with guiding centers on closed flux surfaces also sample the open field lines due to their finite orbit size. This effect could be relatively easily modeled by allowing some annihilation effects for the ions on the closed field lines near the sheath.

b) Neo-classical as opposed to classical transport coefficients

could be used to include the effects of the toroidal drifts. This would require some thought about global drift surface averaging and the differences between various classes of particles (trapped and passing particles on closed and open field lines).

c) Anomalous effects could be included in a more careful, consistent fashion by incorporating a turbulent collision operator due to various instabilities (Buneman, Lower-Hybrid-Drift).

d) The use of orbit averaged mirror losses would account for the fact that in a narrow sheath, a particle samples a wide range of environments in the course of its orbit. The difficulty would be that the non-local losses alter the character of the equations, i.e., one obtains integro-differential equations including averaging integrals.

e) The large ion-orbit size fundamentally limits the usefulness of fluid equations, so that a kinetic description is necessary for more quantitative results. This yields a set of partial differential-integral equations since the other phase space variables appear as well as integrals to determine current and charge densities for self-consistency.

f) The classical collision operator could be treated more realistically via Fokker-Planck rather than Krook collision terms in a kinetic theory. The Fokker-Plank terms introduce further differential operators and phase space integrals making this approach forbiddingly complex.

Appendix A

In this appendix, the collisionless poloidal flow velocity on open field lines is determined for both ions and electrons as a function of the pressure anisotropy.

In the closed field line region of Tormac, arbitrary fluid flows may exist parallel to $\underline{B}$ in the collisionless equilibrium, resulting in arbitrary poloidal flows for the case of helical field lines (the arbitrariness would be removed by the equations first order in collisionality $\equiv$ the transport equations). In contrast, on open field lines poloidal flow is inhibited by material boundaries intersecting the flux surfaces. In order to circulate poloidally, the flow must be orthogonal to the flux surface in some region near the cusps (see Fig. 3). Fluid flows across flux surfaces may be related to the stress tensor and electric field, removing the arbitrariness. The condition that the flow be divergence free, $\nabla\cdot n\underline{u} = 0$, provides a connection from the cusp region to the slab-like portions of the sheath, allowing a determination of the poloidal flow in terms of local slab quantities.

To see this explicitly, examine the collisionless fluid equilibrium equations to lowest order in ρ_i/Δ_s, with:

A1 a) $\underline{\underline{P}}_i = P_\perp (\underline{\underline{I}} - \hat{b}\hat{b}) + P_\parallel \hat{b}\hat{b}$

b) $\underline{\underline{P}}_e = P_e \underline{\underline{I}}$

Assume also that $m_i \underline{u}_i \nabla \underline{u}_i$ is first order in (ρ_i/Δ_s) i.e., the electric field drift and parallel streaming velocity are not too large for the ions. The force balance equation is (for both species)

A2 $$\nabla\cdot\underline{\underline{P}}_s - e_s n(\underline{E} + \underline{u}_s \times \underline{B}) = 0$$

Inverting for $\underline{u}_s$ gives:

A3 $$\underline{u}_s = \underline{u}_{\parallel_s} + \frac{\underline{E} \times \underline{B}}{B^2} - \frac{\nabla\cdot P_s \times \underline{B}}{e_s n B^2}$$

where $\underline{B} = \underline{B}_p + B_\theta\hat{\theta}$ $\hat{\theta}$ = toroidal unit vector; $\underline{B}_p$ = poloidal $\underline{B}$

Take $\underline{B}\cdot$equation A2:

A4 $$B\cdot\nabla\cdot\underline{\underline{P}} = e_s n \underline{B}_p\cdot\underline{E}$$

There is no term $\underline{B}_\theta\hat{\theta}\cdot E_\theta$ because of toroidal symmetry and the condition $\nabla\times\underline{E} = 0 \rightarrow E_\theta = 0$. Take $\underline{B}_p\cdot$equation A2:

A5 $$\underline{B}_p\cdot(\nabla\cdot\underline{\underline{P}} - e_s n\underline{E}) = e_s n\underline{B}_p\cdot(\underline{u}\times\underline{B})$$

Combining A4, A5 allows the elimination of the electric field term, yielding:

A6 $$\hat{P}\cdot(\underline{u}\times\hat{\theta}) = \frac{-(\nabla\cdot\underline{\underline{P}})_\theta}{e_s n B_p} \qquad \hat{p} \equiv \frac{\underline{B}_p}{B_p}$$

If a triad of unit vectors $\hat{n}$, $\hat{P}$, $\hat{\theta}$ are introduced, $\hat{n} \times \hat{P} = \hat{\theta}$ (i.e. $\hat{n}$ is normal to the flux surface) then A6 yields:

A7 $$u_n = \frac{(\nabla\cdot\underline{\underline{P}})_\theta}{e_s n B_p}$$

i.e., the flow <u>across</u> the flux surfaces is proportional to the toroidal stress. For electrons $(\nabla\cdot\underline{\underline{P}}_e)_\theta = 0$ because of toroidal symmetry, so

A8 $$u_{ne} = 0$$

The continuity equation then demands that the poloidal flow of electrons must vanish:

$$\nabla\cdot n\underline{u} = \alpha_n \frac{\partial}{\partial x_n} \beta_n u_n + \alpha_p \frac{\partial}{\partial x_p} \beta_p \, nu_p = 0$$

A9 $\qquad 0$

so

$$nu_{pe} = \frac{f(X_n)}{\beta_p}$$

α_p β_p are metric factors

$= 1$ for straight field lines

On open field lines the boundary condition nu_{pe} $(x_p = x_{wall}) = 0$ must be applied, i.e., there is no flux of electrons into the walls in the collisionless state. Equation A9 then yields

A10 $\qquad \underline{u_{pe} = 0}$

This result may be summarized as follows: the fluid flow across flux surfaces is diamagnetic ($\alpha\nabla P_e$) and $\underline{E}\times\underline{B}$. Pressure balance <u>along</u> $\underline{B}$ places a constraint between $\underline{E}$ and ∇P_e causing a cancellation of the diamagnetic and $\underline{E}\times\underline{B}$ terms.* Thus, fluid flow exists only parallel to the flux surfaces. Continuity of the flow and toroidal symmetry demand $u_{pol_e} = 0$ on open field lines.

For the ions:

A11 $$\nabla\cdot\underline{\underline{P}} = \nabla P_\perp + \nabla\cdot\left((P_\parallel - P_\perp)\hat{b}\hat{b}\right)$$

$$= + \frac{B}{R}\cdot\nabla\left((P_\parallel - P_\perp)\frac{B_\theta R}{B^2}\right) \qquad R = \text{major radius}$$

Using A11 in A7 yields

*There are still $\underline{E}\times\underline{B}$ and diamagnetic flows <u>within</u> the flux surface.

A12 $$u_{ni} = \frac{+B}{enRB_p} \cdot \nabla \left\{ (P_{\parallel} - P_{\perp}) \frac{B_\theta R}{B^2} \right\}$$

To estimate the poloidal flow associated with this flow across flux surfaces, ignore the metric factors, $\alpha_{n,p}$, $\beta_{n,p}$, which gives: (let $\theta \rightarrow \hat{Z}$ and $R \rightarrow$ constant)

$$\nabla \cdot n\underline{u} = \frac{\partial n u_n}{\partial x_n} + \frac{\partial}{\partial x_p} n u_p = 0$$

A13

$$\frac{\partial}{\partial x_p} n u_p = - \frac{\partial}{\partial x_n} n \left(\frac{+1}{en} \frac{\partial}{\partial x_p} (P_{\parallel} - P_{\perp}) \frac{B_z}{B^2} \right)$$

$$= \frac{-1}{e} \frac{\partial^2}{\partial x_n \partial x_p} (P_{\parallel} - P_{\perp}) \frac{B_z}{B^2}$$

Integrating from the center of the flux surface ($x_p = 0$) to the walls ($x_p = x_{wall}$) and applying the boundary condition $nu_{pi}(X_p = X_w) = 0$ gives

A14 $$nu_{pi}\Big|_{x_p=0} = \frac{-1}{e} \frac{\partial}{\partial x} \left((P_{\parallel} - P_{\perp}) \frac{B_z}{B^2} \right)$$

$x_n \rightarrow x$ in the coordinates defined in Fig. 2.

Appendix B

In this appendix, it is shown that the thermal force term in the electron-ion drag is negligible compared to the other terms first order in ε = the collisionality parameter.

The thermal force is proportional to $\nabla_{\parallel} T_e$.[16] A simple argument shows that this effect is of higher order because of the rapid equilibration of electron temperature parallel to $\underline{B}$. If a flux tube is followed in its passage across the sheath, the relaxation of the temperature parallel to $\underline{B}$ is given roughly in the collisionless limit by:

$$\text{B1} \qquad \frac{dT_e}{dt} \sim v_e \nabla_{\parallel} T_e = v_{eth} \frac{B_y}{B} \frac{\partial T_e}{\partial y} \sim v_{eth} \frac{\partial T_e}{\partial y}$$

Replacing d/dt by the characteristic rate of the sheath

$$\text{B2} \qquad \frac{dT_e}{dt} \sim \frac{T_e}{\tau_{coll}} \sim v_{eth} \frac{\partial T_e}{\partial y}$$

which yields

$$\text{B3} \qquad r_p \frac{\partial T_e}{\partial y} \sim \frac{r_p}{v_e \tau_{coll}} T_e \sim \frac{v_i}{v_e} \varepsilon T_e \qquad \varepsilon \equiv \frac{r_p}{v_i \tau_{coll}}$$

As discussed in Chapter II, collisions introduce a weak y dependence: $r_p \frac{\partial}{\partial y}(\ ) = O(\varepsilon(\ ))$. From equation B3, $r_p \frac{\partial T_e}{\partial y}$ is smaller than the other terms by a factor $v_{ith}/v_{eth} \ll 1$.

Appendix C

In this appendix, electron recycling from the walls is accounted for in a different (more drastic) fashion than the method described in chapter III. Here it will be assumed that the walls provide an arbitrarily large source of zero temperature electrons in just the right quantities to short out any large electric fields across the sheath, $E_x = \mathcal{O}(T/e\Delta_s)$. Relatively weak electric fields E_x, $E_y = \mathcal{O}(T/er_p)$ will be assumed to persist so that the plasma may float at $\phi_{plasma} = \mathcal{O}(T/e) \neq \phi_{wall} \equiv 0$. Within the context of the ordering scheme used in Chapter II, the above ansatz requires

C1 $$\frac{d\phi_0}{dx} = 0 \quad \text{on open field lines.}$$

To simplify the analysis, two additional approximations will be made for the open field line region:

C2 a) $$\frac{dB_z}{dx} \cong 0 \quad \text{or} \quad nu_{yi}\Big|_{\substack{\text{zeroth order}\\ \text{in collisions}}} \cong 0$$

b) $$\frac{\partial \underline{u}_i}{\partial y} \times \underline{B} = 0$$

The first approximation is verified numerically; no solutions have been found with significant variation of B_z on open field lines. The second approximation neglects cross-field flows in the ion annihilation flux, i.e., ions are assumed to stream out parallel to $\underline{B}$. This approximation is needed only for calculating $\perp \rightleftarrows \parallel$ energy exchange terms in the ion energy equations and is found numerically to have small effect on solutions.

The electron particle and energy annihilation fluxes are altered by a source, S(X),

C3 a) $\Gamma_e \rightarrow \Gamma_e - S$

b) $\frac{\partial q_{ye}}{\partial y} \rightarrow \frac{\partial q_{ye}}{\partial y} - \phi S$ [Source electrons enter the plasma with energy $e\phi$]

The relevant equations, II.50, become (in normalized variables)

C4

$$\text{a)}\quad \frac{\partial P_{\perp i}}{\partial x} + \frac{\partial P_e}{\partial x} + J_z B_y = 0$$

$$\text{b)}\quad u_{xi}\frac{\partial P_{\perp i}}{\partial x} + P_{\perp i}\left(2\frac{\partial u_{xi}}{\partial x} + \frac{\partial u_{yi}}{\partial y}\right) = -\frac{\partial q^{\perp}_{yi}}{\partial y} - \frac{\nu_i}{3}(P_\perp - P_\parallel) - \nu_{ie}(P_\perp - P_e)$$

$$\text{c)}\quad u_{xi}\frac{\partial P_{\parallel i}}{\partial x} + P_{\parallel i}\left(\frac{\partial u_{xi}}{\partial x} + 3\frac{\partial u_{yi}}{\partial y}\right) = -\frac{2}{3}\nu_i(P_\parallel - P_\perp) - \nu_{ie}(P_\parallel - P_e)$$

$$\text{d)}\quad u_{xe}\frac{\partial P_e}{\partial x} + \frac{5}{3}P_e\left(\frac{\partial u_{xe}}{\partial x} + \frac{\partial u_{ye}}{\partial y} - S\right) = -\frac{2}{3}\left(\frac{\partial q_{ye}}{\partial y} - \phi S\right) + \frac{2}{3}\eta J_z^2 - \nu_{ie}\left(P_e - \frac{2}{3}P_\perp - \frac{P_\parallel}{3}\right)$$

$$\text{e)}\quad n\frac{\partial u_{xi}}{\partial x} = -u_{xi}\frac{\partial n}{\partial x} - n\Gamma_{yi}$$

$$\text{f)}\quad n\frac{\partial u_{xe}}{\partial x} = -u_{xe}\frac{\partial n}{\partial x} - n\Gamma_{ye} + nS$$

$$\text{C4}\quad \begin{cases} \text{g)}\ \dfrac{\partial u_{zi}}{\partial x} = B_y\left(\dfrac{u_{xi}-u_{xe}}{u_{xi}}\right)\left(1 - \dfrac{(P_\parallel - P_\perp)}{2B^2}\right) \\ \qquad\qquad\qquad\qquad \text{(result II.54 is used in C4g)} \\ \text{h)}\ \dfrac{\partial B_y}{\partial x} = \dfrac{J_z}{2} \\ \text{i)}\ \dfrac{\partial B_z}{\partial x} = 0 \\ \text{j)}\ \dfrac{\partial P_{\perp i}}{\partial x} = -\, nu_{zi}B_y \\ \text{k)}\ J_z = \dfrac{E_z + u_{xe}B_y}{\eta} \end{cases}$$

To obtain equations suitable for numerical integration, i.e., in the form II.39, equations C4b, e, j are combined to give an expression for $\partial n/\partial x$:

$$\text{C5}\qquad \frac{\partial n}{\partial x} = \frac{-n^2 u_{zi}B_y}{2P_\perp} + \frac{n}{2P_\perp u_{xi}}\left(\frac{\partial q^\perp_{yi}}{\partial y} + \frac{\nu_i}{3}(P_\perp - P_\parallel) + \nu_{ie}(P_\perp - P_e) - P_\perp \Gamma_i\right)$$

Equations C4g,j are combined to give an equation for the electron pressure:

$$\text{C6}\qquad \frac{\partial P_e}{\partial x} = (nu_{zi} - J_z)B_y$$

The electron energy equation must be consistent with this pressure variation. Inserting C6 and C4f into C4d, the energy equation, yields a relation for the source function S(X):

C7 $$S(X) = \frac{1}{\phi}\frac{\partial q_{ye}}{\partial y} + \frac{3u_{xe}}{2\phi}\left\{(nu_{zi}-J_z)B_y - \frac{5}{3}\frac{P_e}{n}\frac{\partial n}{\partial x} - \frac{2}{3}\frac{nJ_z^2}{u_{xe}} - \frac{\nu_{ie}}{u_{xe}}\left(P_e - \frac{2}{3}P_\perp - P_\parallel/3\right)\right\}$$

The closed set of equations is then:

C8
$$\left\{\begin{aligned}
&\text{a)}\quad \frac{\partial n}{\partial x} = \frac{-n^2u_{zi}B_y}{2P_\perp} + \frac{n}{2P_\perp u_{xi}}\left(\frac{\partial q_{yi}^\perp}{\partial y} + \frac{\nu_i}{3}(P_\perp - P_\parallel) + \nu_{ie}(P_\perp - P_e) - P_\perp\Gamma_i\right)\\
&\text{b)}\quad \frac{\partial P_\perp}{\partial x} = -nu_{zi}B_y\\
&\text{c)}\quad \frac{\partial P_\parallel}{\partial x} = \frac{P_\parallel}{n}\frac{\partial n}{\partial x} - \frac{2P_\parallel}{u_{xi}}\Gamma_i - \frac{2\nu_i}{3u_{xi}}(P_\parallel - P_\perp) - \frac{\nu_{ie}}{u_{xi}}(P_\parallel - P_e)\\
&\text{d)}\quad \frac{\partial P_e}{\partial x} = (nu_{zi}-J_z)B_y\\
&\text{e)}\quad \frac{\partial u_{xi}}{\partial x} = -\frac{u_{xi}}{n}\frac{\partial n}{\partial x} - \Gamma_i\\
&\text{f)}\quad \frac{\partial u_{xe}}{\partial x} = -\frac{u_{xe}}{n}\frac{\partial n}{\partial x} - \Gamma_e + S\\
&\text{g)}\quad \frac{\partial B_y}{\partial x} = \frac{J_z}{2}\\
&\text{h)}\quad \frac{\partial B_z}{\partial x} = 0
\end{aligned}\right.$$

$$\text{C8} \quad \begin{cases} \text{i)} \quad \dfrac{\partial u_{zi}}{\partial x} = B_y \left(\dfrac{u_{xi} - u_{xe}}{u_{xi}} \right) \left(1 - \dfrac{(P_{\parallel} - P_{\perp})}{2B^2} \right) \\ \\ \text{j)} \quad \dfrac{\partial \phi}{\partial x} = 0 \end{cases}$$

where S(X) is given in C7 and J_z in C4k.

REFERENCES

1. L.S. Combes, C.C. Galagher, & M.A. Levine, Phys. Fluids 5, 1070 (1962).

2. C.C. Galagher, L.S. Combes, and M.A. Levine, Phys. Fluids 13, 1617 (1970).

3. M.A. Levine, A.H. Boozer, G. Kalman, O.P. Bakshi, Phys. Rev. Lett., 28, 1323 (1972).

4. W. Grossman, Jr., Phys. Fluids 9, 2478 (1960).

5. H. Grad, Phys. Rev. Lett. 4, 222 (1960).

6. J.D. Lawson, Proc. Phys. Soc. (London), B70:6 (1957).

7. I.J. Spalding, Advances in Plasma Physics 4, 79, Interscience (1971).

8. H.A. Bodin, et al. Plasma Phys. and Controlled Fusion Research II, 537, I.A.E.A., Vienna (1968).

9. J.H. Hammer & W.B. Kuntel, Phys. Fluids 19, 438 (1976).

10. A.H. Boozer & M.A. Mostrom, to be published.

11. E. Hameiri & J.H. Hammer, to be published.

12. N. Krall & A. Trivelpiece, "Principles of Plasma Physics," McGraw-Hill, New York (1973).

13. A. Futch, et al., Plasma Physics, 14, 211 (1972).

14. A.H. Boozer, PPPL-EPRI-5 (1976).

15. P.L. Bhatnager, E.P. Gross, & M. Krook, Phys. Rev. 94, 511 (1954).

16. S.I. Braginskii, "Reviews of Plasma Physics," Vol. 1, Consultants Bureau, New York (1965).

17. L.A. Artsimovich, Nucl. Fus. 12, 215 (1972).

18. A.H. Boozer and M.A. Levine, Phys. Rev. Lett. 31, 1287 (1973).

19. H. Mynick, Ph.D. Thesis, U.C. Berkeley.

20. H. Grad, Phys. Fluids 4, 1366 (1961).

21. P. Channell, Phys. Fluids 19, 1541 (1976).

22. H. Mynick, W. Sharp, & A. Kaufman, to be published.

23. R.C. Davidson & N.T. Gladd, Phys. Fluids 20, 1516 (1977).

24. N.T. Gladd, et al., Phys. Fluids 20, 1876 (1977).

25. A.H. Boozer, Phys. Fluids 19, 1210 (1976).

26. M.A. Mostrom, to be published.

27. M. Vella, to be published.

28. A. McMahon, Phys. Fluids 8, 1840 (1965).

29. R. Courant & D. Hilbert, "Methods of Mathematical Physics," Vol. 2, Interscience, New York (1953).

30. V.P. Pastukhov, Nucl. Fusion 14, 3 (1974).

31. R.H. Cohen, et al., Nucl. Fusion 18, 1229 (1978).

32. L. Spitzer Jr., "Physics of Fully Ionized Gases," Interscience, New York (1956).

33. N.A. Krall and P.C. Liewer, Phys. Fluids 15, 1166 (1972).

34. C. Risk, "A Guide to Frequently used Differential Equation Solvers," UCID-3703 (1974).

35. J.P. Chandler, "STEPIT," Physics Dept., Indiana Univ. (1965).

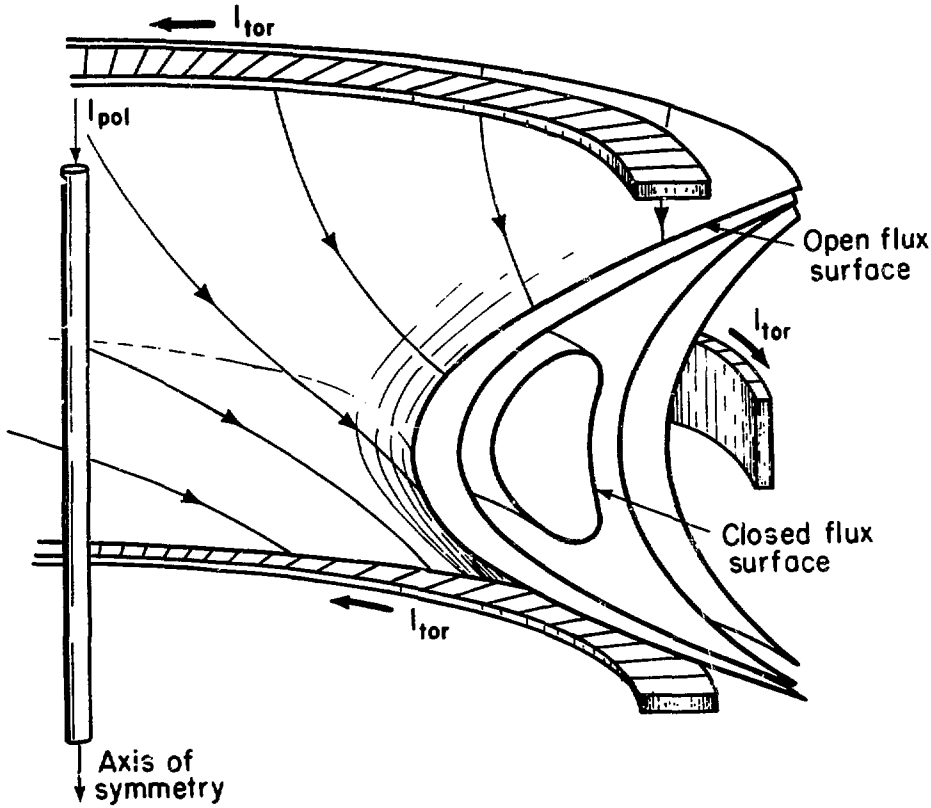

Tormac coils and flux surfaces

XBL 793-696

Fig. 1

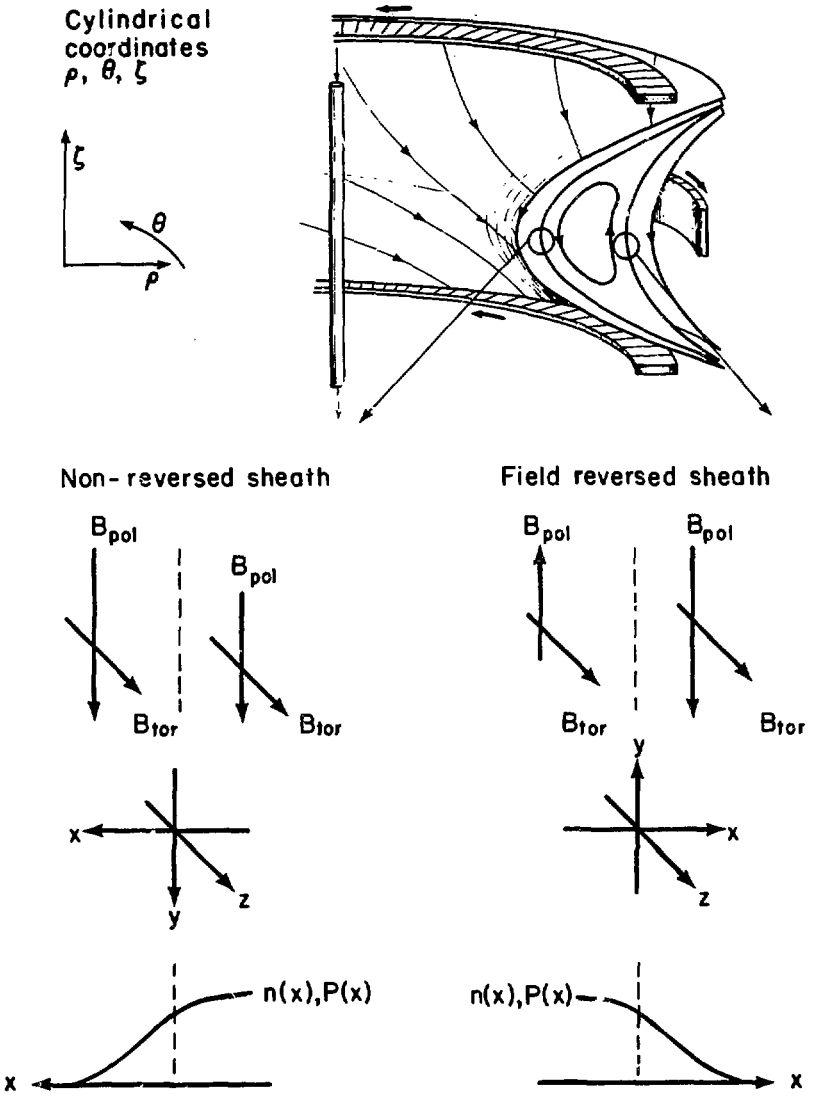

--- the dividing line between open and closed flux surfaces

XBL 793-695

Fig. 2

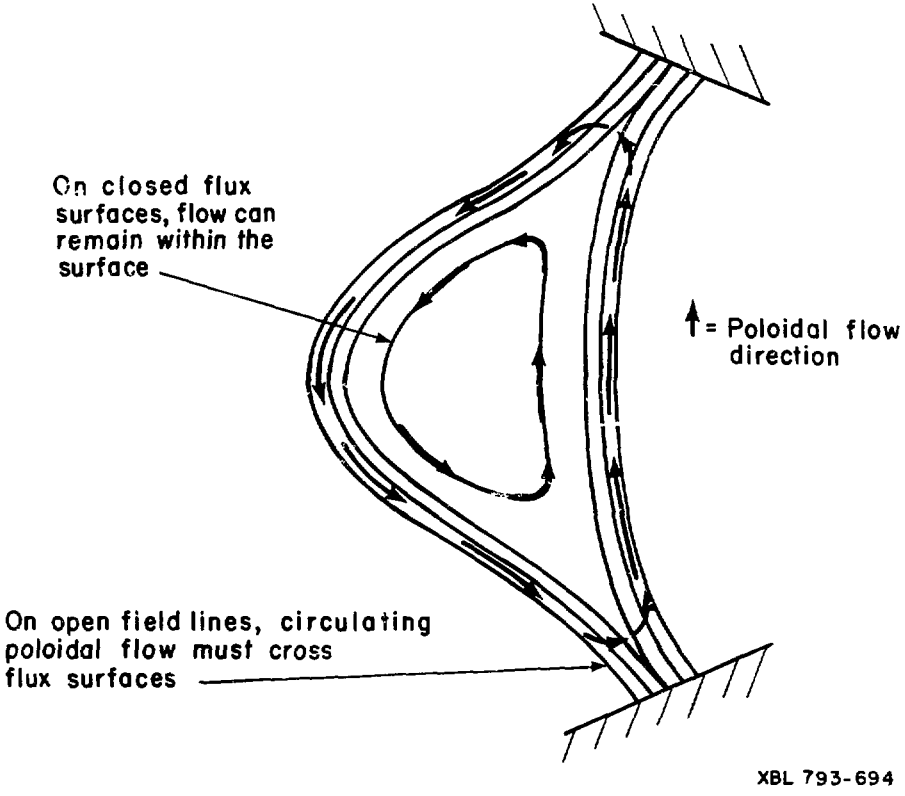
On closed flux surfaces, flow can remain within the surface
= Poloidal flow direction
On open field lines, circulating poloidal flow must cross flux surfaces
XBL 793-694

Fig. 3

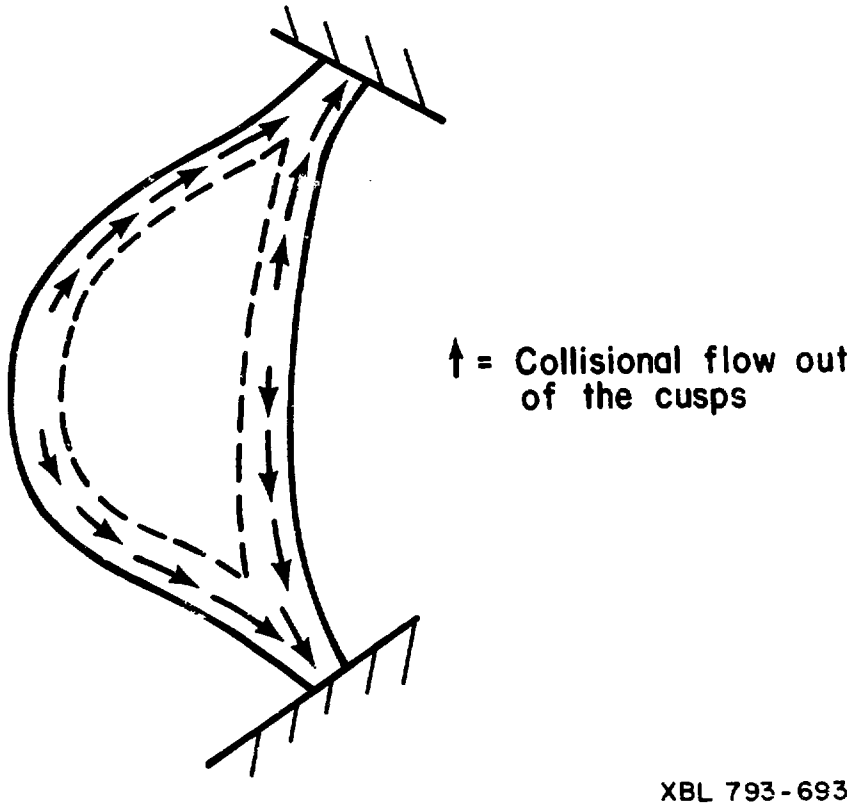

Fig. 4

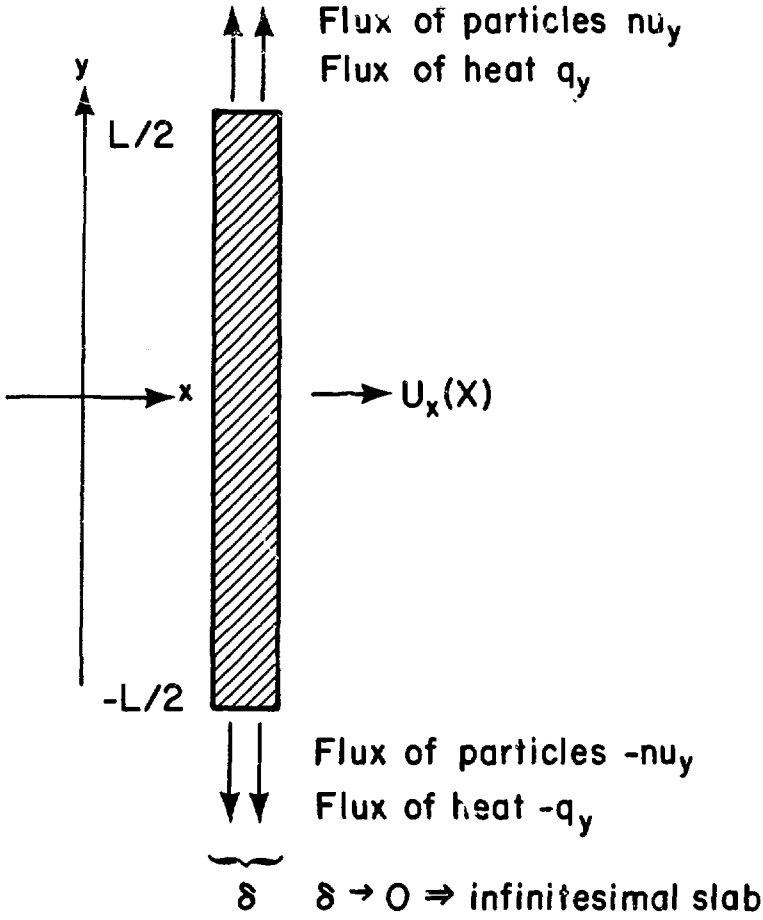

XBL 793-690

Fig. 5

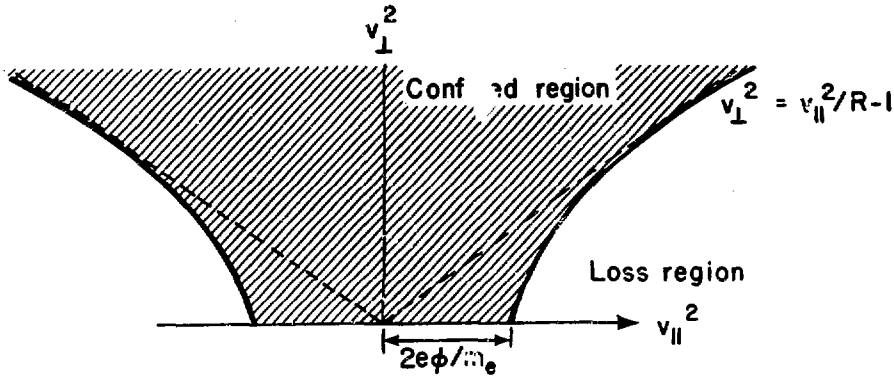

a) Electron loss boundary

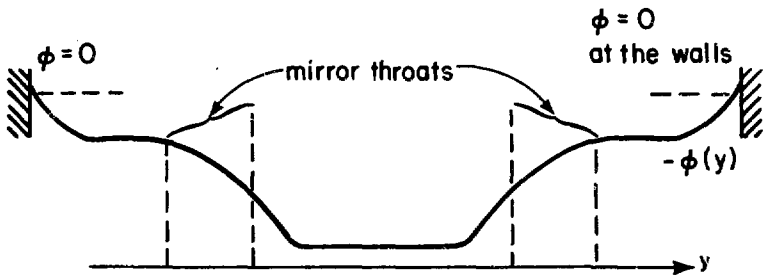

b) Electrostatic well for electrons

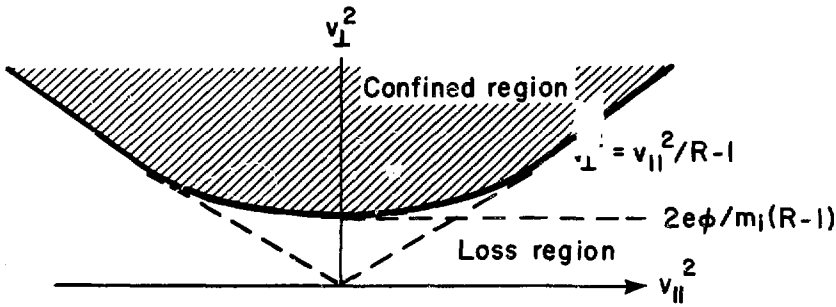

c) Ion loss boundary

XBL 793-691

Fig. 6

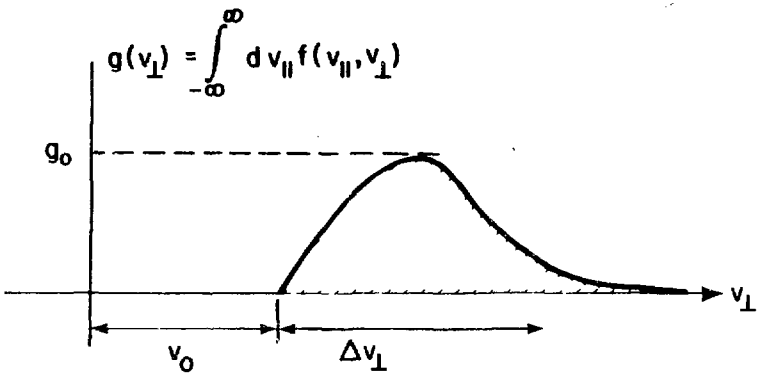

$v_o = \sqrt{2e\phi/m\,(R-1)}$

$\bar{g}(v_\perp)$ = rough approximation to g for calculating moments

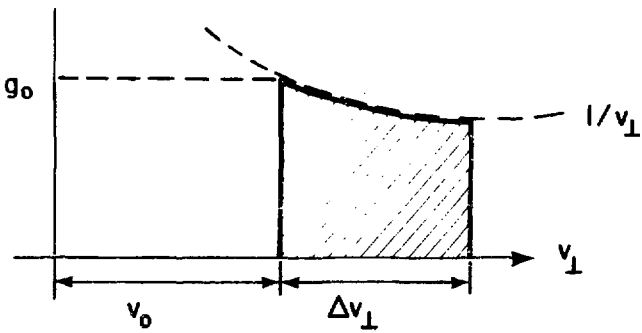

$\Delta v_\perp$ defined so that $\int dv_\perp v_\perp g = \int dv_\perp v_\perp \bar{g}$

XBL 793-692

Fig. 7

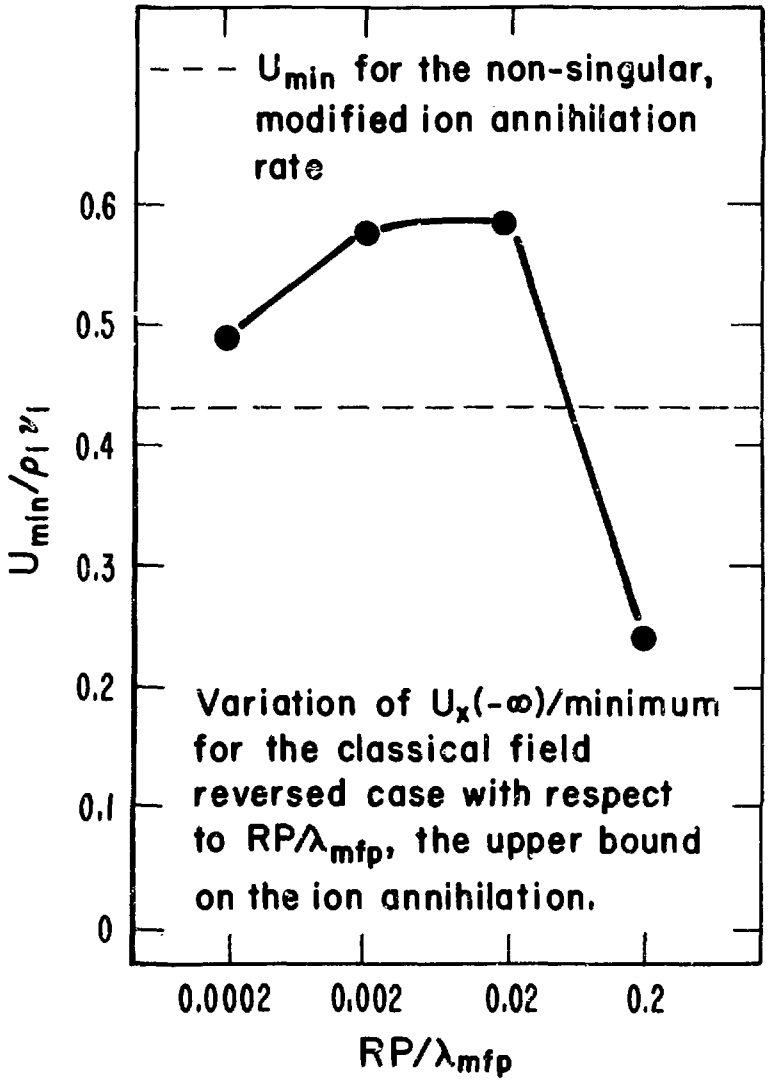
U_{min} for the non-singular, modified ion annihilation rate
0.6
0.5
0.4
0.3
0.2
0.1
0
$U_{min}/\rho_1 v_1$
Variation of $U_x(-\infty)$/minimum for the classical field reversed case with respect to RP/λ_{mfp}, the upper bound on the ion annihilation.
0.0002
0.002
0.02
0.2
RP/λ_{mfp}
XBL 793-679

Fig. 8

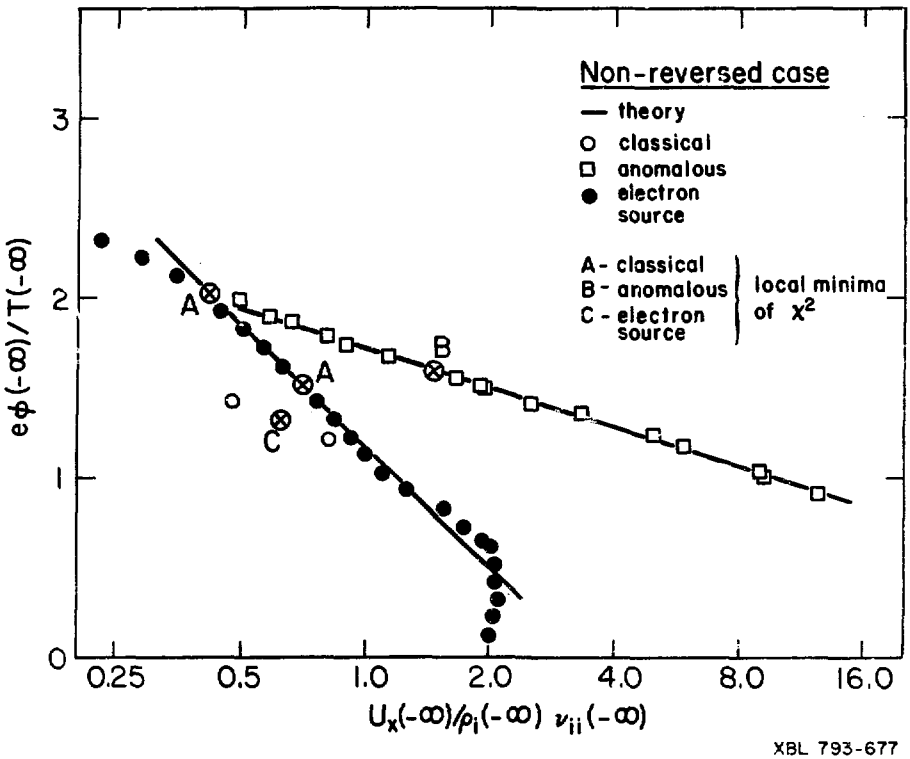
Non-reversed case
— theory
O classical
□ anomalous
● electron source
A - classical
B - anomalous
C - electron source
local minima of χ^2
A
B
A
C
$e\phi(-\infty)/T(-\infty)$
0
1
2
3
0.25
0.5
1.0
2.0
4.0
8.0
16.0
$U_x(-\infty)/\rho_i(-\infty)\ \nu_{ii}(-\infty)$
XBL 793-677

Fig. 9

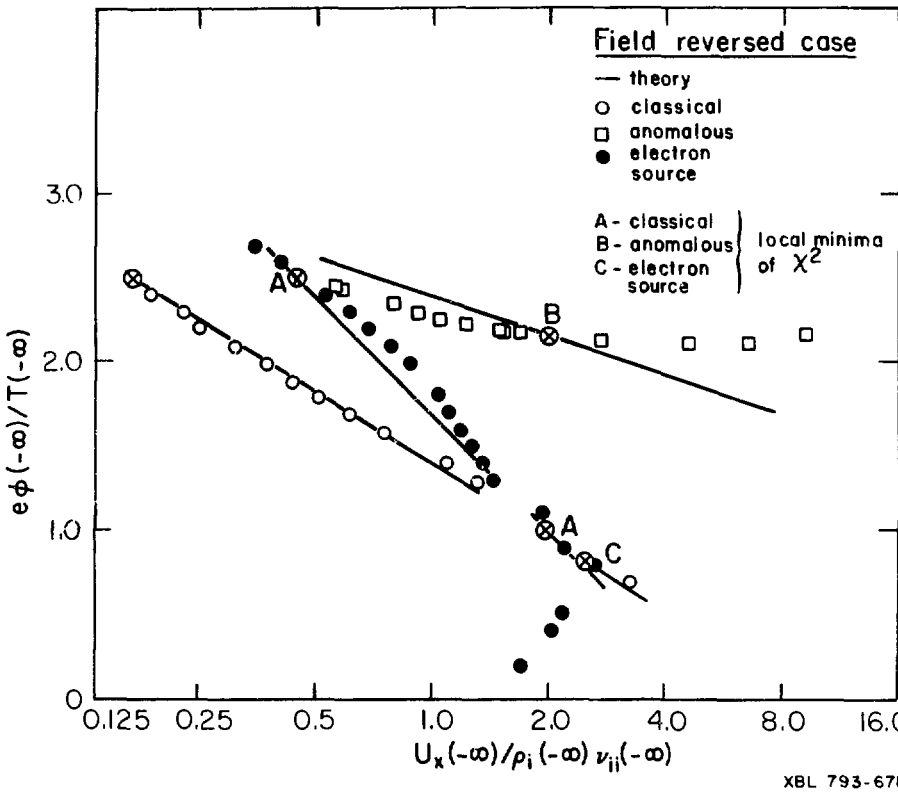
Field reversed case
— theory
○ classical
□ anomalous
● electron source
A - classical
B - anomalous
C - electron source
local minima of χ^2
A
B
A
C
3.0
2.0
1.0
0
0.125
0.25
0.5
1.0
2.0
4.0
8.0
16.0
$e\phi(-\infty)/T(-\infty)$
$U_x(-\infty)/\rho_i(-\infty)\,\nu_{ii}(-\infty)$
XBL 793-678

Fig. 10

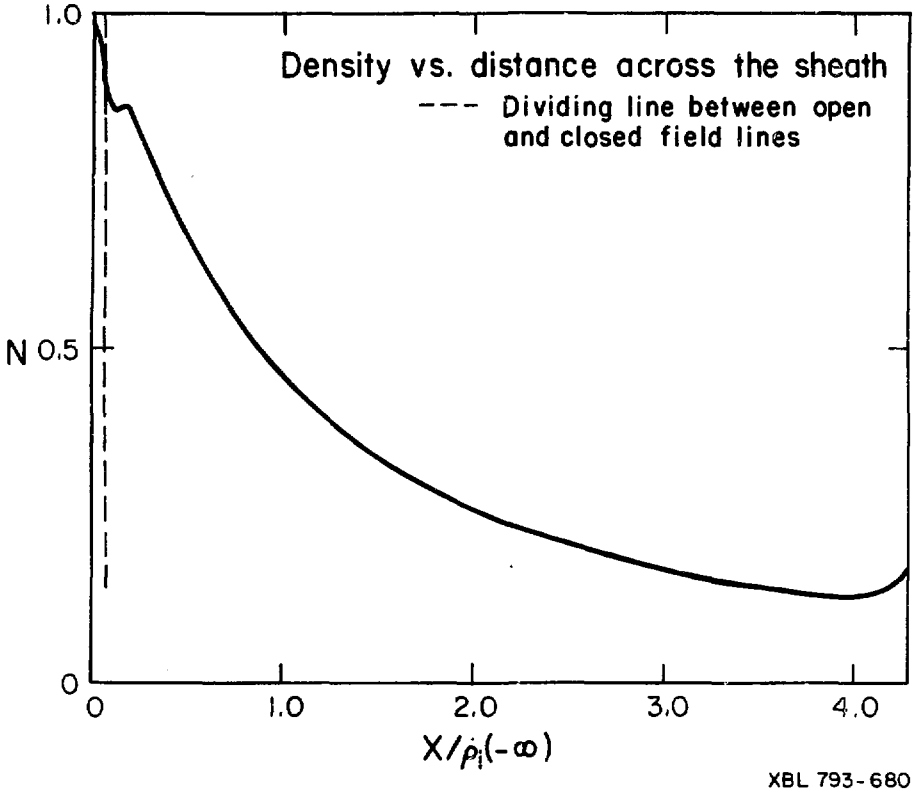
Density vs. distance across the sheath
--- Dividing line between open and closed field lines
1.0
N 0.5
0
0
1.0
2.0
3.0
4.0
X/ρi(-∞)
XBL 793-680

Fig. 11

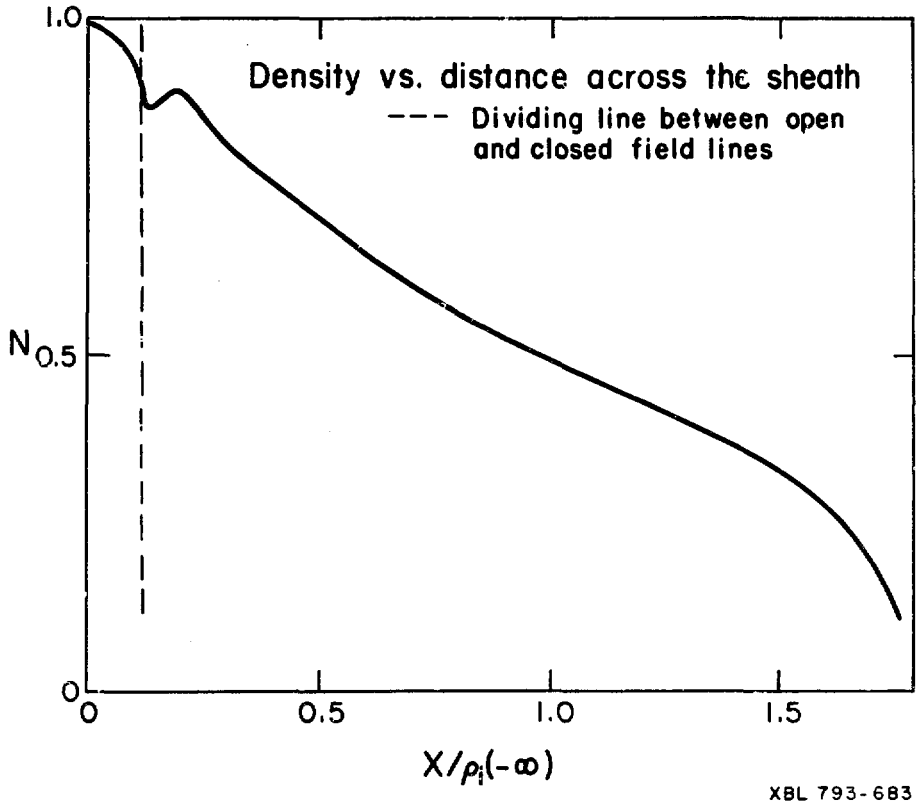
1.0
Density vs. distance across the sheath
--- Dividing line between open and closed field lines
N 0.5
0
0
0.5
1.0
1.5
X/ρi(-∞)
XBL 793-683

Fig. 12

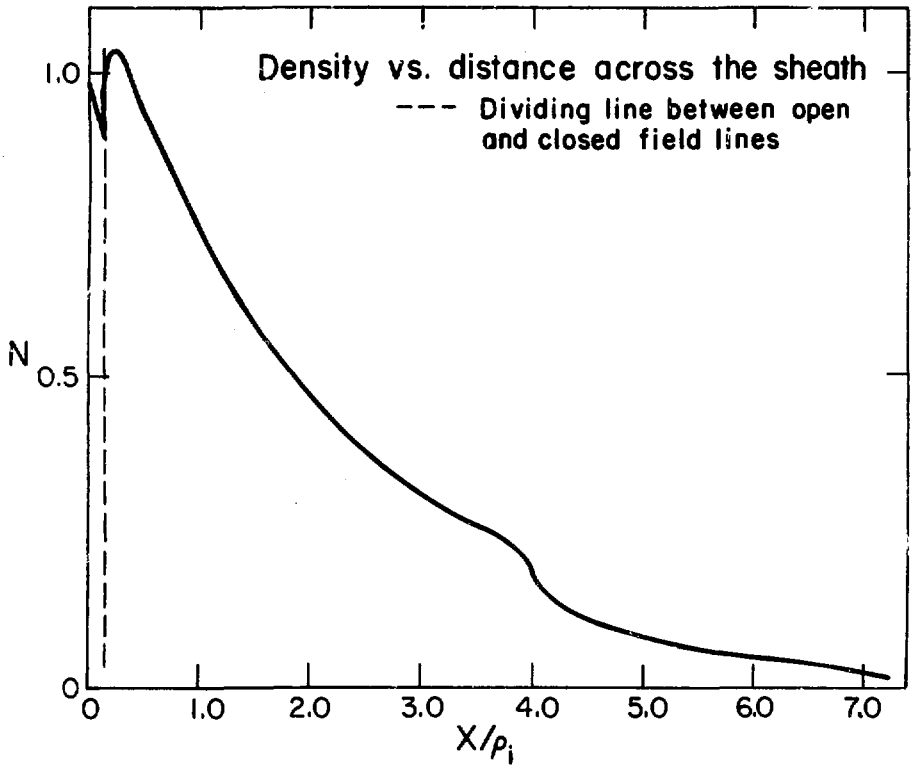

XBL 793-691

Fig. 13

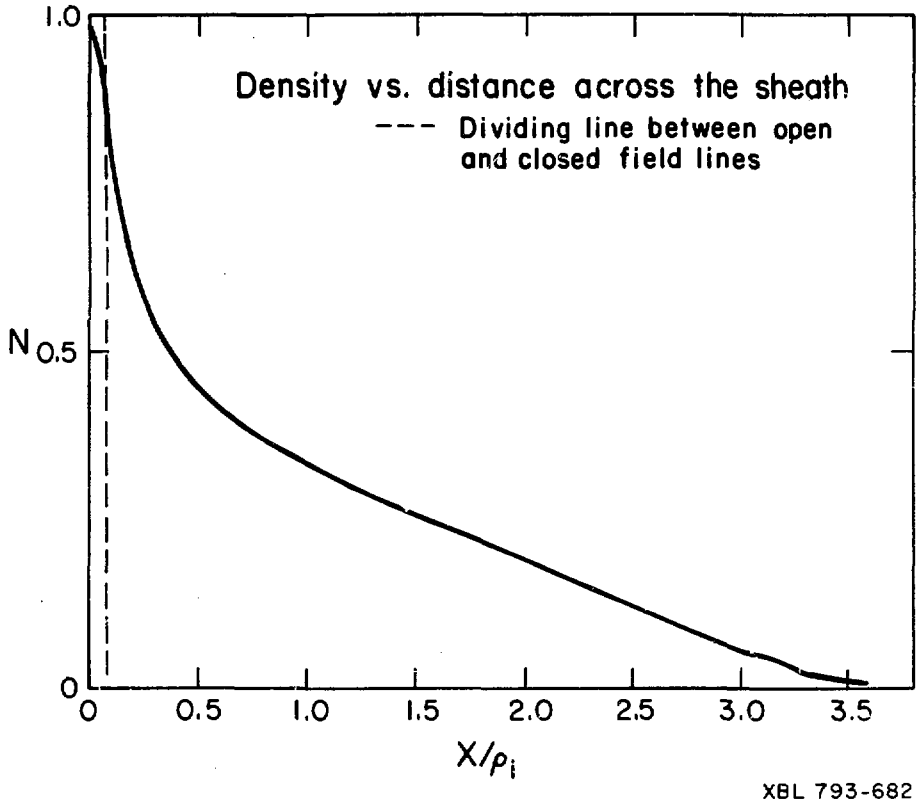
Density vs. distance across the sheath
--- Dividing line between open and closed field lines
1.0
N 0.5
0
0
0.5
1.0
1.5
2.0
2.5
3.0
3.5
X/ρi
XBL 793-682

Fig. 14

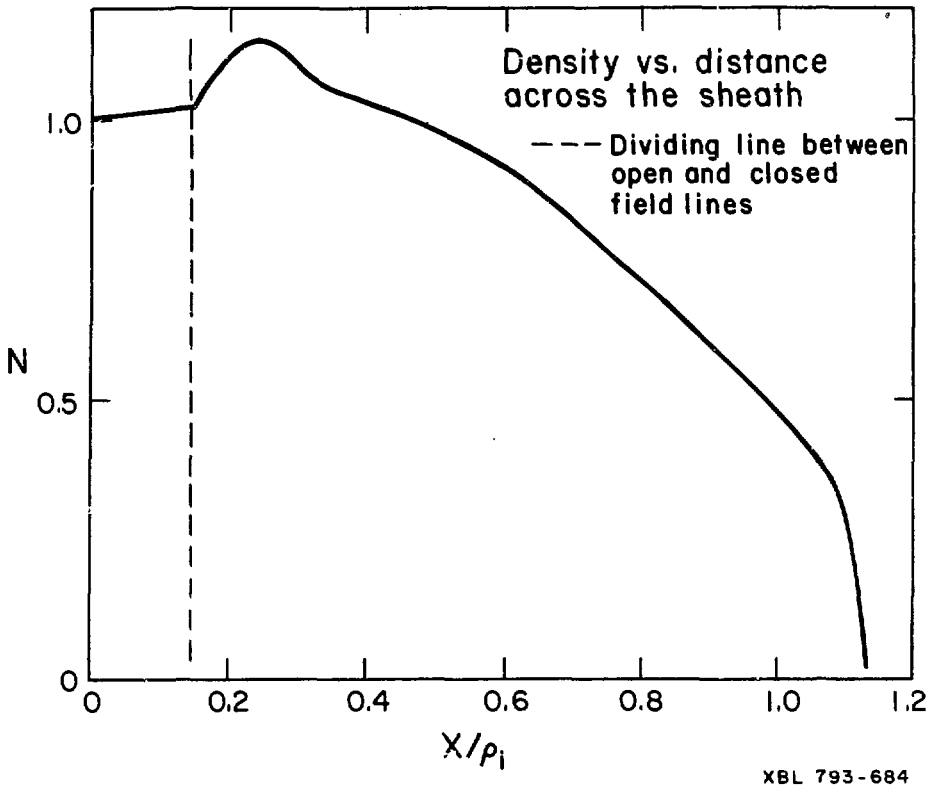
Density vs. distance across the sheath
--- Dividing line between open and closed field lines
N
1.0
0.5
0
0
0.2
0.4
0.6
0.8
1.0
1.2
X/ρi
XBL 793-684

Fig. 15

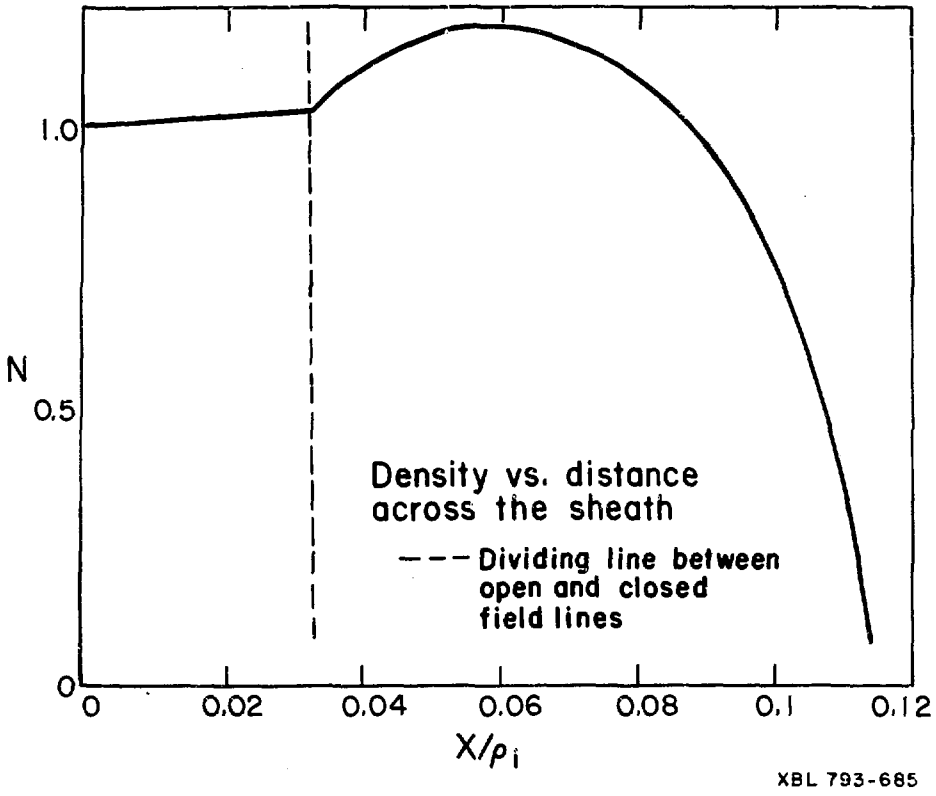
1.0
N
0.5
0
0
0.02
0.04
0.06
0.08
0.1
0.12
X/ρi
Density vs. distance across the sheath
--- Dividing line between open and closed field lines
XBL 793-685

Fig. 16

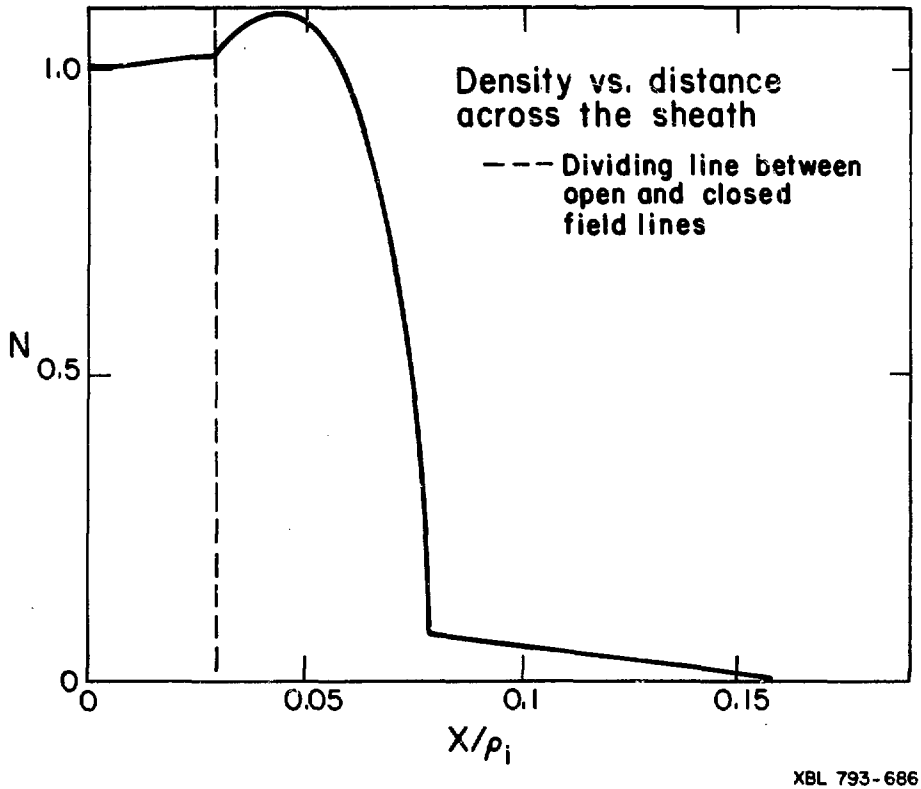
Density vs. distance across the sheath
--- Dividing line between open and closed field lines
1.0
N
0.5
0
0
0.05
0.1
0.15
X/ρi
XBL 793-686

Fig. 17

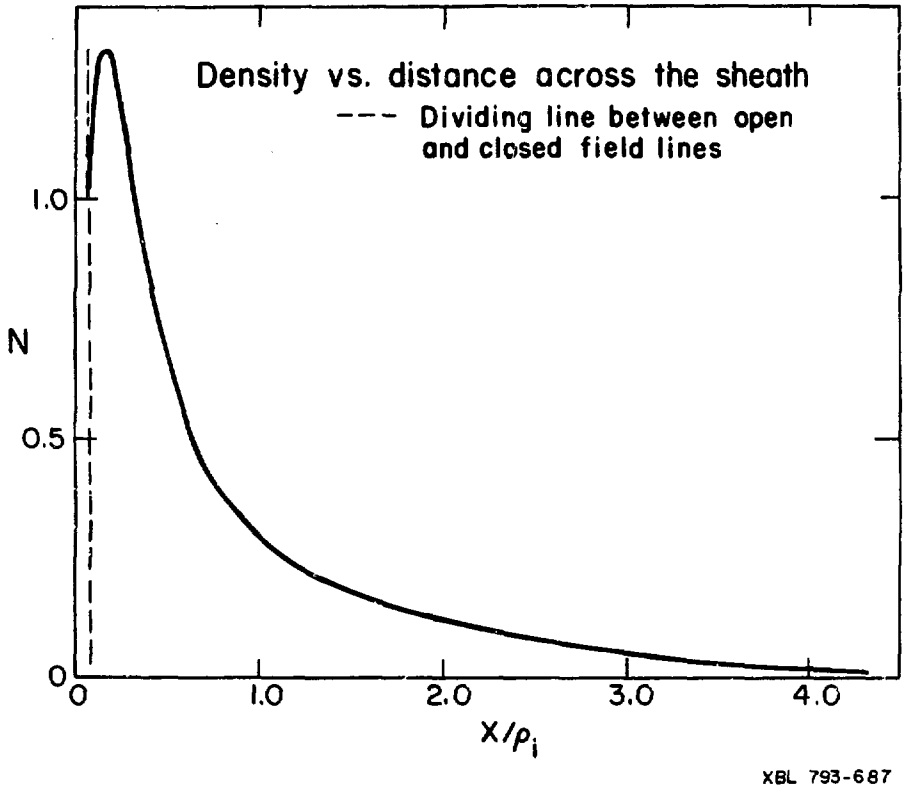
Density vs. distance across the sheath
--- Dividing line between open and closed field lines
N
1.0
0.5
0
0
1.0
2.0
3.0
4.0
X/ρi
XBL 793-687

Fig. 18

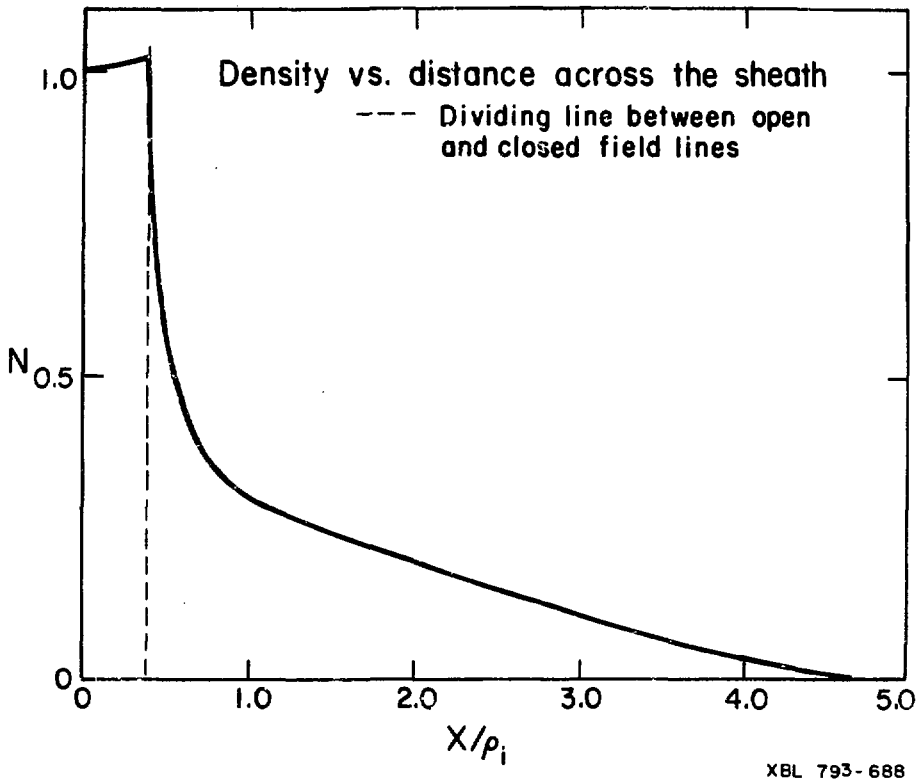
Density vs. distance across the sheath
--- Dividing line between open and closed field lines
1.0
N 0.5
0
0
1.0
2.0
3.0
4.0
5.0
X/ρi
XBL 793-688

Fig. 19

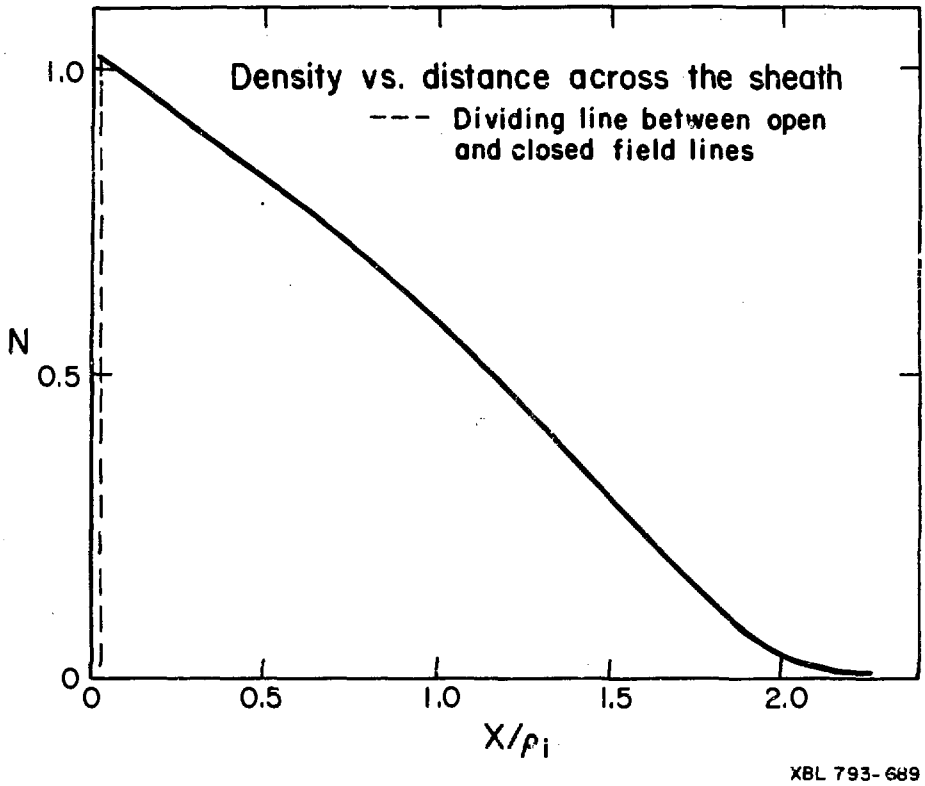

Fig. 20

U.S.GPO:1979-689-058(F)33